Japanese Journal of Veterinary Research 68(3): 133-150, 2020

JJVR

REVIEW ARTICLE Regional Study

Review on counter measures to coronavirus disease 2019 (COVID-19) pandemic, May 2020

Taishi Kidaka[1, 2, *)], Sithumini M.W. Lokupathirage[1, 2, *)], Bungiriye Devinda Shameera Muthusinghe[1, 3, *)], Boniface Lombe Pongombo[1, 2, *)], Christida Estu Wastika[1, 2, *)], Zhouxing Wei[1, 3, *)], Shizuka Yoshioka[1, 4)], Mayumi Ishizuka[1, 4)], Yoshihiro Sakoda[1, 4)], Hiroaki Kariwa[1, 4)] and Norikazu Isoda[1, 2, **)]

[1)] WISE-COVID-19 Tackling Team, WISE Program for One Health Frontier, Graduate School of Excellence, Hokkaido University

[2)] Research Center for Zoonosis Control, Hokkaido University, Kita 20 Nishi 10, Kita-ku, Sapporo, 001-0020, Japan

[3)] Institute for Genetic Medicine, Hokkaido University, Kita 15, Nishi 7, Kita-ku, Sapporo, 060-0815, Japan

[4)] Faculty of Veterinary Medicine, Hokkaido University, Kita18 Nishi 9, Kita-ku, Sapporo, 060-0818, Japan

[*)] Co-first authors

Received for publication, June 9, 2020; accepted, June 25, 2020

Abstract

An outbreak of novel coronavirus infection occurred in China at the end of 2019, which was designated as coronavirus disease 2019 (COVID-19), and spread to regions across Asia and ultimately all over the world. As of 21 May 2020, a total of more than 5 million cases with more than 350 thousand deaths were reported worldwide. Evaluation of the pathogenicity of the disease and determining the efficacy of control measures are essential for rapid containment of the disease. However, the world is facing difficulties in controlling COVID-19 at both of the national and global levels due to variations in pathogenicity of infection by severe acute respiratory syndrome coronavirus 2, the causal agent of COVID-19, and to diverse measures applied in each country based on their control capacities and policies. In the present review, we summarize the basic information and findings related to the COVID-19 pandemic, including pathogen agent, epidemiology, disease transmission, and clinical manifestations. Diagnosis, treatment, and preventive measures applied or under development all over the world are also reviewed to provide the opportunity to establish a more effective scenario for disease containment. Humanity has progressed by developing countless great technologies and immense scientific theories, however it may be a fact that we cannot conquer all risks to humanity. New findings and challenges for the unprecedented pandemic at the global level, such as COVID-19, should also contribute to preparedness for unknown diseases in future, similar to the lessons learnt from severe acute respiratory syndrome and the pandemic A(H1N1)pdm09 influenza.

Key Words: COVID-19

Introduction

Since the dawn of history, humanity has confronted infectious diseases. Human history is, so to speak, the history of infectious diseases. Symptoms of tuberculosis have been confirmed in

**Corresponding author: Dr Norikazu Isoda, PhD, D.V.M.
WISE-COVID-19 Tackling Team, WISE Program for One Health Frontier, Graduate School of Excellence, Hokkaido University, Kita 18, Nishi 9, Kita-ku, Sapporo, 060-0018, Japan
e-mail: isoda@czc.hokudai.ac.jp
doi: 10.14943/jjvr.68.3.133

Egyptian mummies, and the disease was described in early Egyptian texts [10, 106]. Among the greatest plague pandemics ever experienced is the Black Death, which occurred in 1347-1351 and killed 25 million people in Europe [58]. The "Spanish flu" pandemic of 1918-1919 killed approximately 50 million people with mortality of more than 2.5% [73]. Medical science has progressed to conquer infectious diseases by discovering effective treatment methods such as antibiotics and by developing the scientific field of public health. On the other hand, since the 1980s, we have been exposed to a variety of health risks owing to industrialization and increased population; thereby, many infectious diseases spread worldwide quickly. These emerging diseases have become one of the major concerns in public health.

In the 21st century, we have experienced several pandemics. Severe acute respiratory syndrome (SARS) emerged in 2002-2003, causing a total of 8,096 cases with 774 deaths in 29 countries and regions [88]. Pandemic A(H1N1)pdm09 influenza spread from April 2009, and the WHO declared a pandemic from June 2009 to August 2010 [12]. Middle East respiratory syndrome (MERS), which was firstly identified in 2012 mainly caused respiratory symptoms with approximately 35 deaths and has been reported in 27 countries as of the end of 2019 [89]. The largest outbreak of Ebola virus disease, which is an acute and severe disease with high mortality, since its discovery occurred in 2014-2016 caused approximately 11 thousand deaths out of 28 thousand cases in West Africa [91]. All of these diseases spreading at regional or global levels threatened lives and led to updates of control measures.

In 2020, most countries have come to consider a newly emerging disease, coronavirus disease 2019 (COVID-19), which spread worldwide in the three months since its emergence in January 2020. This article highlights characteristics of COVID-19, including pathogens, epidemiology, and disease symptoms to identify effective control measures including diagnosis, treatments, and prevention methods.

Pathogen

The causal virus of COVID-19 was identified as a group of SARS-like coronaviruses and was named 2019 novel coronavirus (2019-nCov) before the International Committee on Taxonomy of Viruses (ICTV) designated the official name of the virus, on 11 February 2020, as severe acute respiratory syndrome coronavirus 2 (SARS-CoV-2) based on the similarity of genomic structure with SARS-CoV [1, 19, 94]. At the same time, the WHO announced the official name of the disease as COVID-19 [84].

Due to the crown-like spike on the surface of the virus, a new type of virus was first found in organ cultures in 1965 and named as coronavirus [75]. This virus belongs to the Coronaviridae family in the Nidovirales order. Coronaviruses are single-strand positive RNA viruses, consisting of nucleocapsid protein, envelope protein (E), spike protein (S), membrane glycoprotein (M) and lipid bilayer [42].

SARS-CoV and MERS-CoV, which cause SARS and MERS, respectively, are also coronavirus targeting the respiratory system in humans. The subgroups of coronavirus families are alpha, beta, gamma and delta; and all three previously mentioned human coronaviruses belong to the betacoronaviruses. When compared with other coronaviruses, SARS-CoV-2 shares 79% sequence identity with SARS-CoV [24].

The S protein of SARS-CoV-2 binds to the cellular receptor angiotensin converting enzyme II (ACE2) for cell entry, and conformation changing in the S protein through an endosomal pathway mediates fusion between the virus envelope and cell membrane. The open reading frame (ORF) 1a and ORF 1b are made by genome RNA and translated into viral replicase protein pp1a and pp1ab, and then cleaved into 16 nonstructural proteins by viral proteinases. Some of these nonstructural proteins form a replication/transcription complex (RNA-dependent RNA polymerase, RdRp), which use the positive strand genomic RNA as a template. The positive strand genomic RNA produced through the replication process becomes the genome of the new

virus particle. Subgenomic RNAs produced through the transcription are translated into corresponding structural proteins for forming a viral particle. Since the translated viral proteins and transcribed viral RNA in the cell are subsequently assembled into virions in endoplasmic reticulum and Golgi, and then virions are released out of the cell by exocytosis [27, 72].

There are indications that COVID-19 patients show heightened levels of leukocytes and plasma pro-inflammatory cytokines [44], while the main pathogenesis of COVID-19 is severe pneumonia with incidence of ground-glass opacities [38]. Significantly high blood levels of cytokines and chemokines have been noted in patients of COVID-19, including IL1-β, IL1RA, IL7, IL8, IL9, IL10, basic FGF2, GCSF, GMCSF, IFNγ, IP10, MCP1, MIP1α, MIP1β, PDGFB, TNFα, and VEGFA [38]. Some severe cases that were admitted to the intensive care unit showed high levels of pro-inflammatory cytokines including IL2, IL7, IL10, GCSF, IP10, MCP1, MIP1α, and TNFα that were suspected to enhance disease severity [38].

Epidemiology, Transmission, and Situation

Early case of COVID-19

The WHO received the first official report from China on 31 December 2019 about an outbreak of pneumonia of unknown etiology in Wuhan City, Hubei Province of China [86]. Further investigation revealed that the first patient showed clinical symptoms on 1 December 2019 without any links to the later cases. The first fatal case was connected to a market in Wuhan and the individual's wife also showed similar symptoms, though she did not have any history of being exposed at the market [38].

Human-to-human transmission

In late January, the WHO announced that SARS-CoV-2 could be transmitted from human to human by droplets, contact, and fomites, similar to the previous outbreaks of MERS and SARS [90]. Cases related to the Wuhan market decreased in time and family-related clusters were confirmed, supporting the case for human-to-human transmission by close contact, some of which caused asymptomatic infection [15]. The first case outside China was reported on 13 January 2020 in Thailand followed by Japan (16 January 2020), South Korea and United States (20 January 2020) [37, 68, 70, 71].

A German case likely transmitted by a woman from China who was diagnosed as positive to SARS-CoV-2 after travel back from Germany led to suspicions that the virus transmission could occur during incubation period and asymptomatic infection [62]. A similar finding was reported in China from a family cluster [6]. Moreover, Zou et al, proposed the possibility of disease transmission from asymptomatic or mildly symptomatic cases based on viral load analysis in nasal and throat swabs [107]. In April, the WHO reported three mechanisms of human-to-human transmission: symptomatic, pre-symptomatic, and asymptomatic transmissions. Symptomatic transmission refers to the transmission from a person manifesting the typical clinical symptoms to others. During the incubation period of COVID-19 estimated 5-14 days, in which the infected host has not shown apparent symptoms, an infected person could be contagious and transmit the virus, a case of pre-symptomatic transmission. The third type was identified by a COVID-19 case transmitted from a laboratory-confirmed asymptomatic carrier [87].

Human to human transmission by indirect contact could be happen when the virus was transferred by the surface of objects. Under the experimental condition, SARS-CoV-2 remained its infectivity in aerosols for 3 hours and was stable on plastic and stainless steel for 72 and 48 hours, respectively [76, 78].

SARS-CoV-2 infection in animals

The first animal infection was reported in two dogs in Hong Kong, whose owner had been diagnosed as positive for COVID-19 [66]. It was reported that several big cats in a zoo in the United States were infected with SARS-CoV-2 via transmission from an asymptomatic zookeeper.

In total, four tigers and three lions showed clinical signs such as dry cough, wheezing, and inappetence. SARS-CoV-2 was isolated from the samples taken from the first affected tiger, and other animals were assumed to be infected with the same virus [93].

Under laboratory conditions, it was confirmed that cats and ferrets were highly susceptible to SARS-CoV-2, while dogs only showed low susceptibility with poor viral replication [65, 67]. In contrast, domestic animals such as pigs, chickens, and ducks were not susceptible to the virus [65]. Similar to humans, cynomolgus macaques were also susceptible to the infection but did not show severe clinical signs [61]. Another study in cats demonstrated effective transmission of the virus from an infected to healthy cat in the same cage [33].

During the COVID-19 pandemic, there is a possibility of the occurrence of SARS-CoV-2 transmission from human to animal as described above. Thus, all infected animals have been reported to cohabit with infected humans. Even though the animals were positive in the viral detection test, further investigation in the field are required to assess whether the infected animals can play a key role in the spread of COVID-19 by transmitting the virus back to humans.

Potential origin of the virus in animals

Since an animal market in Wuhan was related to most of the early cases of COVID-19, the virus was suspected being transmitted from an animal host before causing human-to-human infection. The first comparative genomic analysis reported that SARS-CoV-2 was related to a bat coronavirus which is yet unknown [57]. It also suspected that the virus emerged as the result of recombination events and that a snake is an intermediate host, a finding which was ruled out after further analysis [57, 100].

Metagenomic analysis on bronchoalveolar lavage fluid from a patient in Wuhan revealed that SARS-CoV-2 had 89.1% nucleotide identity with bat-coronavirus SL-CoVZC45 previously isolated in China [94]. Another meta-metagenomic investigation found that SARS-CoV-2 sequence was highly similar to a virus sequence in pangolin lung and to a bat coronavirus (RaTG13) [78]. Furthermore, a genome analysis reported that the SARS-CoV-2 uses ACE2, which is the same entry point as SARS-CoV [104]. A study on SARS-CoV-2 entry points described that the virus was using ACE2 and was supported by the cellular transmembrane protease serine 2 [36].

The intermediate host from bat to human has been investigated in detail by genomic analysis and virus characterization and isolation. Phylogenetic analysis based on full-genome sequences showed that the pangolin coronavirus had 91.0% identity to SARS-CoV-2 and 90.6% identity to RaTG13 [102]. The receptor binding protein on the S1 protein which is one of the subunits of the S protein and could interact with ACE2 receptor, of SARS-CoV-2 is similar to a pangolin coronavirus. However, neither pangolin coronavirus nor RaTG13 has polybasic furin cleavage site at the S1-S2 junction but SARS-CoV-2 does [4, 102]. This mutation allows the S protein of SARS-CoV-2 to be cleaved by furin and other proteases and is a determinant of the viral infectivity and host range [4].

Worldwide spread

Due to the rapid increase of COVID-19 cases outside China, the WHO declared the pandemic of COVID-19 on 11 March 2020 which brought global awareness to this outbreak [20]. Following the lockdown of Hubei Province in China [17], several countries tightening their border control resulted in a decrease in the infection. Hong Kong, Taiwan, and Singapore closed their border in March [2, 54, 56, 69, 72]. Although China authority has banned domestic and international flights from Wuhan since 23 January [17].

The global spread of COVID-19 was initially due to exported cases from China followed by local transmission within the countries. According to the WHO situation reports, COVID-19 was mainly reported as being imported through over-23-day-international travels outside the West Pacific region (Fig. 1). Through genomic epidemiology, Fauver et al. describe that the transmission shifts in the

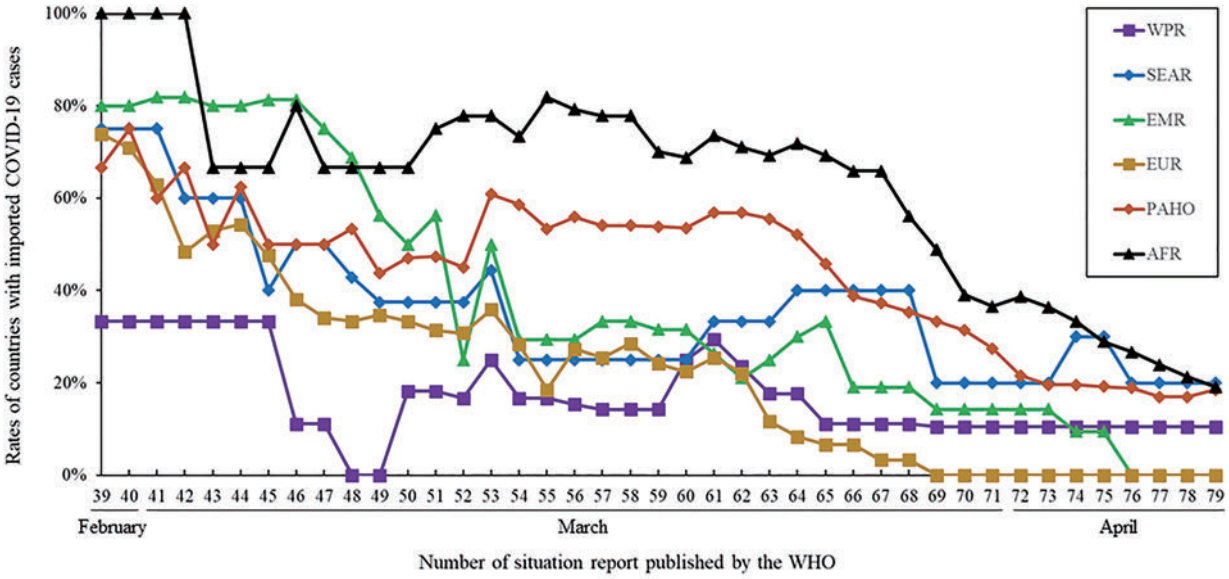

Fig. 1
Dynamics of COVID-19 transmission in member states. Proportions of member states with imported COVID-19 cases confirmed in the region were calculated by the World Health Organization situation reports from No. 39, (on 28 February 2020) to No. 79 (on 8 April 2020). WPR: Western Pacific Region, SEAR: South-East Asia Region, EMR: Eastern Mediterranean Region, EUR; European Region PAHO; Regions of the Americas, AFR; African Region.

United States has been observed since March. Moreover, inter-state air travels were predicted to be the main factor for the domestic spreading in the US, especially in Connecticut [26, 33, 54].

As of 21 May 2020, COVID-19 cases have reach 4.9 million cases including 324,766 deaths with 1,717,407 patients having recovered worldwide [40]. The epi-center of COVID-19 has moved from East-Asia to Europe and the US with a combined 1,532,974 cases followed by Russia (308,705 cases) and Brazil (275,087 cases). In Japan, a total of 16,367 COVID-19 cases has been reported, of which 768 have died and 11,564 recovered.

Signs and Symptoms

General symptoms

A wide spectrum of clinical signs and severity have been reported in cases of COVID-19, ranging from asymptomatic to critical, and, ultimately, death. The most common complication of this disease is acute hypoxaemic respiratory insufficiency and ventilation therapies [59]. At the time of onset, fever, cough, difficulty in breathing, muscle pain, and fatigue were observed as common signs [43]. Most of the signs were observed on the respiratory system, however, digestive symptoms were also observed with or without respiratory symptoms [34]. Among digestive symptoms, diarrhea was the most commonly confirmed in both children and adults, with signs being observed a later rather than early stages of disease onset [74].

Olfactory and gustatory dysfunction was also reported, most of which were rapid onsets, although numbers of patients with this symptom varied depending on region [30]. The mechanism of these symptoms has not yet been clarified but SARS-CoV-2 can grow in olfactory cells at the early phase of infection, possibly causing smell dysfunction in the patient [7].

Elderly and younger patients

All ages are susceptible to SARS-CoV-2, however, the young people less than 20 years of age, the elderly, and patients with chronic disease, heart disease, or immunocompromised

individuals are considered to be generally at higher risk of adverse outcomes [39]. A strong immune response, such as a cytokine storm, that results in worsening the outcome has been recently reported as well [35]. Though the mechanism of a cytokine storm triggered by SARS-CoV-2 infection has not yet been well understood, administration of corticosteroid appears to reduce excessive inflammatory response, although the timing of administration remains challenging [96].

Diagnosis

Molecular methods

It has been shown that COVID-19 patients harborhigh viral loads in their upper and lower respiratory tract at 5-6 days after manifesting clinical symptoms [56, 83]. Nasopharyngeal and oropharyngeal swabs are commonly collected as upper respiratory samples for screening and early diagnosis of COVID-19. For COVID-19 patients with symptoms of severe pneumonia, sputum or bronchoalveolar lavage are collected as lower respiratory tract specimens to obtain samples with a high viral load [99]. Several studies have shown that SARS-CoV-2 RNA can also be detected in blood and stool specimens, suggesting the safer applicability of rectal swabs for detecting SARS-CoV-2 from severe COVID-19 patients [97, 98, 103]. Specimen processing should be carried out in a biosafety level (BSL) 2 cabinet or ideally in a BSL3 environment.

Most of the molecular diagnostics currently applied to COVID-19 involve real-time RT-PCR, while other molecular methods such as loop-mediated isothermal amplification and multiplex isothermal amplification followed by microarray detection are under development or on trial all over the world [2]. Targets of these tests are viral genes encoding structural proteins of SARS-CoV-2, such as the S, E, M, helicase, and nucleocapsid (N) proteins, RdRp, hemagglutinin-esterase, and open reading frames ORF 1a and ORF 1b [14, 18]. In the United States, the Center for Disease Control (CDC) recommends two protein targets in the nucleocapsid (N1 and N2) while the WHO recommends E gene assay followed by a confirmatory assay using the RdRp gene as a first line screening test [18, 37].

Serology

Out of the four structural proteins of SARS-CoV, N protein shows high immunodominance, suggesting its applicability as an antigen of serological diagnosis for COVID-19 [16]. A rapid lateral flow assay and other serological tests have been developed and for detection of IgM and IgG antibodies against SARS-CoV-2 [28, 47, 101]. As it takes several days for the production of antibodies, these tests are less likely to be useful for early diagnosis of infection [32, 46].

Radiological diagnosis

Single or multiple ground-glass opacities, especially on the peripheral and lower lobes in the lung in the early phase, and bilateral multiple lobular and subsegmental areas of consolidation were typical findings of chest X-ray or CT image among serious cases [38, 64].

Treatments

Antivirals

Though many of the specific treatment or medicines are under development, soon after the emergence of COVID-19, several drugs, already developed or approved for therapeutic purpose in other diseases, were applied to COVID-19. Several antiviral agents have shown their efficacies to treat COVID-19 in vitro and in animal models.

Inhibiting the RdRp

Remdesivir

Remdesivir, originally developed as a treatment of Ebola virus infection, was successfully used in several COVID-19 patients in China [3]. As the structure resembles adenosine, remdesivir acts via adding into the synthesizing viral RNA

chain followed by its premature termination. It is currently undergoing multiple trials in different countries, including two randomized phase III trials in China that had been scheduled to be completed in April/May 2020 [53].

Favipiravir

Favipiravir, developed by Toyama Chemical, Japan, which is an approved treatment for influenza has a structure resembling the endogenous guanine which works as a competitive inhibitor of the RdRp [29]. This was approved as the first anti-COVID-19 drug in China by the National Medical Products Administration of China, due to the results of a clinical trial demonstrating its efficacy with few side effects [8].

Inhibiting the Viral Protease

Ivermectin

This FDA-approved anti-parasitic agent has been also revealed to stimulate antiviral activities toward both human immunodeficiency virus and dengue virus [77]. At 48 hours of infection with SARS-CoV-2, ivermectin reduces viral RNA up to 5,000-fold [9].

Blocking Virus–Cell Membrane Fusion

Recombinant Human Angiotensin-converting Enzyme 2 (rhACE2)

It was reported that rhACE2 which blocks the S protein from interacting with cellular ACE2 could inhibit SARS-CoV-2 replication in vitro by a factor of 1,000-5,000 [52]. APN01 (rhACE2), originally developed by Apeiron Biologics, has already undergone phase II trial for acute respiratory distress syndrome.

Hydroxychloroquine

The effect of this antimalarial agent against SARS CoV-2 has been demonstrated in China and France to varying degrees. Considering this evidence, the US FDA issued the European Unit of Account for the use of hydroxychloroquine to treat COVID-19 in the USA. However, the latest study done using a combination of hydroxychloroquine and azithromycin for the treatment of severe COVID-19 patients found no evidence of clinical benefit [51].

In addition to the above mentioned antiviral drugs, monoclonal antibodies against interleukins and SARS-CoV-2-specific neutralizing antibodies identified from recovered patients of COVID-19 are being tested for their efficacies. As of 20 May, the National Institute of Health, clinical trials database records 2,276 trials related to COVID-19 and SARS CoV-2 in total [53], while the WHO International Clinical Trials Registry Platform lists 2,738 clinical trial records as of 19 May 2020 [48].

Vaccines

As of 18 May 2020, 169 total vaccine candidates are on the run in pre-clinical, phase I and phase II trials according to the tracker developed by the Vaccine Centre at the London School of Hygiene & Tropical Medicine. They have categorized these candidates in to 8 vaccine types: RNA (n=21), DNA (n=12), non-replicating viral vector (n=16), replicating viral vector (n=15), Inactivated (n=6), live-attenuated (n=3), protein subunit (n=51) and other/unknown (n=45) [48].

mRNA-1273

US-based company ModernaTX, Inc made a synthetic messenger RNA (mRNA) strand namely mRNA-1273, encapsulated in lipid nanoparticle envelope that encodes the prefusion-stabilized viral spike protein that is expected to elicit a specific antiviral response. Recruitment of participants for the phase I clinical trial is ongoing in the United States and is estimated to be completed by September 2020 [79].

INO-4800

This is a candidate DNA vaccine created by Inovio Pharmaceuticals that can elicit an immune response after being translated into its protein inside host cells [67]. Phase I Open-label Study to Evaluate the Safety, Tolerability and Immunogenicity has started and currently recruiting the healthy study participants. It is expected to be completed in April 2021 [48].

ChAdOx1 nCoV-19

A phase I/II single-blinded, randomized, multi-center study to determine efficacy, safety and immunogenicity of the vaccine candidate ChAdOx1 nCoV-19 created by University of Oxford, UK is currently recruiting study participants and is expected to be completed by May 2021. This vaccine is composed of a non-replicating adenovirus vector carrying the S protein sequence of SARS-CoV-2 [55].

Prevention at the individual level

To date, there is no effective vaccination available for COVID-19 and there is a high risk of acquiring the infection through respiratory droplets and contact. Therefore, the best way to protect oneself is to follow the conventional prevention methods at the individual and community level.

Hand hygiene practices

SARS-CoV-2, like other viruses, has a lipid envelope which hand washing with soap can break apart, there by destroying the infectivity of the virus [63]. Hence, handwashing with soap and water is more important than any other prevention method thus far established. Furthermore, according to the CDC guidelines, an effective handwashing technique includes 5 steps: wet, lather, scrub, rinse, and dry, all of which should last at least 20 minutes [13]. Due to the unavailability of clean water and soap for those who are travelers, the use of 75% alcohol, hand sanitizer gel, or and disinfected wipes are suggested as an instant hand hygiene alternative. A recent study showed that hand wiping using a wet towel soaked in water containing 1.00% soap powder, 0.05% active chlorine, or 0.25% active chlorine from sodium hypochlorite removed 98.4%, 96.6%, and 99.9% of the virus from hands, respectively [49].

Proper use of face masks

The size of SARS-CoV-2 is estimated to be about 125 nm in diameter. The smallest of them are estimated to be 60 nm and the largest are 140 nm [105]. There are several types of masks used by the general public and healthcare workers, each of which has different filter capacities [25]. Surgical mask is conventionally used in hospitals or publics to prevent dissemination of pathogen spread in exhalation and causing a potential infection by it, whereas N95 respirator is specifically used for protecting individuals from being exposed to any kinds of contamination including infectious agents. According to the guidelines issued by the WHO for the usage of face masks, face masks can be used as a physical barrier for individuals showing respiratory symptoms and health-care workers. Whether healthy members of the public should use face masks is still under discussion. The WHO on 6 April 2020 released advice to decision makers on the use of masks for healthy people in community settings [92]. In addition, there are potential advantages to using masks by healthy individuals such as reducing the risk of exposure during the pre-symptomatic period from infected peoples well as reducing the stigmatization of individuals wearing masks for source control. Furthermore, it is important to pay attention to appropriate use and disposal of face masks to avoid any increase in transmission [92].

Disinfection of surfaces

SARS-CoV-2 spreads mostly through contaminated surfaces and respiratory droplets. Therefore, it is not enough to protect oneself only from respiratory droplets using masks. Recent studies have shown that SARS-CoV-2 can persist for hours to days depending on the material of the surfaces [41, 76]. Hence, the CDC recommends cleaning and disinfecting the surfaces of residential and public spaces regularly using appropriate disinfectant [11]. It has been proven that disinfectants with 62-71% ethanol or 0.1% sodium hypochlorite are effective for the disinfection of surfaces contaminated with SARS-CoV-2 [41]. Cleaning of the surfaces should be done followed by the disinfection of the surfaces.

Also, it is important to pay attention to shared instruments and electronic devices such as public telephones and shared computers. Disinfection should be applied prior to usage or hand hygiene methods should be applied after the usage of shared devices.

Implementation of social distancing

Social distancing is a widely accepted method worldwide to fight COVID-19 infection. Social distancing can also be described as "physical distancing" which can be applied to individual and community levels. According to the WHO guidelines for the individual level social distancing involves non-contact greetings, keeping distance of at least one meter between two individuals, staying home or self-isolating even with mild symptoms such as fever, cough, headache until recovery, and avoiding crowded places. As for the community level social distancing involves closure or postponement of mass-gatherings including schools, public sectors, and social and sports events [85]. Furthermore, it is important to make sure that people follow good respiratory hygiene such as cough and sneeze etiquettes to avoid contact with the virus [85].

Contact authorities for help

Seeking medical attention and contacting to the local health authority as soon as possible, can reduce the transmission of the infection. National and local authorities have the most up-to-date information regarding the COVID-19 situation of the respective area. Contacting in advance will allow the health-care provider to direct the patients to the nearest health-care facility without any delay. Contact to the authorities for help when:

- you or someone you know has fever, cough, chills or other respiratory symptoms.
- you or someone you know has been in contact with a patient who is suspected or has tested positive with COVID-19.
- you or someone you know has respiratory symptoms and had been travelling to COVID-19 highly affected areas.

This will also protect the patient from the illness and help prevent spreading the virus into the community.

Measures at the Community and Nation Levels

SARS-CoV-2 is currently spreading, sometimes subclinically, with high transmissibility among susceptible populations around the world, creating an important public health concern [21, 82]. Neither vaccines nor specific treatment are currently available to prevent or cure COVID-19 [23, 31, 95]. The key strategies to control SARS-CoV-2 in the community involve controlling the infection in order to slow its transmission by preventing amplification events and further spread there by protecting susceptible people [21, 60, 95]. As environmental contamination (fomites) influence the spread of infectious diseases, environmental cleaning and disinfection are fundamental for COVID-19 prevention and control [31]. Compounding the problem, the incubation time for COVID-19 is approximately 5-6 days, with presymptomatic infectiousness and increased viral excretion upon appearance of symptoms [5]. Better coordination of quick case detection along with immediate implementation of traditional non-pharmaceutical interventions such as isolation, confinement, tracing all contacts and medical observation of COVID-19 patients and suspected cases, and social distancing are successful ways to limit its spread [1, 23, 95]. When implemented early in accordance with the local context and complementary to individual prevention measures, these containment measures reduce the number of super-spreading events, slow virus amplification and greatly reduce virus spread from symptomatic and non-symptomatic cases as observed in Singapore, Hong Kong and China [5, 60].

SARS-CoV-2 is transmitted by respiratory droplets and therefore requires certain proximity among people for its effective transmission [81]. Limiting individual interactions and physical distancing between individuals can interrupt its transmission and subsequent virus amplification [81]. There is no clear distinction in social distancing,

quarantine or landlock with significant movement restrictions for everyone. At the national level, governments implement community-wide containment (e.g., restrictive lock-down policies) in addition to non-pharmaceutical public health measures [1, 81]. In practice, these measures allow the separation of sick people with contagious diseases from uninfected ones and allow individuals follow-ups [81]. Ethically, such measures challenge individual human rights and have major economic consequences [21, 81]. Therefore, it is important for science-based public health education to provide the reasons for quarantine or landlock, as well as to provide comfort and practical advice in order to prevent or reduce anxiety and distress [22, 95]. This implementation requires partnerships and cooperation with law enforcement at the local and national levels, often involving checkpoints, and may require legal sanctions for breaching quarantine [21, 81]. Community quarantines are currently underway in COVID-19 affected countries worldwide on an order of a magnitude that humanity has never known [81].

Conclusion

After the emergence of COVID-19 at the end of 2019, the disease has spread all over the world, recording nearly 5.5 million cases and more than 34 thousand deaths as of 26 May 2020. Many of the countries implemented strong control strategies such as lockdown and ban on international human movement as measures of containment of COVID-19. Even so, cases and deaths are increasing day by day. Humans now confront a threat which is similar to that of the "Spanish flu" during 1918 to 1919, about a century ago. Since the COVID-19 pandemic may continue or repeat for a long period of time, it is crucially important to know what counter measures are effective. Though several candidates of vaccines and drugs are being developed, no effective vaccine or therapeutic drug exists so far.

Under such conditions, we should re-evaluate general hygiene practices as the measures to prevent COVID-19. Since the main transmission routes of SARS-CoV-2 are droplets and contact, reducing virus loads in these transmission routes should result in decreased chance of infection. There is a controversy whether wearing a mask is effective to prevent the infection. Human seasonal coronavirus from the infected individuals can be effectively filtered by a surgical mask [45]. Therefore, it is highly possible that community-wide wearing of face masks can reduce the total number of infections in the community [50]. To prevent droplet spread, the effect of wearing a mask should be further emphasized. Proper hand hygiene through washing hands and using hand sanitizers can reduce the possibility of virus transfer from contaminated hands to susceptible organs such as eyes and mouth. Social distancing which is related to changing behaviors is also effective: avoiding shaking hands, or hugging for greetings and staying at home whenever possible may also reduce the chance of infection. Combining these general hygiene practices at the individual level may enhance the protection efficacy.

Finding appropriate measures to control COVID-19 at the community and nation levels is essential for reducing the number of cases and deaths. Some countries are implementing strong strategies, like lockdowns, while others are relying on controlling clusters of infection. Since variety of strategies have been implemented, and some countries seem to have succeeded in controlling the first wave of COVID-19, a large epidemiological survey should be conducted to identify the appropriate approaches.

One of the unique features of SARS-CoV-2 infection argued is to cause the subclinical infection, and, thereby, it produces the asymptomatic careers of the virus, which would play a critical role of disease spread widely [80]. Calculation of the sero-positivity in the population is important to understand the disease dynamics more precisely and to estimate the probability to acquire high level of herd-immunity enough to halt the epidemic.

Infection of SARS-CoV-2 in animals should also be more investigated to assess the risk of COVID-19 in animals. Since SARS-CoV-2 can infect domestic cats and dogs [65, 66], the significance of companion animals for virus transmission to humans should be urgently clarified. SARS-CoV-2 may have originated from bat species but more surveys are required. It is also unknown whether SARS-CoV-2 has intermediate host species. Identification of the natural host is a base of control of zoonoses, which can be transmitted among humans and animals including COVID-19 and elucidate the route of transmission from the original host animal(s) to humans. Moreover, surveillance of wild animals should be strengthened to seek for potential pathogens in humans. As zoonotic events occurred at human-animal interface, research activities and control measures for zoonoses would be implemented under the One Health Concept.

Many challenges remain to be revealed in SARS-CoV-2 and COVID-19. The efforts to understand the virus, the disease, and the epidemiology at multi-sectional levels can minimize the social damage caused by COVID-19.

Acknowledgements

We would like to thank whole of the team members and their supervisors contribute their effort to completing this review paper. Ms. Precious Bwalya, Mr. Chizimu Yamweka Joseph, Ms. Mai Kishimoto, Mr. Vuong Tuan Phong, Ms. Chayada Piantham, and Mr. Misheck Shawa, participated in summarizing the contents. Mr. Michael Henshaw contributed to proof-reading of the draft. Prof. Motohiro Horiuchi organized this team.

Reference

1) Adam B, Guido D, Valenti K, David VD. The COVID-19 Pandemic: Government vs. Community Action Across the United States. INET Oxford Working Paper 2020-06, 2020.
2) Ai JW, Zhang Y, Zhang HC, Xu T, Zhang WH. Era of molecular diagnosis for pathogen identification of unexplained pneumonia, lessons to be learned. Emerg Microbes Infect 9, 597-600, 2020, doi:10.1080/22221751.2020.1738905.
3) Al-Tawfiq JA, Al-Homoud AH, Memish ZA. Remdesivir as a possible therapeutic option for the COVID-19. Travel Med Infect Dis, 2020, doi:10.1016/j.tmaid.2020.101615.
4) Andersen KG, Rambaut A, Lipkin WI, Holmes EC, Garry RF. The proximal origin of SARS-CoV-2. Nat Med 26, 450-452, 2020, doi:10.1038/s41591-020-0820-9.
5) Anderson RM, Heesterbeek H, Klinkenberg D, Hollingsworth TD. How will country-based mitigation measures influence the course of the COVID-19 epidemic? Lancet 395, 931-934, 2020, doi:10.1016/S0140-6736(20)30567-5.
6) Bai Y, Yao L, Wei T, Tian F, Jin DY, Chen L, Wang M. Presumed Asymptomatic Carrier Transmission of COVID-19. JAMA, 2020, doi:10.1001/jama.2020.2565.
7) Butowt R, Bilinska K. SARS-CoV-2: Olfaction, Brain Infection, and the Urgent Need for Clinical Samples Allowing Earlier Virus Detection. ACS Chem Neurosci 11, 1200-1203, 2020, doi:10.1021/acschemneuro.0c00172.
8) Cai Q, Yang M, Liu D, Chen J, Shu D, Xia J, Liao X, Gu Y, Cai Q, Yang Y, Shen C, Li X, Peng L, Huang D, Zhang J, Zhang S, Wang F, Liu J, Chen L, Chen S, Wang Z, Zhang Z, Cao R, Zhong W, Liu Y, Liu L. Experimental Treatment with Favipiravir for COVID-19: An Open-Label Control Study. Engineering, 2020, doi:https://doi.org/10.1016/j.eng.2020.03.007.
9) Caly L, Druce JD, Catton MG, Jans DA, Wagstaff KM. The FDA-approved drug ivermectin inhibits the replication of SARS-CoV-2 in vitro. Antiviral Res 178, 104787, 2020, doi:10.1016/j.antiviral.2020.104787.
10) Cave AJE. The evidence for the incidence of tuberculosis in ancient Egypt. British

Journal of Tuberculosis 33, 142-152, 1933, doi:10.1016/S0366-0850(39)80016-3.
11) Center for Disease Control. Detailed Disinfection Guidance in Coronavirus Disease 2019. https://www.cdc.gov/coronavirus/2019-ncov/prevent-getting-sick/cleaning-disinfection.html (accessed 01 June 2020) 2020.
12) Center for Disease Control. 2009 H1N1 pandemic timeline. https://www.cdc.gov/flu/pandemic-resources/2009-pandemic-timeline.html. (accessed 01 June 2020) 2020.
13) Center for Disease Control. Handwashing: Clean Hands Save Lives. https://www.cdc.gov/handwashing/index.html. (accessed 17 May 2020) 2020.
14) Chan JF, Yip CC, To KK, Tang TH, Wong SC, Leung KH, Fung AY, Ng AC, Zou Z, Tsoi HW, Choi GK, Tam AR, Cheng VC, Chan KH, Tsang OT, Yuen KY. Improved Molecular Diagnosis of COVID-19 by the Novel, Highly Sensitive and Specific COVID-19-RdRp/Hel Real-Time Reverse Transcription-PCR Assay Validated In Vitro and with Clinical Specimens. J Clin Microbiol, 2020, doi:10.1128/JCM.00310-20.
15) Chan JF, Yuan S, Kok KH, To KK, Chu H, Yang J, Xing F, Liu J, Yip CC, Poon RW, Tsoi HW, Lo SK, Chan KH, Poon VK, Chan WM, Ip JD, Cai JP, Cheng VC, Chen H, Hui CK, Yuen KY. A familial cluster of pneumonia associated with the 2019 novel coronavirus indicating person-to-person transmission: a study of a family cluster. Lancet 395, 514-523, 2020, doi:10.1016/S0140-6736(20)30154-9.
16) Chen Z, Pei D, Jiang L, Song Y, Wang J, Wang H, Zhou D, Zhai J, Du Z, Li B, Qiu M, Han Y, Guo Z, Yang R. Antigenicity analysis of different regions of the severe acute respiratory syndrome coronavirus nucleocapsid protein. Clin Chem 50, 988-995, 2004, doi:10.1373/clinchem.2004.031096.
17) Chinazzi M, Davis JT, Ajelli M, Gioannini C, Litvinova M, Merler S, Pastore YPA, Mu K, Rossi L, Sun K, Viboud C, Xiong X, Yu H, Halloran ME, Longini IM, Jr., Vespignani A. The effect of travel restrictions on the spread of the 2019 novel coronavirus (COVID-19) outbreak. Science 368, 395-400, 2020, doi:10.1126/science.aba9757.
18) Corman VM, Landt O, Kaiser M, Molenkamp R, Meijer A, Chu DK, Bleicker T, Brunink S, Schneider J, Schmidt ML, Mulders DG, Haagmans BL, van der Veer B, van den Brink S, Wijsman L, Goderski G, Romette JL, Ellis J, Zambon M, Peiris M, Goossens H, Reusken C, Koopmans MP, Drosten C. Detection of 2019 novel coronavirus (2019-nCoV) by real-time RT-PCR. Euro Surveill, 2020, doi:10.2807/1560-7917.ES.2020.25.3.2000045.
19) Coronaviridae Study Group of the International Committee on Taxonomy of V. The species Severe acute respiratory syndrome-related coronavirus: classifying 2019-nCoV and naming it SARS-CoV-2. Nat Microbiol 5, 536-544, 2020, doi:10.1038/s41564-020-0695-z.
20) Cucinotta D, Vanelli M. WHO Declares COVID-19 a Pandemic. Acta Biomed 91, 157-160, 2020, doi:10.23750/abm.v91i1.9397.
21) Davenne E, Giot JB, Huynen P. Coronavirus and COVID-19 : focus on a galopping pandemic (in French). Rev Med Liege 75, 218-225, 2020.
22) DeBaun B. Looking Forward-Infection Prevention in 2017. AORN J 104, 531-535, 2016, doi:10.1016/j.aorn.2016.09.016.
23) Ebrahim SH, Memish ZA. COVID-19 - the role of mass gatherings. Travel Med Infect Dis 34, 101617, 2020, doi:10.1016/j.tmaid.2020.101617.
24) Fan W, Su Z, Bin Y, Yan-Mei C, Wen W, Yi H, Zhi-Gang S, Tao. Z-W, Jun-Hua T, Yuan-Yuan P, Ming-Li Y, Fa-Hui D, Yi L, Qi-Min W, Jiao-Jiao Z, Lin X, Edward CH, Yong-Zhen Z. Complete genome characterization of a novel coronavirus associated with severe human respiractory disease in Wuhan, China. bioRxiv, 2020, doi:doi.org/10.1101/2020.01.24.919183.

25) Fathizadeh H, Maroufi P, Momen-Heravi M, Dao S, Kose S, Ganbarov K, Pagliano P, Esposito S, Kafil HS. Protection and disinfection policies against SARS-CoV-2 (COVID-19). Infez Med 28, 185-191, 2020.
26) Fauver JR, Petrone ME, Hodcroft EB, Shioda K, Ehrlich HY, Watts AG, Vogels CBF, Brito AF, Alpert T, Muyombwe A, Razeq J, Downing R, Cheemarla NR, Wyllie AL, Kalinich CC, Ott IM, Quick J, Loman NJ, Neugebauer KM, Greninger AL, Jerome KR, Roychoudhury P, Xie H, Shrestha L, Huang ML, Pitzer VE, Iwasaki A, Omer SB, Khan K, Bogoch, II, Martinello RA, Foxman EF, Landry ML, Neher RA, Ko AI, Grubaugh ND. Coast-to-Coast Spread of SARS-CoV-2 during the Early Epidemic in the United States. Cell 181, 990-996, 2020, doi:10.1016/j.cell.2020.04.021.
27) Fehr AR, Perlman S. Coronaviruses: an overview of their replication and pathogenesis. Methods Mol Biol 1282, 1-23, 2015, doi:10.1007/978-1-4939-2438-7_1.
28) Food and Drug Administration. Emergency Use Authorizations. https://www.fda.gov/medical-devices/emergency-situations-medical-devices/emergency-use-authorizations#covid19ivd. (accessed 01 June 2020) 2020.
29) Furuta Y, Komeno T, Nakamura T. Favipiravir (T-705), a broad spectrum inhibitor of viral RNA polymerase. Proc Jpn Acad Ser B Phys Biol Sci 93, 449-463, 2017, doi:10.2183/pjab.93.027.
30) Gautier JF, Ravussin Y. A New Symptom of COVID-19: Loss of Taste and Smell. Obesity (Silver Spring) 28, 848, 2020, doi:10.1002/oby.22809.
31) Geller C, Varbanov M, Duval RE. Human coronaviruses: insights into environmental resistance and its influence on the development of new antiseptic strategies. Viruses 4, 3044-3068, 2012, doi:10.3390/v4113044.
32) Guo L, Ren L, Yang S, Xiao M, Chang, Yang F, Dela Cruz CS, Wang Y, Wu C, Xiao Y, Zhang L, Han L, Dang S, Xu Y, Yang Q, Xu S, Zhu H, Xu Y, Jin Q, Sharma L, Wang L, Wang J. Profiling Early Humoral Response to Diagnose Novel Coronavirus Disease (COVID-19). Clin Infect Dis, 2020, doi:10.1093/cid/ciaa310.
33) Halfmann PJ, Hatta M, Chiba S, Maemura T, Fan S, Takeda M, Kinoshita N, Hattori SI, Sakai-Tagawa Y, Iwatsuki-Horimoto K, Imai M, Kawaoka Y. Transmission of SARS-CoV-2 in Domestic Cats. N Engl J Med, 2020, doi:10.1056/NEJMc2013400.
34) Han C, Duan C, Zhang S, Spiegel B, Shi H, Wang W, Zhang L, Lin R, Liu J, Ding Z, Hou X. Digestive Symptoms in COVID-19 Patients With Mild Disease Severity: Clinical Presentation, Stool Viral RNA Testing, and Outcomes. Am J Gastroenterol, 2020, doi:10.14309/ajg.0000000000000664.
35) Henderson LA, Canna SW, Schulert GS, Volpi S, Lee PY, Kernan KF, Caricchio R, Mahmud S, Hazen MM, Halyabar O, Hoyt KJ, Han J, Grom AA, Gattorno M, Ravelli A, De Benedetti F, Behrens EM, Cron RQ, Nigrovic PA. On the Alert for Cytokine Storm: Immunopathology in COVID-19. Arthritis Rheumatol, 2020, doi:10.1002/art.41285.
36) Hoffmann M, Kleine-Weber H, Schroeder S, Kruger N, Herrler T, Erichsen S, Schiergens TS, Herrler G, Wu NH, Nitsche A, Muller MA, Drosten C, Pohlmann S. SARS-CoV-2 Cell Entry Depends on ACE2 and TMPRSS2 and Is Blocked by a Clinically Proven Protease Inhibitor. Cell 181, 271-280, 2020, doi:10.1016/j.cell.2020.02.052.
37) Holshue ML, DeBolt C, Lindquist S, Lofy KH, Wiesman J, Bruce H, Spitters C, Ericson K, Wilkerson S, Tural A, Diaz G, Cohn A, Fox L, Patel A, Gerber SI, Kim L, Tong S, Lu X, Lindstrom S, Pallansch MA, Weldon WC, Biggs HM, Uyeki TM, Pillai SK, Washington State -nCoV Case Investigation Team. First Case of 2019 Novel Coronavirus in the United States. N Engl J Med 382, 929-936, 2020,

doi:10.1056/NEJMoa2001191.
38) Huang C, Wang Y, Li X, Ren L, Zhao J, Hu Y, Zhang L, Fan G, Xu J, Gu X, Cheng Z, Yu T, Xia J, Wei Y, Wu W, Xie X, Yin W, Li H, Liu M, Xiao Y, Gao H, Guo L, Xie J, Wang G, Jiang R, Gao Z, Jin Q, Wang J, Cao B. Clinical features of patients infected with 2019 novel coronavirus in Wuhan, China. Lancet 395, 497-506, 2020, doi:10.1016/S0140-6736(20)30183-5.
39) Jeng MJ. COVID-19 in children: Current status. J Chin Med Assoc, 2020, doi:10.1097/JCMA.0000000000000323.
40) Coronavirus Resource Center of Johns Hopkins University Medicine. World map. https://coronavirus.jhu.edu/map.html. (accessed 01 June 2020) 2020.
41) Kampf G, Todt D, Pfaender S, Steinmann E. Persistence of coronaviruses on inanimate surfaces and their inactivation with biocidal agents. J Hosp Infect 104, 246-251, 2020, doi:10.1016/j.jhin.2020.01.022.
42) Lai MM, Cavanagh D. The molecular biology of coronaviruses. Adv Virus Res 48, 1-100, 1997, doi:10.1016/S0065-3527(06)66005-3.
43) Lake MA. What we know so far: COVID-19 current clinical knowledge and research. Clin Med (Lond) 20, 124-127, 2020, doi:10.7861/clinmed.2019-coron.
44) Lei J, Li J, Li X, Qi X. CT Imaging of the 2019 Novel Coronavirus (2019-nCoV) Pneumonia. Radiology 295, 18, 2020, doi:10.1148/radiol.2020200236.
45) Leung NHL, Chu DKW, Shiu EYC, Chan KH, McDevitt JJ, Hau BJP, Yen HL, Li Y, Ip DKM, Peiris JSM, Seto WH, Leung GM, Milton DK, Cowling BJ. Respiratory virus shedding in exhaled breath and efficacy of face masks. Nat Med 26, 676-680, 2020, doi:10.1038/s41591-020-0843-2.
46) Li Z, Yi Y, Luo X, Xiong N, Liu Y, Li S, Sun R, Wang Y, Hu B, Chen W, Zhang Y, Wang J, Huang B, Lin Y, Yang J, Cai W, Wang X, Cheng J, Chen Z, Sun K, Pan W, Zhan Z, Chen L, Ye F. Development and clinical application of a rapid IgM-IgG combined antibody test for SARS-CoV-2 infection diagnosis. J Med Virol, 2020, doi:10.1002/jmv.25727.
47) Liu Y, Liu Y, Diao B, Ren F, Wang Y, Ding J, Huang Q. Diagnostic Indexes of a Rapid IgG/IgM Combined Antibody Test for SARS-CoV-2. medRxiv, 2020, doi:10.1101/2020.03.26.20044883.
48) London School of Hygiene and Tropical Medicine. COVID-19 vaccine development pipeline. https://vac-lshtm.shinyapps.io/ncov_vaccine_landscape/ (accessed 01 June 2020) 2020.
49) Ma QX, Shan H, Zhang HL, Li GM, Yang RM, Chen JM. Potential utilities of mask-wearing and instant hand hygiene for fighting SARS-CoV-2. J Med Virol, 2020, doi:10.1002/jmv.25805.
50) MacIntyre CR, Chughtai AA. Facemasks for the prevention of infection in healthcare and community settings. BMJ 350, h694, 2015, doi:10.1136/bmj.h694.
51) Molina JM, Delaugerre C, Le Goff J, Mela-Lima B, Ponscarme D, Goldwirt L, de Castro N. No evidence of rapid antiviral clearance or clinical benefit with the combination of hydroxychloroquine and azithromycin in patients with severe COVID-19 infection. Med Mal Infect 50, 384, 2020, doi:10.1016/j.medmal.2020.03.006.
52) Monteil V, Kwon H, Prado P, Hagelkruys A, Wimmer RA, Stahl M, Leopoldi A, Garreta E, Hurtado Del Pozo C, Prosper F, Romero JP, Wirnsberger G, Zhang H, Slutsky AS, Conder R, Montserrat N, Mirazimi A, Penninger JM. Inhibition of SARS-CoV-2 Infections in Engineered Human Tissues Using Clinical-Grade Soluble Human ACE2. Cell 181, 905-913 e907, 2020, doi:10.1016/j.cell.2020.04.004.
53) National Institute of Health, U.S. Clinical Trials. https://clinicaltrials.gov/ct2/results?cond=COVID-19 (accessed 01 June 2020) 2020.
54) Nikkei Asian Review. Taiwan's battle against

coronavirus began in late 2019. https://asia.nikkei.com/Spotlight/Coronavirus/Taiwan-s-battle-against-coronavirus-began-in-late-2019 (accessed 8 April 2020) 2020.

55) University of Oxford. Oxford COVID-19 vaccine begins human trial stage. httpps://oxfordbrc.nihr.ac.uk/okford-covid-19-vaccine-begins-human-trial-stage/ (accessed 17 May 2020) 2020.

56) Pan Y, Zhang D, Yang P, Poon LLM, Wang Q. Viral load of SARS-CoV-2 in clinical samples. Lancet Infect Dis 20, 411-412, 2020, doi:10.1016/S1473-3099(20)30113-4.

57) Paraskevis D, Kostaki EG, Magiorkinis G, Panayiotakopoulos G, Sourvinos G, Tsiodras S. Full-genome evolutionary analysis of the novel corona virus (2019-nCoV) rejects the hypothesis of emergence as a result of a recent recombination event. Infect Genet Evol 79, 104212, 2020, doi:10.1016/j.meegid.2020.104212.

58) Prentice MB, Rahalison L. Plague. Lancet 369, 1196-1207, 2007, doi:10.1016/S0140-6736(07)60566-2.

59) Price S, Singh S, Ledot S, Bianchi P, Hind M, Tavazzi G, Vranckx P. Respiratory management in severe acute respiratory syndrome coronavirus 2 infection. Eur Heart J Acute Cardiovasc Care 9 229-238, 2020, doi:10.1177/2048872620924613.

60) Qian X, Ren R, Wang Y, Guo Y, Fang J, Wu ZD, Liu PL, Han TR. Members of Steering Committee SoGHCPMA. Fighting against the common enemy of COVID-19: a practice of building a community with a shared future for mankind. Infect Dis Poverty 9, 34, 2020, doi:10.1186/s40249-020-00650-1.

61) Rockx B, Kuiken T, Herfst S, Bestebroer T, Lamers MM, Oude Munnink BB, de Meulder D, van Amerongen G, van den Brand J, Okba NMA, Schipper D, van Run P, Leijten L, Sikkema R, Verschoor E, Verstrepen B, Bogers W, Langermans J, Drosten C, Fentener van Vlissingen M, Fouchier R, de Swart R, Koopmans M, Haagmans BL. Comparative pathogenesis of COVID-19, MERS, and SARS in a nonhuman primate model. Science, 2020, doi:10.1126/science.abb7314.

62) Rothe C, Schunk M, Sothmann P, Bretzel G, Froeschl G, Wallrauch C, Zimmer T, Thiel V, Janke C, Guggemos W, Seilmaier M, Drosten C, Vollmar P, Zwirglmaier K, Zange S, Wolfel R, Hoelscher M. Transmission of 2019-nCoV Infection from an Asymptomatic Contact in Germany. N Engl J Med 382, 970-971, 2020, doi:10.1056/NEJMc2001468.

63) Sahu KK, Mishra AK, Lal A. COVID-2019: update on epidemiology, disease spread and management. Monaldi Arch Chest Dis, 2020, doi:10.4081/monaldi.2020.1292.

64) Shi H, Han X, Jiang N, Cao Y, Alwalid O, Gu J, Fan Y, Zheng C. Radiological findings from 81 patients with COVID-19 pneumonia in Wuhan, China: a descriptive study. Lancet Infect Dis 20, 425-434, 2020, doi:10.1016/S1473-3099(20)30086-4.

65) Shi J, Wen Z, Zhong G, Yang H, Wang C, Huang B, Liu R, He X, Shuai L, Sun Z, Zhao Y, Liu P, Liang L, Cui P, Wang J, Zhang X, Guan Y, Tan W, Wu G, Chen H, Bu Z. Susceptibility of ferrets, cats, dogs, and other domesticated animals to SARS-coronavirus 2. Science, 2020, doi:10.1126/science.abb7015.

66) Sit THC, Brackman CJ, Ip SM, Tam KWS, Law PYT, To EMW, Yu VYT, Sims LD, Tsang DNC, Chu DKW, Perera R, Poon LLM, Peiris M. Infection of dogs with SARS-CoV-2. Nature, 2020, doi:10.1038/s41586-020-2334-5.

67) Smith TRF, Patel A, Ramos S, Elwood D, Zhu X, Yan J, Gary EN, Walker SN, Schultheis K, Purwar M, Xu Z, Walters J, Bhojnagarwala P, Yang M, Chokkalingam N, Pezzoli P, Parzych E, Reuschel EL, Doan A, Tursi N, Vasquez M, Choi J, Tello-Ruiz E, Maricic I, Bah MA, Wu Y, Amante D, Park DH, Dia Y, Ali AR, Zaidi FI, Generotti A, Kim KY, Herring TA, Reeder S, Andrade VM, Buttigieg K, Zhao G, Wu JM, Li D, Bao L, Liu J, Deng W, Qin C, Brown AS, Khoshnejad M, Wang N, Chu J, Wrapp D, McLellan JS, Muthumani K, Wang B, Carroll

MW, Kim JJ, Boyer J, Kulp DW, Humeau L, Weiner DB, Broderick KE. Immunogenicity of a DNA vaccine candidate for COVID-19. Nat Commun 11, 2601, 2020, doi:10.1038/s41467-020-16505-0.

68) Song JY, Yun JG, Noh JY, Cheong HJ, Kim WJ. Covid-19 in South Korea - Challenges of Subclinical Manifestations. N Engl J Med 382, 1858-1859, 2020, doi:10.1056/NEJMc2001801.

69) South China Morning Post. Coronavirus: after Singapore and Taiwan close borders, calls for Hong Kong to do the same. https://www.scmp.com/news/hong-kong/health-environment/article/3076348/coronavirus-after-singapore-and-taiwan-close. (accessed 22 March 2020) 2020.

70) SouthChina Morning Post. Wuhan pneumonia: Thailand confirms first case of virus outside China. https://www.scmp.com/news/hong-kong/health-environment/article/3045902/wuhan-pneumonia-thailand-confirms-first-case. (accessed 13 January 2020) 2020.

71) The Straits Times. Japan confirms first case of infection from Wuhan coronavirus; Vietnam quarantines two tourists. https://www.straitstimes.com/asia/east-asia/japan-confirms-first-case-of-infection-with-new-china-coronavirus. (accessed 16 January 2020) 2020.

72) Su S, Wong G, Shi W, Liu J, Lai ACK, Zhou J, Liu W, Bi Y, Gao GF. Epidemiology, Genetic Recombination, and Pathogenesis of Coronaviruses. Trends Microbiol 24, 490-502, 2016, doi:10.1016/j.tim.2016.03.003.

73) Taubenberger JK, Morens DM. 1918 Influenza: the mother of all pandemics. Emerg Infect Dis 12, 15-22, 2006, doi:10.3201/eid1201.050979.

74) Tian Y, Rong L, Nian W, He Y. Review article: gastrointestinal features in COVID-19 and the possibility of faecal transmission. Aliment Pharmacol Ther 51, 843-851, 2020, doi:10.1111/apt.15731.

75) Tyrrell DA, Bynoe ML. Cultivation of a Novel Type of Common-Cold Virus in Organ Cultures. Br Med J 1, 1467-1470, 1965, doi:10.1136/bmj.1.5448.1467.

76) van Doremalen N, Bushmaker T, Morris DH, Holbrook MG, Gamble A, Williamson BN, Tamin A, Harcourt JL, Thornburg NJ, Gerber SI, Lloyd-Smith JO, de Wit E, Munster VJ. Aerosol and Surface Stability of SARS-CoV-2 as Compared with SARS-CoV-1. N Engl J Med 382, 1564-1567, 2020, doi:10.1056/NEJMc2004973.

77) Wagstaff KM, Sivakumaran H, Heaton SM, Harrich D, Jans DA. Ivermectin is a specific inhibitor of importin alpha/beta-mediated nuclear import able to inhibit replication of HIV-1 and dengue virus. Biochem J 443, 851-856, 2012, doi:10.1042/BJ20120150.

78) Wahba L, Jain N, Fire AZ, Shoura MJ, Artiles KL, McCoy MJ, Jeong DE. An Extensive Meta-Metagenomic Search Identifies SARS-CoV-2-Homologous Sequences in Pangolin Lung Viromes. mSphere, 2020, doi:10.1128/mSphere.00160-20.

79) Wang F, Kream RM, Stefano GB. An Evidence Based Perspective on mRNA-SARS-CoV-2 Vaccine Development. Med Sci Monit 26, e924700, 2020, doi:10.12659/MSM.924700.

80) Wilder-Smith A, Chiew CJ, Lee VJ. Can we contain the COVID-19 outbreak with the same measures as for SARS? Lancet Infect Dis 20, e102-e107, 2020, doi:10.1016/S1473-3099(20)30129-8.

81) Wilder-Smith A, Freedman DO. Isolation, quarantine, social distancing and community containment: pivotal role for old-style public health measures in the novel coronavirus (2019-nCoV) outbreak. J Travel Med, 2020, doi:10.1093/jtm/taaa020.

82) Wilson ME, Chen LH. Travellers give wings to novel coronavirus (2019-nCoV). J Travel Med, 2020, doi:10.1093/jtm/taaa015.

83) Wolfel R, Corman VM, Guggemos W, Seilmaier M, Zange S, Muller MA, Niemeyer D, Jones TC, Vollmar P, Rothe C, Hoelscher

M, Bleicker T, Brunink S, Schneider J, Ehmann R, Zwirglmaier K, Drosten C, Wendtner C. Virological assessment of hospitalized patients with COVID-2019. Nature, 2020, doi:10.1038/s41586-020-2196-x.

84) World Health Organization. Novel Coronavirus (2019-nCoV): Situation Report-22. https://www.who.int/docs/default-source/coronaviruse/situation-reports/20200211-sitrep-22-ncov.pdf?sfvrsn=fb6d49b1_2. (accessed 01 June 2020) 2020.
85) World Health Organization. Coronavirus disease (COVID-19) advice for the public. https://www.who.int/emergencies/diseases/novel-coronavirus-2019/advice-for-public (accessed 01 June 2020) 2020.
86) World Health Organization. Pneumonia of unknown cause - China. https://www.who.int/csr/don/05-january-2020-pneumonia-of-unkown-cause-china/en/. (accessed 05 January 2020) 2020.
87) World Health Organization. Novel Coronavirus (2019-nCoV): Situation Report-73. https://www.who.int/docs/default-source/coronaviruse/situation-reports/20200402-sitrep-73-covid-19.pdf?sfvrsn=5ae25bc7_6. (accessed 01 June 2020) 2020.
88) World Health Organization. Summary of probable SARS cases with onset of illness from 1 November 2002 to 31 July 2003. https://www.who.int/csr/sars/country/table2004_04_21/en/. (accessed 01 June 2020) 2020.
89) World Health Organization. Middle East Respiratory Syndrome coronavirus. https://www.who.int/en/news-room/fact-sheets/detail/middle-east-respiratory-syndrome-coronavirus-(mers-cov). (accessed 01 June 2020) 2020.
90) World Health Organization. Novel Coronavirus(2019-nCoV): Situation Report-4. https://www.who.int/docs/default-source/coronaviruse/situation-reports/20200124-sitrep-4-2019-ncov.pdf?sfvrsn=9272d086_8. (accessed 01 June 2020) 2020.
91) World Health Organization. Ebola virus disease. https://www.who.int/csr/disease/ebola/en/. (accessed 01 June 2020) 2020.
92) World Health Organization. Advice on the use of masks in the context of COVID-19: interim guidance, 6 April 2020. https://apps.who.int/iris/handle/10665/331693. (accessed 01 June 2020) 2020.
93) World Organisation for Animal Health (OIE). SARS-CoV-2/COVID-19, United States of America. https://www.oie.int/wahis_2/public/wahid.php/Reviewreport/Review?page_refer=MapFullEventReport&reportid=33885. (accessed 01 June 2020) 2020.
94) Wu F, Zhao S, Yu B, Chen YM, Wang W, Song ZG, Hu Y, Tao ZW, Tian JH, Pei YY, Yuan ML, Zhang YL, Dai FH, Liu Y, Wang QM, Zheng JJ, Xu L, Holmes EC, Zhang YZ. A new coronavirus associated with human respiratory disease in China. Nature 579, 265-269, 2020, doi:10.1038/s41586-020-2008-3.
95) Xiao Y, Torok ME. Taking the right measures to control COVID-19. Lancet Infect Dis 20, 523-524, 2020, doi:10.1016/S1473-3099(20)30152-3.
96) Ye Q, Wang B, Mao J. The pathogenesis and treatment of the `Cytokine Storm' in COVID-19. J Infect 80, 607-613, 2020, doi:10.1016/j.jinf.2020.03.037.
97) Yeo C, Kaushal S, Yeo D. Enteric involvement of coronaviruses: is faecal-oral transmission of SARS-CoV-2 possible? Lancet Gastroenterol Hepatol 5, 335-337, 2020, doi:10.1016/S2468-1253(20)30048-0.
98) Yong Z, Cao C, Shuangli Z, Chang S, Dongyan W, Jingdong S, Yang S, Wei Z, Zijian F, guizhen W, Jun X, Wenbo X. Isolation of 2019-nCoV from a stool specimen of a laboratory-confirmed case of the coronavirus disease 2019 (COVID-19). China CDC Weekly 2, 123-124, 2020.
99) Yu F, Yan L, Wang N, Yang S, Wang L, Tang Y, Gao G, Wang S, Ma C, Xie R, Wang F, Tan C, Zhu L, Guo Y, Zhang F. Quantitative Detection and Viral Load Analysis of SARS-

CoV-2 in Infected Patients. Clin Infect Dis, 2020, doi:10.1093/cid/ciaa345.

100) Zhang C, Zheng W, Huang X, Bell EW, Zhou X, Zhang Y. Protein Structure and Sequence Reanalysis of 2019-nCoV Genome Refutes Snakes as Its Intermediate Host and the Unique Similarity between Its Spike Protein Insertions and HIV-1. J Proteome Res 19, 1351-1360, 2020, doi:10.1021/acs.jproteome.0c00129.

101) Zhang P, Gao Q, T. W, Ke Y, Mo F, Jia R, Liu W, Liu L, Zheng S, Liu Y, Li L, Wang Y, Xu L, Hao K, Yang RM, Li S, Lin C, Zhao Y. Evaluation of recombinant nucleocapsid and spike proteins for serological diagnosis of novel coronavirus disease 2019 (COVID-19). 2020, doi:10.1101/2020.03.17.20036954.

102) Zhang T, Wu Q, Zhang Z. Probable Pangolin Origin of SARS-CoV-2 Associated with the COVID-19 Outbreak. Curr Biol 30, 1346-1351 e1342, 2020, doi:10.1016/j.cub.2020.03.022.

103) Zhang W, Du RH, Li B, Zheng XS, Yang XL, Hu B, Wang YY, Xiao GF, Yan B, Shi ZL, Zhou P. Molecular and serological investigation of 2019-nCoV infected patients: implication of multiple shedding routes. Emerg Microbes Infect 9, 386-389, 2020, doi:10.1080/22221751.2020.1729071.

104) Zhou P, Yang XL, Wang XG, Hu B, Zhang L, Zhang W, Si HR, Zhu Y, Li B, Huang CL, Chen HD, Chen J, Luo Y, Guo H, Jiang RD, Liu MQ, Chen Y, Shen XR, Wang X, Zheng XS, Zhao K, Chen QJ, Deng F, Liu LL, Yan B, Zhan FX, Wang YY, Xiao GF, Shi ZL. A pneumonia outbreak associated with a new coronavirus of probable bat origin. Nature 579, 270-273, 2020, doi:10.1038/s41586-020-2012-7.

105) Zhu N, Zhang D, Wang W, Li X, Yang B, Song J, Zhao X, Huang B, Shi W, Lu R, Niu P, Zhan F, Ma X, Wang D, Xu W, Wu G, Gao GF, Tan W, China Novel Coronavirus Investigating and Research Team. A Novel Coronavirus from Patients with Pneumonia in China, 2019. N Engl J Med 382, 727-733, 2020, doi:10.1056/NEJMoa2001017.

106) Zimmerman MR. Pulmonary and osseous tuberculosis in an Egyptian mummy. Bull N Y Acad Med 55, 604-608, 1979.

107) Zou L, Ruan F, Huang M, Liang L, Huang H, Hong Z, Yu J, Kang M, Song Y, Xia J, Guo Q, Song T, He J, Yen HL, Peiris M, Wu J. SARS-CoV-2 Viral Load in Upper Respiratory Specimens of Infected Patients. N Engl J Med 382, 1177-1179, 2020, doi: 10.1056/NEJMc2001737.

Japanese Journal of Veterinary Research 68(3): 151-158, 2020

JJVR

REGULAR PAPER Experimental Research

The swab-sampled dry fecal cytology in healthy dogs and in dogs with acute and chronic diarrhea: a pilot study

Elena Benvenuti [1], Enrico Bottero [2], Alessio Pierini [1,*], Eleonora Gori [1] and Veronica Marchetti [1]

[1] Department of Veterinary Science, University of Pisa, via Livornese, San Piero a Grado, 56122 Pisa, Italy
[2] Associazione Professionale Endovet Italia, Turin, Italy

Received for publication, September 21, 2019; accepted, April 15, 2020

Abstract

Dry-mount fecal cytology is a little explored procedure that is potentially useful for dogs with gastrointestinal diseases. This study describes fecal cytology using swab sampling in healthy dogs (HD) and in dogs with acute and chronic diarrhea. Forty HD, 40 dogs with acute diarrhea (AD; diarrhea < 5 days) and 40 dogs with chronic diarrhea (CD; diarrhea > 3 weeks) were also enrolled. Sixteen different cytological features were scored for each fecal sample. Twenty HD were used to establish normal reference range for each cytological feature. Exact tests were used to evaluate associations between the three groups. The presence of red blood cells, cocci bacterial monomorphism and spore-forming bacteria were significantly higher in AD than the HD. Neutrophils, lymphocytes and macrophages were significantly higher in AD and CD groups compared to HD. Plasma cells were significantly higher in CD and the HD and AD groups. Bacterial phagocytosis was significantly higher in AD group than CD and HD. In conclusion, swab-sampled fecal cytology, as a cheap and feasible procedure, can be a useful diagnostic and monitoring technique. Although, our pilot study results showed differences between HD and enteropathic dogs, further investigations are necessary.

Key Words: canine, diarrhea, dry-mount fecal cytology, rectal swab

Introduction

Fecal cytology (FC) is used for fecal examination in dogs with gastrointestinal symptoms [2,9]. There are two types of FC: wet-mount FC and dry-mount fecal cytology (DFC). Wet-mount FC consists of the microscopic observation of a fresh stool smear, which ideally is less than five minutes old. Wet-mount FC is suitable for the detection of *Giardia* spp., trichomonides and amoebae, as well as larvae of nematodes (e.g., *Strongiloides* spp.) and bacteria such as *Campylobacter* spp. [2,4]. With DFC, the smear can be collected by various sampling methods [4] (e.g., rectal scraping, rectal lavage and digital examination) and then is air dried and stained. This method is useful for identifying infectious agents (e.g., *Prototheca* spp., *Cryptococcus* spp.), inflammatory or neoplastic cells, and for evaluating the cytological features of the intestinal microbiota [2,5,9,10].

In the DFC of healthy dogs (HD), an extremely polymorphic population of several different bacilli

* Corresponding author: Alessio Pierini, via Livornese, San Piero a Grado, 56122 Pisa, Italy
pierini.alessio2004@libero.it
doi: 10.14943/jjvr.68.3.151

Table 1. Scoring system for fecal cytological feature evaluation.

Cytological features	Power field	Category	
		Normal	Abnormal
Squamous cells	10×	<50	≥50
Columnar cells	10×	<20	≥20
Neutrophils	10×	<10	≥10
Eosinophils	10×	<5	≥5
Lymphocytes	10×	<10	≥10
Plasma cells	10×	<5	≥5
Macrophages	10×	<5	≥5
Immature lymphoid cells	10×	<10	≥10
Red blood cells	40×	Absent	Present
Cyniclomyces spp.	40×	<10	≥10
Yeasts	40×	<30	≥30
Presence of cocci bacterial monomorphism*	100×	Absent	Present
Gull-wing-shaped bacteria	100×	<5	≥5
Spiral-shaped bacteria	100×	<5	≥5
Spore-forming bacteria	100×	<5	≥5
Bacterial phagocytosis	100×	Absent	Present

For cytological features observed with a 10× magnification, all the smear was examined.
For cytological features observed with a 40× and 100× magnification, ten random fields were examined.
* More than 50% of cocci bacteria

is typically observed [4]. There should be fewer than five spore-forming rods/100× field, and cocci should be rare or absent [2,4,11]. Occasionally, a low number of individual or doublet *Cyniclomyces* spp. may be observed, but its real pathogenic power is still unclear [4,6,11]. A monomorphic or oligomorphic bacterial population, an increased number of cocci or an increased amount of yeast (e.g., *Candida*, *Cyniclomyces* spp.) are found in dysbiosis [11]. The presence of neutrophils is abnormal and may be associated with distal colitis or proctitis [2,11]. Fecal cytological patterns in HD have already been reported using several cytological sampling techniques [4]. In Frezoulis' study, FC features collected by various methods, including digital examination (DE), rectal scraping (RS) and rectal lavage (RL) in HD and dogs with diarrhea, are described. In HD, the median number of isolated epithelial cells and lymphocytes was higher when RS was used. This may be because RS is a more aggressive procedure compared to DE and RL, and may collect greater numbers of lymphocytes from the colic lymphoid follicles and columnar epithelial cells from the mucosa [4]. RS may be preferable when the deeper mucosal layers need to be sampled, such as for the diagnosis of colorectal lymphoma [4]. In dogs with diarrhea, the median cluster of epithelial cells and the number of neutrophils in fecal samples have been found to be different among sampling methods. In particular, the presence of clusters of epithelial cells and neutrophils have been shown to be more frequent in RS than in DE and RL [4].

Since there are no available data on swab-sampled DFC on both healthy dogs and dogs with acute and chronic diarrhea, the first aim is to describe swab-sampled DFC features in these populations. In addition, since our second hypothesis is that in dogs with acute and chronic diarrhea may have different various population of inflammatory cells one of each other and different compared to healthy dogs, the second aim is to evaluate potential differences in swab-sampled

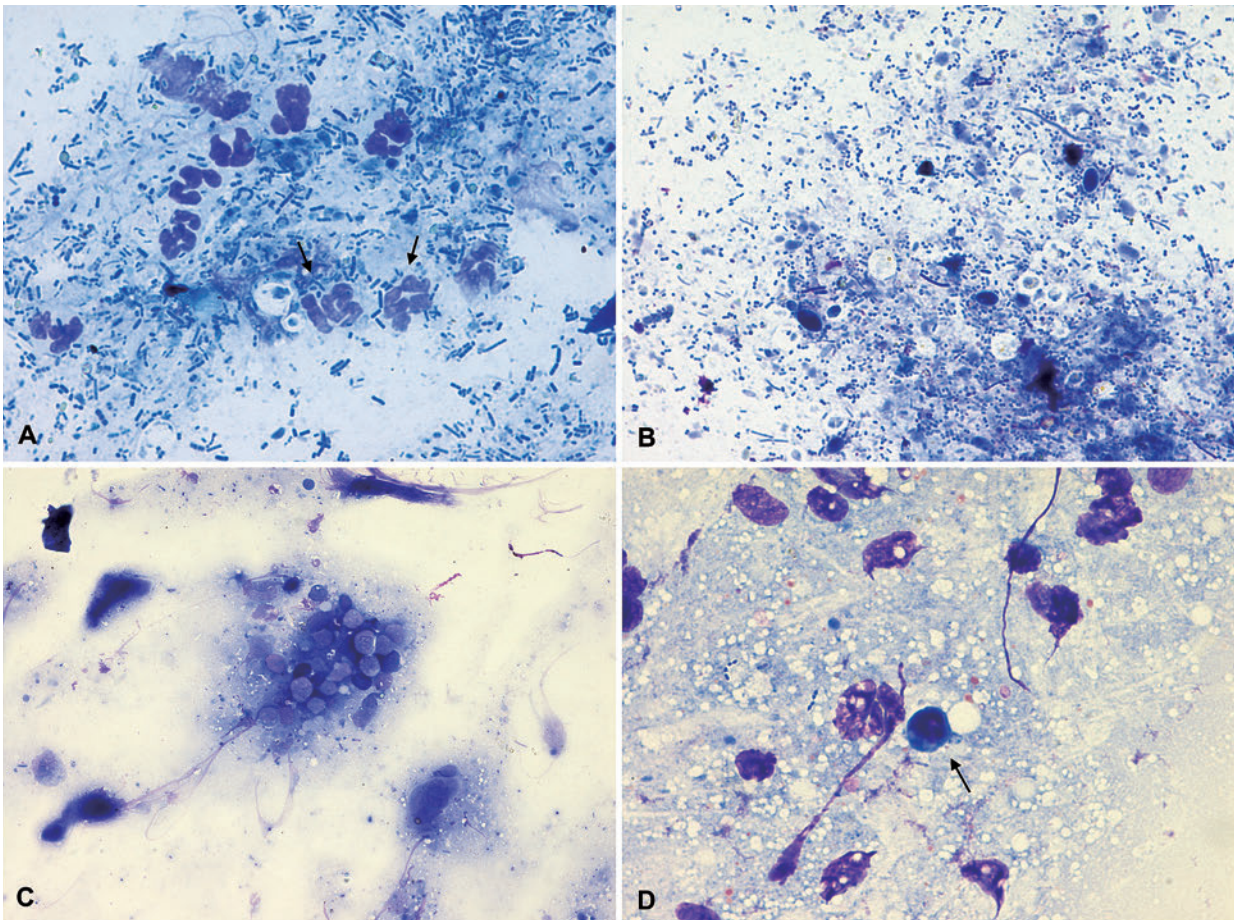

Fig. 1.
Dry-mount fecal cytology findings in canine acute (AD) and chronic diarrhea (CD). Diff Quik® stain. (a) Bacterial phagocytosis. An aggregate of some neutrophils in active phagocytosis (arrows) is present among the microbial flora of an AE dog. 100×, oil. (b) Cocci bacterial monomorphism in AD dog. Abnormal bacterial flora with cocci monomorphism. 100×, oil. (c) Lymphocytes. An aggregate of small lymphocytes from an CD dog. 40×. (d) Plasma cell. An isolated plasm cell in a pale basophilic background with some bacteria from a CD dog. 40×.

DFC between the three study populations.

Materials and Methods

Healthy dogs

Twenty HD were initially used to determine the reference range for each cytological feature (Table 1, column "normal"). A control group was recruited from HD identified during routine physical examination for vaccination. In all dogs, a DFC via rectal swab was performed. A plastic swab was moistened with sterile saline solution, inserted in the rectal ampulla with an inclination of 45° for 1 to 4 cm (according to the size of the patient), rotated on the mucosal surface for 4-5 times, extracted and rolled onto glass slides for cytology. The rectal swab was always performed by the same operator and only one smear for each patient was performed. All smears were stained with a Romanowsky stain (Diff Quik® Bio Optica Milano S.p.A.- Milan, Italy) and examined by a cytopathologist using a light-microscope (Leica DM LB Microscope, Leica Microsystems Srl, Milan, Italy). The highest number for each specific cytological feature detected in the first HD was used as the upper limit of the reference range for that cytological feature. Regarding *Cyniclomyces* spp. [6], gull-wing-shaped

bacteria [2,11], spiral-shaped bacteria [11] and yeasts [11], previously published reference ranges were used. All patients were evaluated using a scoring system established for 16 cytological features (Table 1). The entire smear was evaluated at 10× to estimate the amount of squamous and columnar cells, neutrophils, eosinophils, lymphocytes, plasma cells, macrophages and immature lymphoid cells. The *Cyniclomyces* spp. is a yeast and morphologically identified by its "spectacle case" shape; the length is approximately 1/5th of the diameter of a *Toxocara canis* egg [6]. Presence of red blood cells (RBCs) and number of *Cyniclomyces* spp. and other round-shape yeasts were assessed at 40× magnification in 10 random fields (Table 1). Presence of cocci or rod-shaped bacterial monomorphism and bacterial phagocytosis (Fig. 1-a) and the number of gull-wing-shaped bacteria, spiral-shaped bacteria and spore-forming bacteria were evaluated at 100× magnification in 10 random fields. Cocci bacterial monomorphism was evaluated when cocci exceeded 50% in 10 random fields. (Table 1; Fig. 1-b).

Dogs with acute and chronic diarrhea

Client-owned dogs were enrolled with a diagnosis of acute diarrhea (AD) and chronic diarrhea (CD) that had been referred to our internal medicine service. For each dog, signalment and clinical history were collected and signed informed consent was obtained from their owners. The AD group included dogs with a history of diarrhea for less than five days. The CD group included dogs with a history of diarrhea for at least three weeks. Each CD dog had a hematobiochemical profile, urinalysis, fecal panel and diagnostic imaging performed as a part of routine care. In CD dogs other extra-intestinal diseases, infectious or parasitic diseases and intestinal disease of other etiology (e.g., mechanical obstruction from intussusception, foreign body or intestinal tumors) were ruled out. In all patients, FC was performed at admission or at the time of endoscopy before anesthesia was induced. Dogs with positive fecal flotation or positive in-clinic Giardia test (SNAP® Giardia test, Idexx Laboratories Inc. Europe, Hoofddorp, Netherlands) were excluded. In both groups, administration of symptomatic treatment (spasmolytic, adsorbent, antiemetic or antacid drugs and probiotics) and fleas and tick preventive drugs were permitted. In the AD group, dogs already on antibiotic therapy were excluded. In the CD group, antibiotics, probiotics and immunosuppressive drugs had to have been discontinued at least ten days before the endoscopy. Each dog in CD group had a final diagnosis of chronic lymphoplasmacytic enteritis confirmed at the histopathologic evaluation[3]. Dogs with intestinal lymphoma and with colorectal neoplasia were excluded.

Normal fecal cytological scores were obtained from the HD. The age of the three groups were tested with the D'Agostino Pearson normality test and then compared between the three groups using Kruskal-Wallis test. Fecal cytological features were compared between the three study populations using Chi-square test and then compared between the three pairs of groups (HD vs. AD, HD vs. CD, AD vs. CD) using Fisher's exact test [8]. A P-value < 0.05 was considered significant (GraphPad Prism 7 for Windows, La Jolla, CA).

Results

One hundred and twenty dogs were enrolled and divided into three groups. Forty dogs were included in the HD group, 40 in the AD, and 40 in the CD group. The median age for all dogs was six years (range 1-17 years) and was similar to the three study groups (HD, AD and CD; $P > 0.05$). Fifty-six female dogs (17 spayed) and 64 male dogs (4 neutered) were included in this study and distribution of sex and sexual status was similar between all groups.

Of the 120 dogs included in the study, 51 were mix-breed. The involved breeds were: German Sheperd (13), Labrador Retriever (6), English Setter (5), Cavalier King Charles Spaniel (4), Cocker Spaniel (4), Golden Retriever (3), Jack Russel Terrier (3), West Highland White Terrier

Table 2. Fecal cytological scores for each parameter observed in the three study groups.

Cytological parameters	HD	AD	CD	*P*-value
Presence of RBC	0/40 (0%) [A]	11/40 (27.5%) [B]	4/40 (10%) [A]	0.0008
Squamous cells	0/40 (0%)	0/40 (0%)	0/40 (0%)	NE
Columnar cells	0/40 (0%)	0/40 (0%)	0/40 (0%)	NE
Neutrophils	0/40 (0%) [A]	36/40 (90%) [B]	29/40 (72.5%) [B]	<0.0001
Eosinophils	0/40 (0%)	2/40 (5%)	2/40 (5%)	0.3554
Lymphocytes	0/40 (0%) [A]	7/40 (17.5%) [B]	14/40 (35%) [B]	0.0002
Plasma cells	0/40 (0%) [A]	3/40 (7.5%) [A]	14/40 (35%) [B]	<0.0001
Macrophages	1/40 (2.5%) [A]	9/40 (22.5%) [B]	12/40 (30%) [B]	0.004
Immature lymphoid cells	0/40 (0%)	1/40 (2.5%)	1/40 (2.5%)	0.6014
Cyniclomyces guttulatus	1/40 (2.5%)	1/40 (2.5%)	3/40 (7.5%)	0.4340
Yeasts	14/40 (35%)	12/40 (30%)	15/40 (37.5%)	0.7716
Presence of cocci bacterial monomorphism	0/40 (0%) [A]	12/40 (30%) [B]	4/40 (10%) [A]	0.0003
Gull-wing-shaped bacteria	0/40 (0%) [A]	5/40 (12.5%) [A]	0/40 (0%) [A]	0.0054
Spiral-shaped bacteria	0/40 (0%)	1/40 (2.5%)	1/40 (2.5%)	0.6014
Spore-forming bacteria	2/40 (5%) [A]	9/40 (22.5%) [B]	2/40 (5%) [A]	0.01
Bacterial phagocytosis	0/40 (0%) [A]	25/40 (62.5%) [B]	9/40 (22.5%) [C]	<0.0001

AD = acute diarrhea; CD = chronic diarrhea; HD = healthy dogs; NE = not evaluable; RBC = red blood cell. Fecal cytological scores for each feature were analyzed with Chi-square test between the three groups and if $P < 0.05$ was considered significant. A, B, C, two groups with different letters have a statistically significant difference in the post-hoc Fisher's exact test.

(2), Border Collie (2), Pug (2), Dogo Argentino (2), Shih tzu (2), Rottweiler (2), Poodle (2), Dogue de Bordeaux (2), Yorkshire Terrier (2), Dobermann Pinscher (1), Maremma Sheperd (1), Dalmatian dog (1), Hound (1), Briard (1), Chihuahua (1), Berger Blanc Suisse (1), Maltese (1), Dachshund (1), Beagle (1), Bull Terrier (1), Pinscher (1), Weimaraner (1).

Epithelial cells (squamous and columnar cells), eosinophils, immature lymphoid cells, *Cyniclomyces* spp., other yeasts and spiral-shaped bacteria showed no differences between the three groups, as showed in Table 2.

The presence of RBCs, neutrophils, lymphocytes, plasma cells, macrophages, cocci bacterial monomorphism, as well as gull-wing-shaped bacteria, spore-forming bacteria and bacterial phagocytosis were significantly different between the three groups (Table 2).

In the HD group, no inflammatory cells were observed, except for few macrophages in the sample from one dog. The samples from 35% of dogs in the HD group contained some yeasts, and *Cyniclomyces* spp. was identified in one case. Moreover, samples from two dogs contained increased spore-forming bacteria (Table 2).

The presence of RBCs, cocci bacterial monomorphism and spore-forming bacteria were significantly different between the HD and AD groups ($P = 0.0004$, $P = 0.0002$ and $P = 0.0476$, respectively). HD dogs had significantly different neutrophils, lymphocytes (Fig. 1-c) and macrophages both compared to AD ($P < 0.0001$, $P = 0.0117$, $P = 0.0143$, respectively) and CD groups ($P < 0.0001$, $P < 0.0001$ and $P = 0.0009$, respectively). Plasma cells were significantly different between CD and the HD and AD groups ($P < 0.0001$ and $P = 0.0052$, respectively; Fig. 1-d). Gull-wing-shaped bacteria and bacterial phagocytosis were significantly different between the three groups ($P = 0.0054$ and $P < 0.0001$, respectively). However, gull-wing-shaped bacteria scores were compared between pairs of groups and showed no significant differences. Bacterial phagocytosis scores were significantly different between the three groups (HD

vs AD $P < 0.0001$, HD vs CD $P = 0.0024$, AD vs CD $P = 0.0006$, respectively). Data regarding the scores of each individual cytological feature are shown in Table 2.

Discussion

Dry-mount fecal cytology is not commonly used in clinical practice. To date, few studies have described the technique and interpretation of results [2,4].

In the present study, RBCs and inflammatory cells were absent in HD. In a recent study on thirty-seven healthy dogs, neutrophils and lymphocytes were detected when fecal cytology was collected by DE and RS, however, when RL was used, no RBCs and inflammatory cells were identified in the sample [4]. These findings suggested that more aggressive procedures, such as DE and RS, can lead to falsely increased blood-derived cell levels, making the interpretation of results challenging. In the present study, fecal cytological samples were collected using a moistened plastic swab, which, in the authors' opinion, may be less traumatic than DE and RS, thus reducing the risk of over-diagnosing inflammatory disease or intestinal hemorrhage using FC. In our study, the presence of inflammatory cells in swab-sampled DFC was associated with an intestinal inflammatory condition. According to Mandigers et al., the presence of yeast is not associated to intestinal disease and both round-shape yeast and *Cyniclomyces* spp. can also be present in healthy dogs being its pathogenic role unclear [6].

According to the literature, pleomorphic bacteria (a mixture of cocci and rods) in HD can been seen. As previously reported, our data confirm the microbiota in healthy dogs is variable with a pleomorphic population, with the rod component being the largest [1].

In the present study, macrophages and spore-forming bacteria were detected only in one dog and two dogs of the HD group, respectively. This finding suggests that detection of a low number of macrophages and spore-forming bacteria should be interpreted with caution.

RBCs were significantly more frequently observed in the AD group. During acute enteropathies, RBCs are expected to be detected because hyperemia, inflammatory edema or direct damage of the colonic mucosa are usually present in such conditions [12]. However, in our study population cytologic signs of acute (erythrophagocytosis) or chronic hemorrhage (hemosiderin phagocytosis) were not present.

In our study, neutrophils, lymphocytes and macrophages were significantly increased in dogs with enteropathy compared to HD. Thirty-six out of 40 (90%) dogs in the AE group showed the presence of neutrophils, 25 out of 40 (60%) showed bacterial phagocytosis, and 30% showed cocci bacterial monomorphism. These data suggest the presence of an acute inflammation, besides the involvement of bacteria in the pathological process. With rectal cytology it is not possible to determine whether bacteria are the primary cause or a consequence of the pathological process [1]. In our opinion, it would be interesting to study the associations between bacterial phagocytosis, clinical (e.g., fever) and clinical pathological (e.g., leukocytosis or toxic neutrophils) findings to direct further laboratory investigations (e.g., PCR, specific fecal culture for pathogenic bacteria, immune-enzyme assays for bacterial toxins).

The presence of gull-wing-shaped bacteria was different between groups (Table 2). However, their presence only in the AD group suggests a possible infectious etiology which may be investigated with the laboratory investigation reported above.

In addition, the presence of increased number of spore-forming bacteria in the AD group might warrant further investigations (e.g., *Clostridium perfringens* enterotoxins) into the role of these bacteria in this subset of dogs with acute diarrhea [7].

The presence of small lymphocytes and macrophages was significantly associated with dogs with enteropathy, however the presence of plasma cells (35%) was the only cytological feature associated with CD. Chronic inflammatory

enteropathies are often characterized by the presence of a reactive proliferation of lymphocytes and plasma cells in the gastrointestinal mucosa and submucosa [3]. Regarding inflammatory cells, a previous study described findings in FC in dogs with diarrhea, but no differences were observed between chronic and acute disease [4]. In our case, the findings of plasma cells and bacterial phagocytosis were significantly different between the AD and CD groups.

These results highlight the importance for further studies about the utility of the DFC for the diagnostic work up in enteropathic dogs. This study has some limitations. Primarily, we did not evaluate the absolute number of cytological parameters, however a normal/abnormal basis was estimated from the fecal cytology of twenty healthy dogs. It is therefore not possible to obtain an absolute number in order to establish a ROC curve to determine the actual cut off for each parameter. Furthermore, some evaluations, such as cocci bacterial monomorphism, were a subjective estimation which may differ between cytopathologists. The lack of an etiopathological characterization of the enteropathies and particularly the lack of a clinical severity score, are further limitations of the present study, and therefore the real utility of DFC in clinical practice cannot be determined. On the other hand, since DFC is a cheap, fast and non-invasive procedure that can exclude some life-threating infectious agents (e.g., *Prototheca* spp.), this pilot study is the first step to evaluate the clinical and diagnostic value of DFC.

References

1) AlShawaqfeh MK, Wajid B, Minamoto Y, Markel M, Lidbury JA, Steiner JM, Serpedin E, Suchodolski JS. A dysbiosis index to assess microbial changes in fecal samples of dogs with chronic inflammatory enteropathy. FEMS Microbiol Ecol 93, 700, 2017.
2) Broussard JD. Optimal fecal assessment. Clin Tech Small Anim Pract 18, 218–230, 2003.
3) Day MJ, Bilzer T, Mansell J, Wilcock B, Hall EJ, Jergens A, Minami T, Willard M, Washabau R. World Small Animal Veterinary Association Gastrointestinal Standardization Group Histopathological standards for the diagnosis of gastrointestinal inflammation in endoscopic biopsy samples from the dog and cat: a report from the World Small Animal Veterinary Association Gastrointestinal Standardization Group. J Comp Pathol 138 Suppl 1, S1–43, 2008.
4) Frezoulis PS, Angelidou E, Diakou A, Rallis TS, Mylonakis ME. Optimization of fecal cytology in the dog: comparison of three sampling methods. J Vet Diagn Invest 29, 767–771, 2017.
5) Graves TK, Barger AM, Adams B, Krockenberger MB. Diagnosis of systemic cryptococcosis by fecal cytology in a dog. Vet Clin Pathol 34, 409–412, 2005.
6) Mandigers PJJ, Duijvestijn MBHM, Ankringa N, Maes S, van Essen E, Schoormans AHW, German AJ, Houwers DJ. The clinical significance of Cyniclomyces guttulatus in dogs with chronic diarrhoea, a survey and a prospective treatment study. Vet Microbiol 172, 241–247, 2014.
7) Marks SL, Rankin SC, Byrne BA, Weese JS. Enteropathogenic bacteria in dogs and cats: diagnosis, epidemiology, treatment, and control. J Vet Intern Med 25, 1195–1208, 2011.
8) Shan G, Gerstenberger S. Fisher's exact approach for post hoc analysis of a chi-squared test. PLoS One 12(12), 1–12, 2017.
9) Suchodolski JS. Laboratory approach: stomach and small intestine. In: Canine and Feline Gastroenterology, 1st ed. Washabau RJ, Day MJ. eds. Saunders: St. Louis, MO. pp.177–187, 2013.
10) Vince AR, Pinard C, Ogilvie AT, Tan EO, Abrams-Ogg ACG. Protothecosis in a dog. Canadian Veterinary Journal 55, 950–954, 2014.
11) Wamsley HL. Dry-mount fecal cytology. In:

Canine and Feline Cytology, 3rd ed. Raskin RE, Meyer DJ. eds. Saunders: St. Louis, MO. pp.215–225, 2010.
12) Washabau, RJ. Large intestine. In: Canine and Feline Gastroenterology, 1st ed. Washabau RJ, Day MJ. eds. Saunders: St. Louis, MO. pp.729-777, 2013.

Japanese Journal of Veterinary Research 68(3): 159-170, 2020

JJVR

REGULAR PAPER Experimental Research

Development of a highly sensitive method for the detection of Cryptosporidium parvum virus type 1 (CSpV1)

Ayman Ahmed Shehata[1,2], Hironori Bando[1], Yasuhiro Fukuda[1], Mohammad Hazzaz Bin Kabir[3,4], Fumi Murakoshi[5], Megumi Itoh[6], Atsushi Fujikura[7], Hiroaki Okawa[7], Takuto Endo[8], Akira Goto[9], Masayuki Kachi[10], Toshie Nakayama[11], Yuto Kano[12], Shoko Oishi[13], Konosuke Otomaru[13], Kei Kazama[14], Mohamed Ibrahim Essa[2] and Kentaro Kato[1,3,*]

[1]Laboratory of Sustainable Animal Environment, Graduate School of Agricultural Science, Tohoku University, 232-3 Yomogida, Naruko-onsen, Osaki, Miyagi 989-6711, Japan
[2]Department of Animal Medicine, Infectious Diseases, Faculty of Veterinary Medicine, Zagazig University, El-Shohada, Moawwad, Qesm Awel AZ Zagazig, 44511, Egypt
[3]National Research Center for Protozoan Diseases, Obihiro University of Agriculture and Veterinary Medicine, Inada-cho, Obihiro, Hokkaido 080-8555, Japan
[4]Department of Microbiology and Parasitology, Sher-e-Bangla Agricultural University, Sher-e-Bangla Nagar, Dhaka-1207, Bangladesh
[5]Department of Infectious Diseases, Kyoto Prefectural University of Medicine, 465, Kajiicho, Kawaramachi-hirokoji, Kamigyo-ku, Kyoto 602-8566, Japan
[6]Department of Veterinary Medicine, Obihiro University of Agriculture and Veterinary Medicine, Inada-cho, Obihiro, Hokkaido 080-8555, Japan
[7]Fukuoka Dairy Cattle Artificial Insemination Clinic, Fukuoka Prefecture Dairy Farming Cooperative, 1-13-4, Susenji, Nishiku, Fukuoka, Fukuoka 839-0832, Japan
[8]Kurume Dairy Cattle Artificial Insemination Clinic, Fukuoka Prefecture Dairy Farming Cooperative, 75-2, Airaku, Ohashimachi, Kurume, Fukuoka 839-0832, Japan
[9]Veterinary Medical Center, Obihiro University of Agriculture and Veterinary Medicine, 2-11 Inada-nishi, Obihiro, Hokkaido 080-8555, Japan
[10]Dairy Research Department, Gifu Prefectural Livestock Research Institute, 1975-615 Kubohara, Yamaoka-cho, Ena, Gifu 509-7601, Japan
[11]Miyazaki Agricultural mutual aid association, 17938-5 Nyuta Shintomi-cho, Miyazaki 889-1406, Japan
[12]Soo Agricultural mutual aid association, 2253 Osumicho Tsukino, Soo-shi, Kagoshima 899-8212, Japan
[13]Joint Faculty of Veterinary Medicine, Kagoshima University, 1-21-24 Korimoto, Kagoshima 890-0065 Japan
[14]School of Veterinary Medicine, Azabu University, 1-17-71 Fuchinobe, Chuou-ku, Sagamihara, Kanagawa 252-5201, Japan

Received for publication, February 4, 2020; accepted, April 22, 2020

* Corresponding author: Kentaro Kato, D.V.M., Ph.D
Laboratory of Sustainable Animal Environment, Graduate School of Agricultural Science, Tohoku University, 232-3 Yomogida, Naruko-onsen, Osaki, Miyagi 989-6711, Japan
Phone: +81-229-84-7391, Fax: +81-229-84-7391, E-mail: kentaro.kato.c7@tohoku.ac.jp
doi: 10.14943/jjvr.68.3.159

Abstract

***Cryptosporidium* is an apicomplexan zoonotic parasite that infects most mammals, including humans. Cryptosporidium parvum virus type 1 (CSpV1) is the first member within the Partitiviridae family recognized to infect protozoan hosts. *Cryptosporidium* tracking based on CSpV1 detection has been attempted; however, each study used different conditions for the PCR protocol, primers, and target viral sequences. Accordingly, the sensitivity of PCR-based CSpV1 detection remains unclear. In addition, oocyst purification from clinical samples can be problematic due to small number of oocysts, sample degradation and low yield efficiency of currently used purification methods. Here we show that the second half of the coding region of dsRNA2 can be detected from various types of clinical samples, without the need for oocyst purification, by using a semi-nested-PCR technique. Furthermore, we show that the short sequence targeted in this study has higher diversity than the *Cryptosporidium* GP60 gene. Taken together, our findings suggest that this method could be used as an important tracking marker for *Cryptosporidium* species.**

Key Words: Calves, *Cryptosporidium,* CSpV1, PCR

Introduction

Cryptosporidium is a zoonotic parasite that causes cryptosporidiosis. *Cryptosporidium* can infect a wide range of hosts including domestic animals and humans through ingestion of contaminated food or water[30]. The severe diarrhoea and related high mortality associated with the infection in young animals have a serious impact on animal husbandry[4]. *Cryptosporidium* infection occurs throughout the world but high prevalence rates are more common in poorly developed countries where prevalence was ranged from 20% to 60% in individual calves in Japan and may reach to 98% at herd level in Argentina[1,12,22]. Unfortunately, none of the drugs currently available to treat cryptosporidiosis are completely effective[29]. Therefore, the development of a quick and accurate detection method and genetic surveillance of *Cryptosporidium* are particularly important to predict and prevent the spread of infection.

Historically, microscopic techniques have been relied upon for the detection of *Cryptosporidium* oocysts, even though misdiagnosis is possible due to debris[5,9]. In addition, no major morphological differences among oocysts have been found between different species by using these techniques[8]. More recently, PCR-based techniques are being developed for detection, species identification, and phylogenetic analysis of *Cryptosporidium*[32,34,35]; however, problems remain. For example, although *Cryptosporidium* detection requires the purification of oocysts from faecal samples, the recovery rates of oocysts from frozen stock vary from 22% to 75%[3]. Accordingly, new techniques for *Cryptosporidium* detection and identification are needed.

Cryptosporidium parvum virus type 1 (CSpV1), which is a double-strand (ds) RNA virus belonging to the Cryspo-virus genus in the Partitiviridae family, was first detected in 1997 from C. *parvum*[13,14]. So far, there have been no reports demonstrating the extracellular transmission of the virus to *Cryptosporidium* because CSpV1 is vertically transmitted intracellularly during *Cryptosporidium* division[25]. In addition, it has been reported that *Cryptosporidium* oocysts contain a large number of viral RNAs relative to the number of oocyst genes[31]. Therefore, CSpV1-based techniques have been developed as an alternative approach to *Cryptosporidium* detection and identification[17,33]. In fact, the detection sensitivity of CSpV1-based techniques has been reported to be 2,000-fold higher than that of techniques designed to detect *Cryptosporidium* oocysts because of the stability and abundance of the viral RNA[15,31]. The virus possesses an encapsidated long dsRNA1 segment that encodes the RNA-dependent RNA

polymerase and a short dsRNA2 segment that encodes the capsid protein[24]. The complete sequences of the CSpV1 dsRNAs have been identified in *C. hominis*, *C. felis*, and *C. melegridis* and have been shown to be conserved[18]. Therefore, dsRNA2 has frequently been used for *Cryptosporidium* detection. However, different regions within or outside the coding region of the dsRNAs have been used as the targets for PCR-based detection[17-19], and the effects of differences in the PCR approaches used on the sensitivity of viral detection remain unknown.

Although CSpV1-based techniques show great potential for use in *Cryptosporidium* detection, the purification of *Cryptosporidium* oocysts remains an essential step for viral RNA extraction. Currently used methods for oocyst recovery appear to be unsuitable for samples with a small number of oocysts[7, 28]. Moreover, it has been reported that degradation of oocysts due to excystation or storage can lead to an extreme reduction in the efficiency of oocyst purification[11]. For these reasons, new methods that do not require *Cryptosporidium* oocyst purification are needed.

In the present study, we demonstrate that CSpV1 detection sensitivity is affected by the PCR target site within CSpV1 dsRNA2. In addition, we show that a partial dsRNA2 sequence of CSpV1 can be used to detect CSpV1 from clinical samples without the need for *Cryptosporidium* oocyst purification. Our data suggest that this method has potential as an alternative strategy for *Cryptosporidium* or CSpV1 detection and identification.

Materials and Methods

Clinical sample collection: A total of 62 diarrhoeic faecal samples were kindly provided by the veterinarians in various prefectures of Japan. Samples were from dairy and beef calves that ranged in age from 3 days to 50 days, acquired between October 2018 and March 2019, from eight different Japanese prefectures. In this study, three different breeds of calves were included: Holstein Friesians, Japanese Black, and cross-bred F1 hybrids. Samples were stored at -28 ˚C until use.

Table 1. different primer sequences used in this study.

Primer	Sequence
P1F	5'-ATTACAAGTTTTGAATCAATAGAG-3'
P2F	5'-CCTATGCACCATAGTGGAATTAC-3'
P3F	5'-CCTATCGCTGAGCATCTAACTAGATGG-3'
P4R	5'-ACTAACAGATTGCACTGCTTCCGGC-3'
P5R	5'-TCTGCGCTACACTCCGTCGTTACTAT-3'
P6R	5'-ATGGGAGCGATCTGCGCTACAC-3'

RNA extraction from faecal samples: RNA was extracted from all samples without oocyst purification by using 0.4–0.5 g of faeces according to the protocol of the Quick-RNA Faecal/Soil Microbe Microprep Kit (Zymo Research Corp, Irvine, CA, USA). RNA was stored at -80 ˚C until use. Some samples were examined microscopically for oocysts and were then subjected to at least three freezing-thawing cycles before RNA extraction.

PCR protocol using RNA extracted from C. parvum HNJ-1 strain: *C. parvum* HNJ-1 is maintained in nude mice in the Department of Infectious Diseases, Kyoto Prefectural University of Medicine, Japan. Total RNA was extracted from *C. parvum* HNJ-1 oocysts. In this study, we used seven sets of primer pairs for CSpV1 detection. The CPVS_ORF_1F and CPVS_ORF_6R primers were previously used for CSpV1 detection[20]. The other four primers were designed for this study. All of the primers used in this study are listed in Table 1. First, cDNA was synthesized by using 1000 pg of total RNA extracted from *C. parvum* HNJ-1 with the CPVS_ORF_1F primer by using the Thermo Scientific Verso cDNA Synthesis Kit (Thermo Scientific, Waltham, Massachusetts, CA, USA) according to the manufacturer's instructions. The resulting cDNA was included the in initial and semi-nested

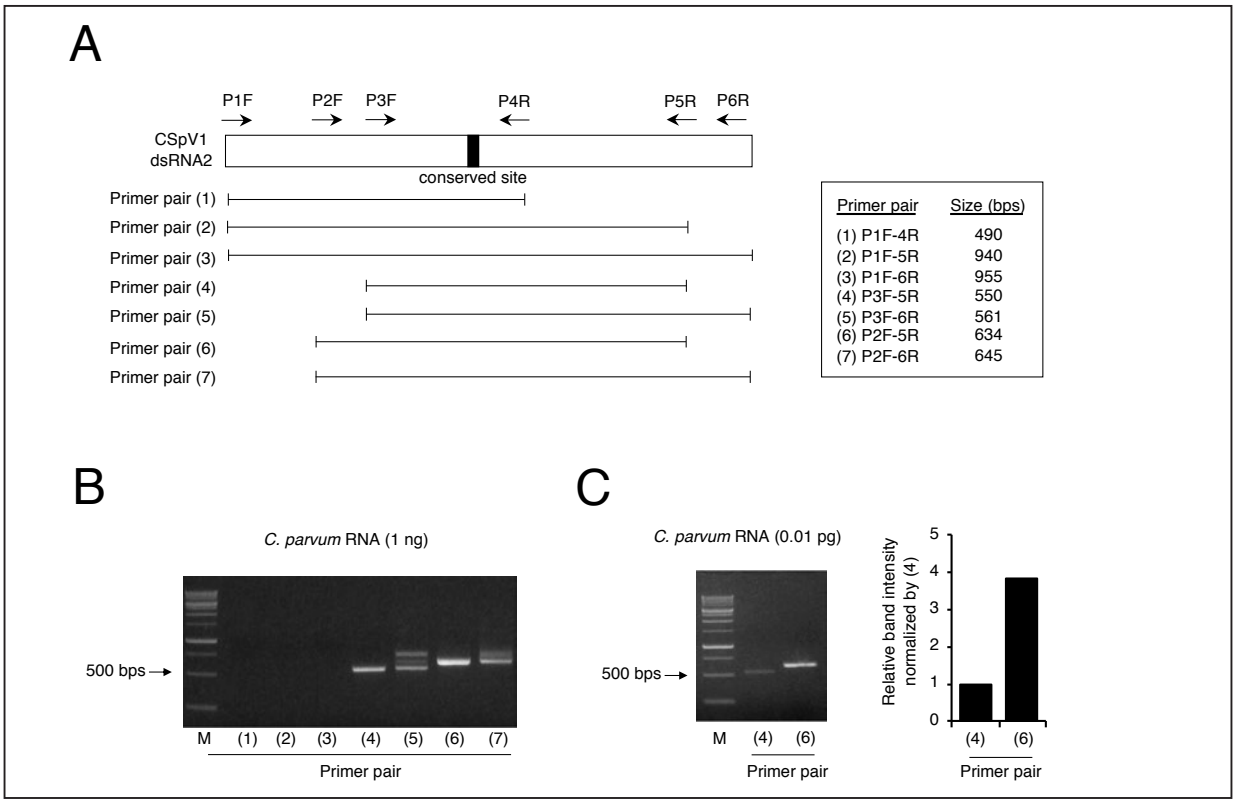

Fig. 1. PCR condition sare important for virus detection
(A) Schematic drawings of PCR analyses for CSpV1 dsRNA2 detection with different primer pairs and targeted sizes. **(B)** Detection of CSpV1 by PCR in 1 µg of RNA from *Cryptosporidium* oocysts was performed using the indicated primer pairs. Results shown in a 1.5% agarose gel. M: molecular weight marker (1-kb DNA ladder). **(C)** Detection of CSpV1 by PCR in 0.01 pg of RNA from *Cryptosporidium* oocysts was performed using the indicated primer pairs. Results shown in a 1.5% agarose gel. M: molecular weight marker (1-kb DNA ladder). The densitometry analysis of the amplified fragments was performed by using NIH Image J.

PCR reaction, which was performed by using the KOD FX Neo kit with the indicated primer pairs (**Fig. 1A**). Then, to evaluate the sensitivity of our protocol, the same procedure was repeated using four different concentrations (10, 1, 0.1, and 0.01 pg/ul) of template total RNA extracted from *C. parvum* HNJ-1 for cDNA synthesis and amplification of the various target fragments. The PCR protocol was as follows: 94 ˚C for 2 min, then 45 cycles of 98 ˚C for 10 s, 60 ˚C for 30 s and 68 ˚C for 1 min, followed by 68 ˚C for 7 min.

Semi-nested PCR protocol using RNA extracted from faecal samples: After optimization of our protocol using RNA from the *C. parvum* HNJ-1 strain, we examined the ability of this method to detect CSpV1 dsRNA2 from total RNA directly extracted from 62 *faecal* samples of calves in the field. Total RNA was extracted from these *faecal* samples as above. cDNA synthesis and the initial PCR, using primer pair 2, were carried out by using the protocol just described. Then, 2 µl of the first PCR product was used for the second PCR reaction, which was performed by using the KOD FX Neo kit (TOYOBO, Osaka, Japan) with the indicated primer pair 6. The PCR protocol was as follows: 94 ˚C for 2 min, then 45 cycles of 98 ˚C for 10 s, 60 ˚C for 30 s and 68 ˚C for 1 min, followed by 68 ˚C for 7 min.

Detection and visualization of CSpV1 and Cryptosporidium genetic diversity: PCR products were separated by electrophoresis through 1.5 % agarose gels and extracted by

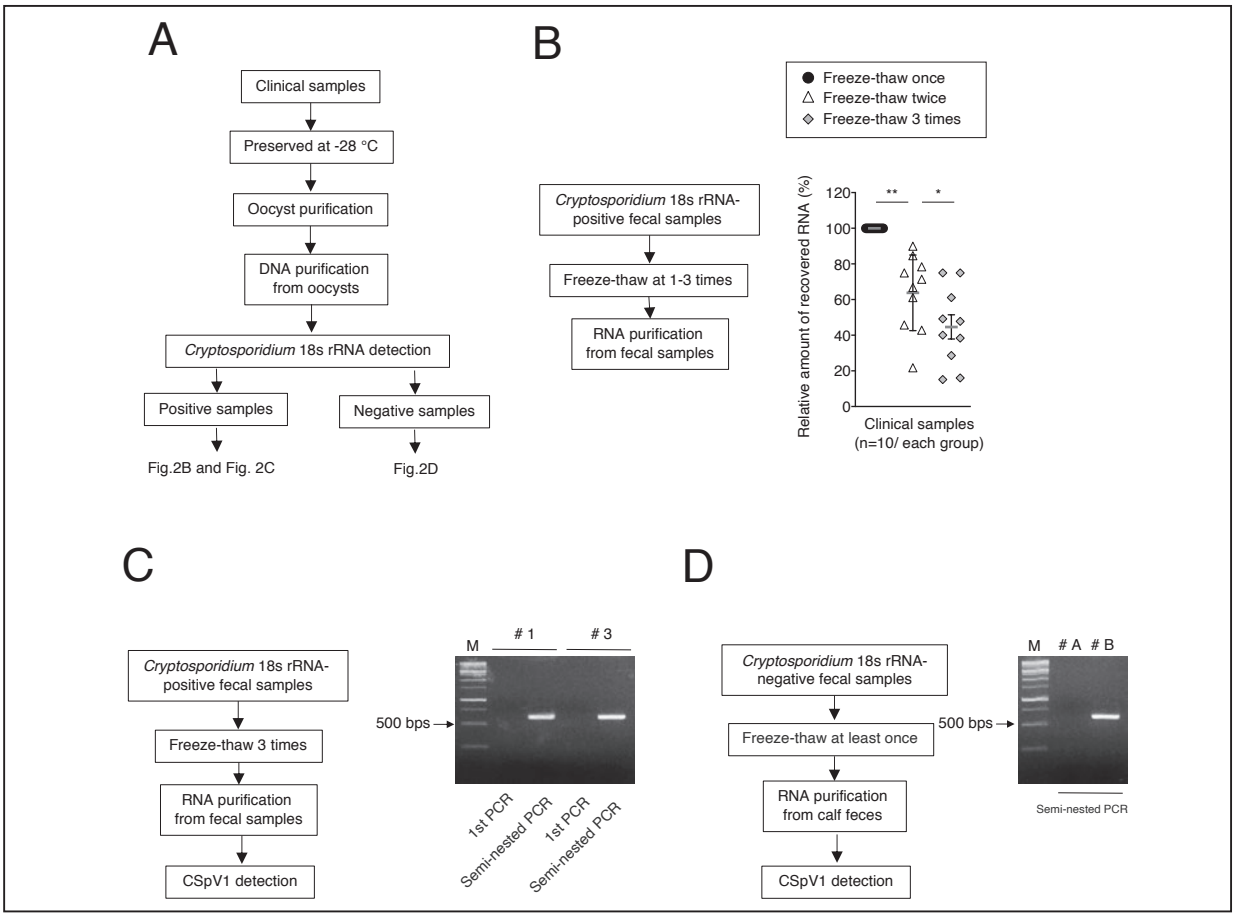

Fig. 2. CSpV1 can be detected in damaged clinical samples.
(A) Scheme of the experimental strategy used to evaluate PCR sensitivity and specificity using clinical samples. **(B)** Effect of frequent freeze-thawing on RNA extraction. Each point represents the mean of one sample (n=10). *$p < 0.05$, ** $p<0.01$; (Student's t-test). **(C)** Detection of CSpV1 in *Cryptosporidium*-positive clinical samples by using primary PCR alone or semi-nested PCR. Results shown in a 1.5% agarose gel. M: molecular weight marker (1-kb DNA ladder) **(D)** Detection of CSpV1 in *Cryptosporidium*-negative clinical samples by using semi-nested PCR. Results shown in a 1.5% agarose gel. M: molecular weight marker (1-kb DNA ladder).

using the NucleoSpin Gel and PCR Clean-up kit (MACHEREY-NAGEL GmbH & Co, Düren, Germany) according to the manufacturer's instructions. An automated sequencer (Applied Biosystems 3130xl Genetic Analyzer; Applied Biosystems, Tokyo, Japan) was used for analysing sequences. The resulting sequences were read on 4Peaks Genetic Analyzer software and aligned using Clustal W on the MEGA7 program. The aligned dsRNA2 sequences in which all gaps were eliminated were applied to the popART software equipped with the integer neighbor-joining (IntNJ) method to visualize genetic diversity by nucleotide substitutions[2]. Similarly, GP60 gene sequences (published data) for the same twenty-five samples were used to construct haplotype networks to be compared with the dsRNA2-based tree.

Results

The PCR target region of CSpV1 has an effect on virus detection sensitivity

To test the PCR amplification efficiency in relation to the PCR conditions, we used 1 ng of RNA extracted from purified *Cryptosporidium parvum* oocysts and different primer pairs targeting dsRNA2 (**Fig. 1A**). We found that

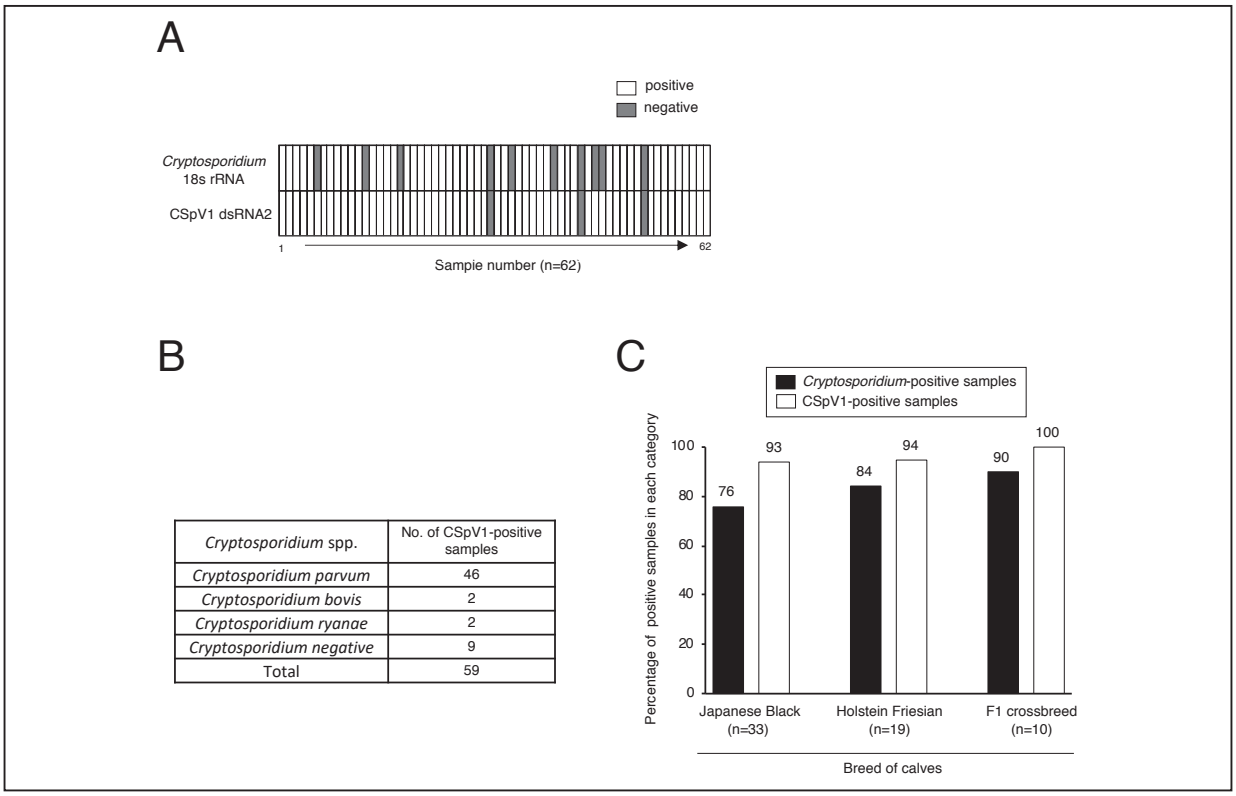

Cryptosporidium spp.	No. of CSpV1-positive samples
Cryptosporidium parvum	46
Cryptosporidium bovis	2
Cryptosporidium ryanae	2
Cryptosporidium negative	9
Total	59

Fig. 3. The CSpV1-based dsRNA2 detection method is applicable to field samples.
(A) CSpV1 and *Cryptosporidium* detection in 62 clinical samples; correlation between the results based on *Cryptosporidium* 18S rRNA and the results based on CSpV1 dsRNA2. **(B)** CSpV1 detection in three *Cryptosporidium* species. **(C)** The infection rates for CSpV1 and *Cryptosporidium* in different breeds of host animals was analysed.

CSpV1 was only detected by primer pairs targeting the second half of dsRNA2 (i.e., primer pairs 4, 5, 6, or 7; **Fig. 1B**). The specificity of each primer pair was confirmed through amplicon sequencing. Additionally, whereas primer pairs 5 and 7 showed non-specific amplification, specific amplicons were clearly produced by primer pairs 4 and 6 (**Fig. 1B**). Therefore, we next tested the limit of detection of CSpV1 by using low RNA concentrations from *C. parvum* oocysts and primer pair 4 or 6 (**Fig. 1C**). We found that CSpV1 was strongly detected by primer pair 6 compared with primer pair 4 (**Fig. 1C**). Taken together, these data indicate that both the viral target sequence and the primer pair combination are important for CSpV1 detection.

Establishment of a direct method for the detection of CSpV1 from faecal samples

Cryptosporidium oocyst purification has been essential for sensitive molecular or serological CSpV1 detection[17, 20], even though the current purification procedures have limitations and drawbacks. Therefore, we assessed whether a PCR-based CSpV1 detection method using primer pair 6 could be used to assess faecal samples without having to purify the *Cryptosporidium* oocysts (**Fig. 2A, 2B, 2C, and 2D**). Storage conditions reportedly affect the extraction efficiency of RNA[11]. We confirmed that the extraction efficiency of RNA from faecal samples was markedly reduced by repeat freeze-thawing (**Fig. 2B**). We tried to detect CSpV1 by using RNA extracted from damaged faecal samples (i.e., samples that had been freeze-thawed three times). However, we failed to detect CSpV1 from these samples even though *Cryptosporidium* infection was confirmed by using a nested-PCR

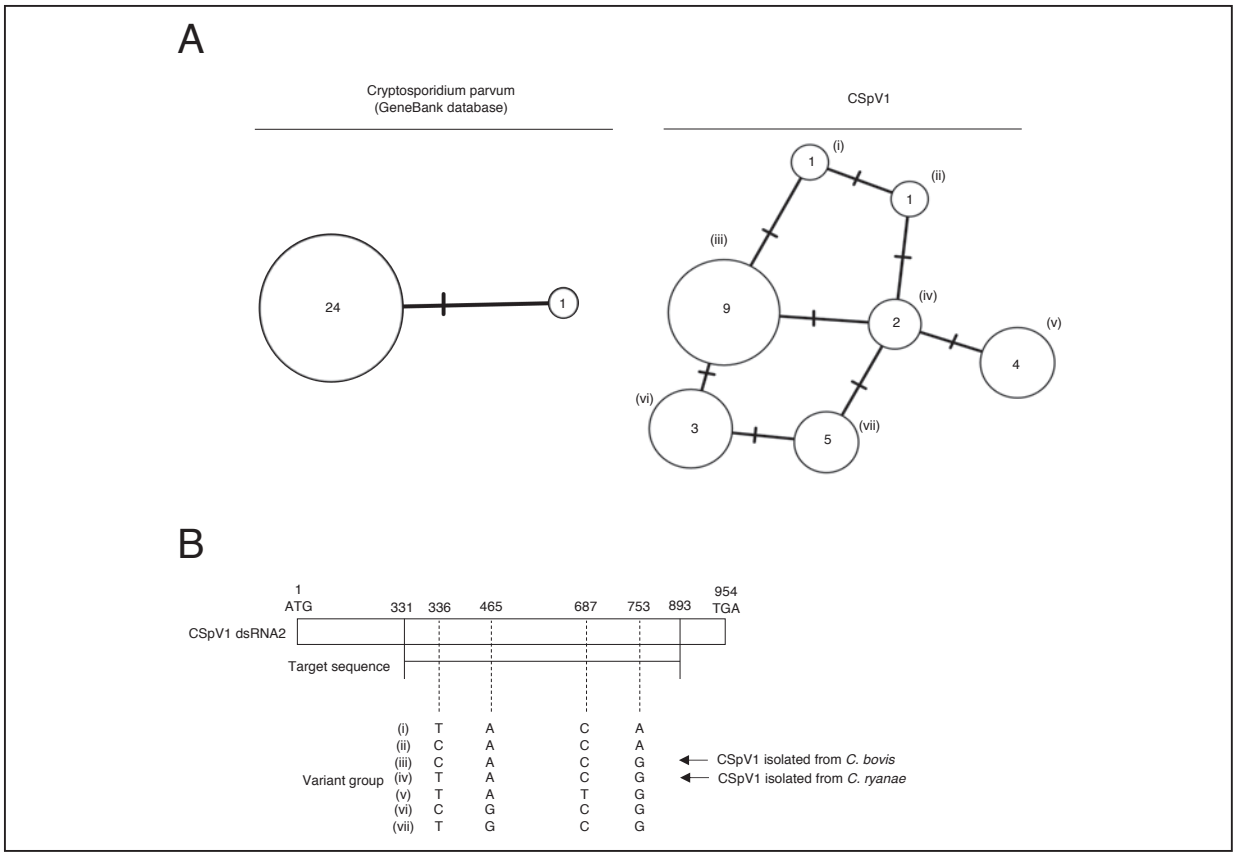

Fig. 4. Partial sequence analysis of dsRNA2 shows high genetic diversity compared with GP60 gene sequences. **(A)** Genetic diversities based on *Cryptosporidium* GP60 and CSpV1 dsRNA2 nucleotide substitutions as visualized by using popART software equipped with the Integer neighbor-joining (IntNJ) method. Numbers inside circles indicate the total number of samples within the group. The number of mutation sites between groups is indicated on each line. Variant groups of CSpV1 dsRNA2 sequences are shown (i–vii). **(B)** Nucleotide substitutions at different sites within the dsRNA2 sequence resulting in variant alignment groups based on virus sequence.

method targeting *Cryptosporidium* 18S rRNA (**Fig. 2C**). Then, we examined whether a semi-nested PCR method, using primer pair 2 for the first PCR and primer pair 6 for the second PCR, could be used to test faecal samples without purification of the *Cryptosporidium* oocysts. By using this approach, we were able to confirm the presence of CSpV1 in the damaged faecal samples (**Fig. 2C**), thereby demonstrating that the semi-nested PCR method could directly detect CSpV1 in damaged faecal samples. To test the sensitivity of the semi-nested PCR method, we attempted to detect CSpV1 from faecal samples that were freeze-thawed at least once and were negative for the parasite by a nested-PCR method targeting *Cryptosporidium* 18s rRNA(**Fig. 2D**). Some of the samples were CSpV1-negative in this assay(**Fig. 2D**), suggesting that our method is highly specific. Other samples were CSpV1-positive (**Fig. 2D**), indicating that our method is more sensitive than the existing method. Taken together, our findings demonstrate that this direct CSpV1 detection method is effective for use with faecal samples.

Direct methods to detect CSpV1 in clinical samples

Our current study has shown that the semi-nested PCR method using primer pair 6 is highly sensitive for the detection of CSpV1 from faecal samples without the need for purification of *Cryptosporidium* oocysts (**Fig. 3A**). We, therefore, next investigated whether this method could be used to detect CSpV1 in 62 clinical samples

that had undergone freeze-thawing at least once; these samples were collected in Japan between October 2018 and March 2019 (**Fig. 3A**). Although a previous study reported that 50 out of these 62 samples were *Cryptosporidium*-positive (personal communication), we found that 59 of the same 62 samples were CSpV1-positive (**Fig. 3A**). Importantly, we found that the CSpV1-positive samples matched completely with the *Cryptosporidium* 18S rRNA-positive samples (**Fig. 3A**). Thus, we detected an additional 9 CSpV1-positive samples among a total of 12 *Cryptosporidium* 18S rRNA-negative samples (**Fig. 3A**). These results demonstrate that our direct viral detection method is highly sensitive even for clinical samples.

CSpV1 is present in C. bovis and C. ryanae

To date, CSpV1 has been reported in only four *Cryptosporidium* species: *C. parvum, C. felis, C. hominis, and C. meleagridis*[17, 18]. Our results suggest that CSpV1 is also present in *C. bovis* and *C. ryanae* (**Fig. 3B**). This is the first report to detect CSpV1 both in *C. bovis* and *C. ryanae*, suggesting that our method can detect CSpV1 regardless of the *Cryptosporidium* species (**Fig. 3B**). Moreover, we found a high number of CSpV1-positive samples in all breeds of beef and dairy calves(**Fig. 3C**), suggesting that our method can detect CSpV1 regardless of the cattle breed. These results demonstrate that our direct viral detection method can be used regardless of parasite species or host breed.

CSpV1 partial sequences show a high level of genetic polymorphism compared with Cryptosporidium GP60

Although the GP60 gene is frequently used for subtyping *Cryptosporidium parvum*, the *C. parvum* subtype IIaA15G2R1 is the most common subtype found in cattle in many countries[26] and is the only subtype of *C. parvum* that has been detected in Japan[1]. In a previous study, the *Cryptosporidium* infection rate was about 80% where *C. parvum* isolates represented 92% of the total positive samples with IIaA15G2R1 as the most common subtype (personal communication). In contrast, previous reports have shown variation in the sequence of CSpV1 dsRNA2[17, 33]. In one study, although 64 of 80 samples were found to be *C. parvum*-positive, GP60 gene sequences were obtained from only 41 samples (personal communication), and only 25 samples were found to express both the GP60 gene and partial CSpV1 dsRNA2 sequences. Therefore, to assess whether our viral target sequence could serve as an alternative marker for *C. parvum*, we attempted a genetic polymorphism analysis using the 25 sequences of the GP60 gene or partial CSpV1 dsRNA2 from these samples (**Fig. 4A**). We found that 24 of the 25 GP60 gene sequences comprised one group, whereas the other group contained only one sequence. In contrast, we obtained seven CSpV1 dsRNA2 variant groups based on the virus sequences: 2 groups contained one sequence, whereas the other 5 groups contained 2, 3, 4, 5, and 9 sequences, respectively. These results suggest that CSpV1 dsRNA2 sequences have greater genetic diversity than the GP60 gene sequence, even though the viral target sequence is shorter (**Fig. 4A**). Four nucleotide substitutions were found within the dsRNA2 target sequences; as a result, distinct nucleotide alignments were obtained and the samples could be clustered into 7 groups (**Fig. 4B**). Specifically, these 4 nucleotide substitutions at base pair positions 336, 465, 687, or 753 of the dsRNA2 target sequence are responsible for genetic diversity of the virus (**Fig. 4B**). In addition, virus sequences recovered from *C. bovis*-infected samples were 100% identical to each other and belonged to group (iii). Similarly, nucleotide sequences of CSpV1 for *C. ryanae* showed complete identity and clustered within group (iv) (**Fig. 4A, 4B**). However, the GP60-based sequence network revealed identical sequences with only one C nucleotide replaced with A at base pair positions 395. Taken together, these findings indicate that the partial dsRNA2 sequence that we targeted in this study could serve as an important tracking marker for *C. parvum*.

Discussion

In the present study, we demonstrated that a PCR method targeting a partial sequence of CSpV1 dsRNA2 can be used for virus detection from *Cryptosporidium* oocysts. Previous studies have shown that a PCR-based CSpV1 detection method has advantages for sensitive detection of *Cryptosporidium*, for example, detection of fewer than 5 oocysts have been reported[19]. However, these studies used various detection conditions, including various PCR protocols, different target regions of the viral RNA, and different primer pairs. Accordingly, the relationship between the efficiency of virus detection and the detection method has remained unclear. In the present study, we found that PCR amplification efficiency is specific for the target region of the viral RNA; whereas the first half of dsRNA2 is difficult to detect, the second half of dsRNA2 is effectively amplified by PCR. In addition, the 3-prime end of the coding sequence can lead to non-specific amplification, possibly because the first half of dsRNA2 contains a highly AT-rich region. In the present study, we clearly demonstrated that the second half of dsRNA2, which lacks the 3-prime end of the coding sequence, is effectively amplified by using our PCR method.

It has been reported that 100 μg of total RNA can be extracted from 10^9 *Cryptosporidium* oocysts[28]. Given that one *Cryptosporidium* oocyst contains 0.1 pg of total RNA, CSpV1 RNA may be present as less than 0.1 pg in one oocyst. Our study showed that 0.01 pg of RNA extracted from a *Cryptosporidium* oocyst is enough for CSpV1 detection, suggesting that our method has the potential to detect a single oocyst. Moreover, it has been reported that a short-conserved region within dsRNA2 is shared among all known virus sequences that have been identified in different *Cryptosporidium* species[18]. Importantly, amplicons produced by our method include this conserved region, which suggests that our method may be useful for tracking sources of *Cryptosporidium* outbreaks.

Most previous CSpV1 detection studies used RNA extracted not from faeces but from oocysts[17, 20]. However, it is difficult to purify *Cryptosporidium* oocysts from the faeces of hosts with a low oocyst load[3]. In addition, degradation of oocysts due to excystation or storage can result in a significant decrease in the efficiency of purification of *Cryptosporidium* oocysts[11]. In fact, the PCR sensitivity with clinical faecal samples stored for 5 weeks was found to be less than 20%[11]. Of note, our method successfully detected CSpV1 from clinical samples that had been stored for more than a year and subjected to frequent freezing-thawing cycles (at least one) before RNA extraction. Thus, we have established a highly sensitive method for CSpV1 detection from clinical samples without the need for purification of *Cryptosporidium* oocysts.

A previous study found that 50 out of 62 samples contained *Cryptosporidium* oocysts based on a *Cryptosporidium* 18S rRNA detection method (personal communication). In contrast, using our detection method, we demonstrated that 59 of those 62 samples are, in fact, CSpV1-positive. Importantly, these CSpV1-positive samples included the 50 *Cryptosporidium* 18S rRNA-positive samples, thereby demonstrating that our PCR method targeting the partial CSpV1 dsRNA2 can be used as an alternative *Cryptosporidium* detection method. Of interest, our current study identified 9 of the *Cryptosporidium* 18S rRNA-negative samples as CSpV1-positive, suggesting that CSpV1 may be a more sensitive marker of *Cryptosporidium* than the 18S rRNA gene of the *Cryptosporidium* genome. Some studies have reported that CSpV1-based methods show greater sensitivity in detecting *Cryptosporidium* in clinical samples than do techniques that use oocyst or sporozoite antigens; however, these studies involved serologic techniques or colloidal gold-based immunochromatographic tests[15, 16, 31]. In contrast, here we demonstrated that a PCR-based method targeting the partial CSpV1 dsRNA2 can detect for *Cryptosporidium* in clinical samples with high sensitivity. *Cryptosporidium* has been

isolated all over the world including rural areas and developing countries[6, 10, 23].Improving PCR-based CSpV1 detection methods for use with clinical samples that have been preserved is important, because such methods are widely applicable for tracking of *Cryptosporidium* infections. Thus, our PCR-based method targeting the partial CSpV1 dsRNA2 could contribute to various characterization studies of *Cryptosporidium* without temporal and spatial constraints.

Although 29 *Cryptosporidium* species have been recognized to date[4], CSpV1 has been reported in only four species: *C. parvum, C. felis, C. hominis, and C. meleagridis*[17, 18]. In the present study, we found CSpV1 in *C. bovis* and *C. ryanae* for the first time. The lack of information about CSpV1 in *C. bovis* and *C. ryanae* may be due to the pathology of these *Cryptosporidium* species; infection with these *Cryptosporidium* species is usually without clinical symptoms or diarrhoea[22]. Therefore, it may be more difficult to detect *C. bovis* and *C. ryanae* from clinical samples compared with *C. parvum*. In addition, most studies have examined clinical samples collected from young stock because of the pathology of *C. parvum*. In contrast, *C. bovis* and *C. ryanae* are found mainly in older calves and stock aged 3–11 months[27], and the clinical samples used in this study came from animals across a wide age range. Whatever the case, our data show that this method can be used to detect the presence of CSpV1 in *C. bovis* and *C. ryanae*. Clearly, this first CSpV1 detection spurs interest in the *Cryptosporidium*-virus interaction, in particular, the host factors that determine or modulate CSpV1 infection. Further studies regarding the identification of animal factors and host interactions in relation to CSpV1 infection are warranted.

Our current study showed that there is no correlation between the presence of CSpV1 and the breed of calf, suggesting that *Cryptosporidium* is widespread regardless of host factors such as breed. Most subtyping studies have focused on the *C. parvum* GP60 gene[21, 26]; therefore, additional high-resolution tools for tracking different *Cryptosporidium* species and subtypes may be required. Here, sequence analysis of 25 samples using the partial dsRNA2 sequence rather than the GP60 gene sequence revealed greater genetic diversity among the virus sequences from several isolates even though the partial dsRNA2 sequence is shorter than the GP60 gene sequence. In addition, CSpV1 seems to be non-species specific based on the similarity observed among the CSpV1 sequences from samples infected with *C. bovis, C. ryanae,* or *C. parvum*. Taken together, our data show that this partial dsRNA2 sequence could be used as an alternative marker for *Cryptosporidium* detection and identification.

In summary, we have shown that a partial dsRNA2 sequence from CSpV1 is a useful PCR target for the detection of *Cryptosporidium* and CSpV1 from clinical samples without the need for purification of *Cryptosporidium* oocysts. This method will be of value in *Cryptosporidium* and CSpV1 detection and identification.

Acknowledgements

The authors would like to thank the veterinarians of the different prefectures for collecting the specimens and collaborating with us. This study was funded by grants-in-aid for Scientific Research (B:17H03913) and (C:16KT0141) and Scientific Research on Innovative Areas (3805) from the Ministry of Education, Culture, Science, Sports, and Technology (MEXT) of Japan, and by a Livestock Promotional Subsidy from the Japan Racing Association. We would like to thank the Ministry of higher Education and Scientific Research, the Arab Republic of Egypt for support during this study in accordance with the Egypt-Japan Education Partnership (EJEP).

References

1) Aita J, Ichikawa-Seki M, Kinami A, Yaita S, Kumagai Y, Nishikawa Y, Itagaki T. Molecular characterization of *Cryptosporidium parvum* detected in Japanese black and Holstein calves in Iwate Prefecture and Tanegashima Island, Kagoshima Prefecture, Japan. J Vet Med Sci 77, 997-999, 2015.
2) Bryant JW. popart: full-feature software for haplotype network construction. Methods Ecol Evol 6, 1110-1116, 2015.
3) Bukhari Z, Smith HV. Effect of three concentration techniques on viability of *Cryptosporidium parvum* oocysts recovered from bovine feces. J Clin Microbiol 33, 2592-2595, 1995.
4) Chalmers RM, Katzer F. Looking for *Cryptosporidium*: the application of advances in detection and diagnosis. Trends Parasitol 29, 237-251, 2013.
5) Connelly L, Craig BH, Jones B, Alexander CL. Genetic diversity of *Cryptosporidium* spp. within a remote population of Soay Sheep on St. Kilda Islands, Scotland. Appl Environ Microbiol 79, 2240-2246, 2013.
6) Del Coco VF, Cordoba MA, Basualdo JA. *Cryptosporidium* infection in calves from a rural area of Buenos Aires, Argentina. Vet Parasitol 158, 31-35, 2008.
7) Ebrahimzade E, Shayan P, Asghari Z, Jafari S, Omidian Z. Isolation of small number of *Cryptosporidium parvum* oocyst using immunochromatography. Iran J Parasitol 9, 482-490, 2014.
8) Elliot A, Morgan UM, Thompson RC. Improved staining method for detecting *Cryptosporidium* oocysts in stools using malachite green. J Gen Appl Microbiol 45, 139-142, 1999.
9) Fayer R, Morgan U, Upton SJ. Epidemiology of *Cryptosporidium*: transmission, detection and identification. Int J Parasitol 30, 1305-1322, 2000.
10) Fayer R, Santin M, Dargatz D. Species of *Cryptosporidium* detected in weaned cattle on cow-calf operations in the United States. Vet Parasitol 170, 187-192, 2010.
11) Fischer P, Taraschewski H, Ringelmann R, Eing B. Detection of *Cryptosporidium parvum* in human feces by PCR. Tokai J Exp Clin Med 23, 309-311, 1998.
12) Garro CJ, Morici GE, Utges ME, Tomazic ML, Schnittger L. Prevalence and risk factors for shedding of *Cryptosporidium* spp. oocysts in dairy calves of Buenos Aires Province, Argentina. Parasite Epidemiol Control 1, 36-41, 2016.
13) Khramtsov NV, Chung PA, Dykstra CC, Griffiths JK, Morgan UM, Arrowood MJ, Upton SJ. Presence of double-stranded RNAs in human and calf isolates of *Cryptosporidium parvum*. J Parasitol 86, 275-282, 2000.
14) Khramtsov NV, Woods KM, Nesterenko MV, Dykstra CC, Upton SJ. Virus-like, double-stranded RNAs in the parasitic protozoan *Cryptosporidium parvum*. Mol Microbiol 26, 289-300, 1997.
15) Kniel KE, Higgins JA, Trout JM, Fayer R, Jenkins MC. Characterization and potential use of a *Cryptosporidium parvum* virus (CPV) antigen for detecting *C. parvum* oocysts. J Microbiol Methods 58, 189-195, 2004.
16) Kniel KE, Jenkins MC. Detection of *Cryptosporidium parvum* oocysts on fresh vegetables and 1 herbs using antibodies specific for a *Cryptosporidium parvum* viral antigen. J Food Prot 68, 1093-1096, 2005.
17) Leoni F, Gallimore CI, Green J, McLauchlin J. Molecular epidemiological analysis of *Cryptosporidium* isolates from humans and animals by using a heteroduplex mobility assay and nucleic acid sequencing based on a small double-stranded RNA element. J Clin Microbiol 41, 981-992, 2003.
18) Leoni F, Gallimore CI, Green J, McLauchlin J. Characterisation of small double stranded RNA molecule in *Cryptosporidium hominis*, *Cryptosporidium felis* and *Cryptosporidium meleagridis*. Parasitol Int 55, 299-306, 2006.

19) Mark Jenkins CO, Fetterer R, Santin M. RT-PCR specific for Cryspovirus is a highly sensitive method for detecting *Cryptosporidium parvum* oocysts. Food and Waterborne Parasitology 5, 14-20, 2016.
20) Murakoshi F, Ichikawa-Seki M, Aita J, Yaita S, Kinami A, Fujimoto K, Nishikawa Y, Murakami S, Horimoto T, Kato K. Molecular epidemiological analyses of Cryptosporidium parvum virus 1 (CSpV1), a symbiotic virus of *Cryptosporidium parvum*, in Japan. Virus Res 211, 69-72, 2016.
21) Murakoshi F, Tozawa Y, Inomata A, Horimoto T, Wada Y, Kato K. Molecular characterization of *Cryptosporidium* isolates from calves in Ishikari District, Hokkaido, Japan. J Vet Med Sci 75, 837-840, 2013.
22) Murakoshi F, Xiao L, Matsubara R, Sato R, Kato Y, Sasaki T, Fukuda Y, Tada C, Nakai Y. Molecular characterization of *Cryptosporidium* spp. in grazing beef cattle in Japan. Vet Parasitol 187, 123-128, 2012.
23) Nagano S, Matsubayashi M, Kita T, Narushima T, Kimata I, Iseki M, Hajiri T, Tani H, Sasai K, Baba E. Detection of a mixed infection of a novel *Cryptosporidium andersoni* and its subgenotype in Japanese cattle. Vet Parasitol 149, 213-218, 2007.
24) Nibert ML, Ghabrial SA, Maiss E, Lesker T, Vainio EJ, Jiang D, Suzuki N. Taxonomic reorganization of family Partitiviridae and other recent progress in partitivirus research. Virus Res 188, 128-141, 2014.
25) Nibert ML, Woods KM, Upton SJ, Ghabrial SA. Cryspovirus: a new genus of protozoan viruses in the family Partitiviridae. Arch Virol 154, 1959-1965, 2009.
26) Rieux A, Chartier C, Pors I, Delafosse A, Paraud C. Molecular characterization of *Cryptosporidium* isolates from high-excreting young dairy calves in dairy cattle herds in Western France. Parasitol Res 112, 3423-3431, 2013.
27) Robertson LJ, Björkman C, Axén C, Fayer R. Cryptosporidiosis in farmed animals. In: *Cryptosporidium* : Parasite and Disease. Cacciò SM, Widmer G. eds. Springer. pp.149-235, 2014.
28) Fayer R, Xiao L. eds. *Cryptosporidium* and Cryptosporidiosis, 2nd ed., CRC Press, Boca Raton, 2008.
29) Shahiduzzaman M, Daugschies A. Therapy and prevention of cryptosporidiosis in animals. Vet Parasitol 188, 203-214, 2012.
30) Smith HV, Caccio SM, Cook N, Nichols RA, Tait A. *Cryptosporidium* and *Giardia* as foodborne zoonoses. Vet Parasitol 149, 29-40, 2007.
31) Tai L, Li J, Yin J, Zhang N, Yang J, Li H, Yang Z, Gong P, Zhang X. A novel detection method of *Cryptosporidium parvum* infection in cattle based on *Cryptosporidium parvum virus* 1. Acta Biochim Biophys Sin (Shanghai) 51, 104-111, 2019.
32) Wang R, Zhang L, Axen C, Bjorkman C, Jian F, Amer S, Liu A, Feng Y, Li G, Lv C, Zhao Z, Qi M, Dong H, Wang H, Sun Y, Ning C, Xiao L. *Cryptosporidium parvum* IId family: clonal population and dispersal from Western Asia to other geographical regions. Sci Rep 4, 4208, 2014.
33) Xiao L, Limor J, Bern C, Lal AA. Tracking *Cryptosporidium parvum* by sequence analysis of small double-stranded RNA. Emerg Infect Dis 7, 141-145, 2001.
34) Zahedi A, Paparini A, Jian F, Robertson I, Ryan U. Public health significance of zoonotic *Cryptosporidium* species in wildlife: Critical insights into better drinking water management. Int J Parasitol Parasites Wildl 5, 88-109, 2016.
35) Ziegler PE, Santucci F, Lindergard G, Nydam DV, Wade SE, Schaaf SL, Chang YF, Mohammed HO. Evaluation of polymerase chain reaction diagnosis of *Cryptosporidium* spp in dairy cattle and wildlife. Vet Ther 8, 148-159, 2007.

Japanese Journal of Veterinary Research 68(3): 171-186, 2020

JJVR

REGULAR PAPER Experimental Research

Therapeutic effect of bovine amniotic fluid in murine dry eye model

Kadri Kulualp[1,*], Servet Kiliç[2], Yesari Eröksüz[3], Hatice Eröksüz[3] and Abdullah Aslan[4]

[1]Department of Surgery, Faculty of Veterinary Medicine, Dokuz Eylul University, İzmir, Turkey
[2]Department of Surgery, Faculty of Veterinary Medicine, Namik Kemal University, Tekirdag, Turkey
[3]Department of Pathology, Faculty of Veterinary Medicine, Firat University, Elazig, Turkey
[4]Department of Molecular Biology and Genetics, Faculty of Science, Firat University, Elazig, Turkey

Received for publication, September 21, 2019; accepted, May 20, 2020

Abstract

This study investigated the therapeutic effect of bovine amniotic fluid (BAF) in dry eye (DE) model in 60 female BALB/c mice divided equally into 6 groups. Control group (CG) received 5 µL formal saline and experimental groups 0.2% benzalkonium chloride in both eyes twice a day during 14 days. From 15 to 30 days while CG and DE group only was administered saline, other groups called BAF20, BAF35, BAF50 and BAF100 received 5 µL 20, 35, 50 and 100% BAF three times a day, respectively. On day 15, in all experimental groups tear production decreased, tear break-up time shortened, corneal fluorescein staining score increased compared to baseline; on day 30, for these parameters the most effective BAF concentrations were 35%, 50% and 100%. According to western blot analysis the lowest levels were obtained in CG and BAF35 groups for tumor necrosis factor α (TNF-α), vascular endothelial growth factor (VEGF) and cytokeratin 10 (K10); CG for adiponectin receptor-1 (AdipoR1); BAF35 and CG for adiponectin receptor-2 (AdipoR2) ($P < 0.05$). In the immunohistochemical analysis the lowest levels were in CG, BAF35, BAF50 and BAF100 groups for TNF-α, VEGF and K10; CG, BAF35 and BAF50 groups for AdipoR1; CG, BAF20, BAF35 and BAF50 groups for AdipoR2 ($P < 0.05$). TUNEL method revealed a lower apoptotic cell score in all BAF groups ($P > 0.05$). In conclusion; moderate to high concentrations of BAF have the more beneficial effects on DE at molecular and clinical signs and it can be used for the treatment.

Key Words: bovine amniotic fluid, dry eye, inflammation, mice, treatment

Introduction

Dry eye (DE) is a chronic multifactorial disorder induced primarily by high rate of inflammatory cytokine release as a result of tear hyperosmolarity, increased precorneal tear film (PTF) instability and hyperactivity of immune components in ocular surface cells[17,57]. DE is characterized by ocular surface impairment, inflammation, precorneal tear film instability and visual disturbances[49,54,57]. The current DE treatment modalities are based on increasing PTF stability, maintaining normal tear osmolarity, preventing apoptosis and inflammation and providing ocular surface homeostasis[52,57]. The main purpose of DE management is to remove the underlying causes of the disease playing roles in its pathogenesis[14,15] with resultants of relieved clinical symptoms and improved the patient of life quality[9,14,27]. Recently, the therapeutic benefits of

* Corresponding author: kadri.kulualp@deu.edu.tr, Department of Surgery, Faculty of Veterinary Medicine, Dokuz Eylul University, 35890, Fax: +90-232-572 3505, İzmir, Turkey
doi: 10.14943/jjvr.68.3.171

some biological agents, similar to natural tears including autologous serum, umbilical cord serum and human amniotic membrane and fluid, on DE widely have been investigated[44,45,53]. In earlier studies indicated that human amniotic membrane and fluid contain high amounts of growth factors vital for fetal development and revealed to induce corneal sensitivity, promote nerve regeneration and decrease epithelial damage as well as scar tissue formation in alkali burn cornea[18,26]. It has also been reported that these agents contain hyaluronic acid which is an anti-inflammatory polysaccharide[11,43,48]. In a mouse DE model study[44] in which the therapeutic effects of some body fluids and tear preparations were compared, it was found that human amniotic fluid yielded better results in terms of corneal fluorescein staining and goblet cell density than artificial tear preparations and human serum. Another study reported[45] that higher concentration of human amniotic fluid has better therapeutic effects on DE than its lower concentrations. Bovine has a well-developed allantoic cavity and a large amount of amniotic fluid. Bovine amniotic fluid (BAF), which is rich in proteins, minerals and cells, has the advantages of being inexpensive and easy to obtain[12]. In a study on acute corneal alkali burns of rat, BAF was found to reduce corneal erosions, edema and keratinization. These results indicate that BAF may be an alternative therapeutic agent in veterinary ophthalmology[16]. To our knowledge, up to now no study has investigated the therapeutic benefits of BAF on DE.

DE models can be established utilizing aquaternary ammonium compound, benzalkonium chloride (BEC), an active ingredient of ophthalmic preparations with antimicrobial action[36,56].BEC rapidly induces DE via disrupting the lipid phase of PTF and disintegrating corneal epithelial cell membrane[36].

The aim of this study was to investigate the therapeutic effects of 4 different concentrations of BAF, a biological fluid, in murine DE model induced with BEC.

Materials and Methods

Experimental procedure: This study was conducted in accordance with the Association for Research in Vision and Ophthalmology (ARVO) Statement for the Use of Animals in Ophthalmic and Vision Research, and it was approved by the Firat University Animal Experiments Local Ethics Committee (2016/4/34). The material in the study consisted of 60 BALB/c female mice with average weights of 18–20 g and average ages of 6–8 weeks. During the study, the subjects were kept in a room with an ambient temperature of 24ºC ± 1ºC, relative humidity of 60% ± 10%, and a light-dark cycle of 12 hours. No food and water restrictions were applied during the study. Following clinical and ophthalmological examinations, the subjects that were determined to be healthy were included the study. One week prior to the experiment, all the subjects were transferred to an independent room, where they were kept in conventional mouse cages. Experimental procedures were performed using a funnel shaped hard plastic restraint[22], the narrower end of which had a hole large enough for a mouse to pass its head through. To obtain the measurements, the animals were encouraged to pass through the restraint several times. Then, they were randomly divided into 6 groups (n=10 x 6). Group I served as the control group (CG); the other 5 groups (1 experimental group, the dry eye [DE] group and 4 BAF treatment groups) were topically administered 5 μL of 0.2% BEC in both eyes twice a day (09:00, 21:00) for 14 days to induce the DE model. During this time, the CG subjects received the same amount of saline and the same time points[55]. The subjects in the CG and DE groups (Group II) received 0.9% saline 3 times a day (09:00, 15:00, and 21:00) for a 15-day therapeutic period; the subjects in the other 4 groups (BAF treatment groups) were administered 20% BAF (Group III, BAF20), 35% BAF (Group IV, BAF35), 50% BAF (Group V, BAF50), and 100% BAF (Group VI, BAF100) at the same intervals and the same time points. At the end of the study, the mice were

decapitated, and the eye tissues were carefully collected and stored at -80°C until the Western blot (WBlot), immunohistochemical (IHC), and terminal deoxynucleotidyl transferase dUTP nick end labeling (TUNEL) analyses were conducted.

Procurement and Preparation of BAF:BAF was obtained from a 270±2 day pregnant cow that had a prolapsed vagina and a closed cervix uterus. The fluid was collected during the caesarean section procedure under sterile conditions, centrifuged at 3,000 rpm for 15 min and stored at -20ºC until used[12]. During use, it was kept at 4ºC to prevent bacterial contamination[12,16]. The BAF in Group III, Group IV, and Group V was diluted at concentrations of 20% (BAF20), 35% (BAF35), and 50% (BAF50), respectively, with isotonic saline; the BAF in Group VI (BAF100) was pure or used without dilution solution.

Procedure of the clinical parametric tests: In all the groups, the tear production rate, tear break-up time (TBUT), and corneal fluorescein staining tests were measured 7 times; baseline (before the experiment) and after inducing the DE model on days 15, 18, 22, 25, 28, and 30 at the same time points (13:00–15:00). During each measurement, any ocular abnormalities (photophobia, ocular discharge and redness, conjunctivitis, keratitis) were also noted.

Measurement of tear production rate with Endodontic Absorbent Paper Point Test (EAPPTT): As test material Roeko Color (Color size 30, Langenau, Germany) brand, a gold standard for this particular measurement[29,30,40] was used. After ensuring the physical restraint, the test strips were placed in the lower conjunctival fornix near the lateral canthus of each eye and left in place for 1 min. Measurement was performed in both eyes simultaneously. After the test strips were removed, the length of wetness on the strips was read on amillimeter scale and average data of both eyes were recorded.

TBUT: With a micro-injector (901 N, Hamilton, USA) 1 µL 0.1% liquid sodium fluorescein (Fertility Chemical Laboratory, Istanbul, Turkey) was instilled into the left and right eyes of each subject. After 3 blinks, the eye lids were withheld with fingers and under the slit-lamp biomicroscope (XL-1, Shin-Nippon, Osaka, Japan) the moment the tear break up occurred the first was noted and the average value of the both eyes was recorded[21,36].

Corneal fluorescein staining test: In all the experimental subjects, 90 sec after the TBUT, the corneal staining rate was assessed using the slit-lamp biomicroscope with a cobalt blue filter; and the detected corneal lesions were photographed under an operation microscope[25,36]. The lesions were scored as 0: no staining on the corneal surface; 1: a staining area equal to or less than 1/8; 2: a staining area equal to or less than 1/4; 3: a staining area equal to or less than 1/2; and 4: a staining area more than 1/2 or covering the entire corneal surface[25].

Total protein isolation:Corneoconjunctival tissue samples (Half of each group; 5 samples of both eyes) were washed with cold phosphate buffered saline (PBS) and protein isolation was performed with UPX Universal Protein Extraction Kit (Expedeon, UK), after protein isolation, the protein samples were kept at -20 °C until analysis[2].

Analysis of VEGF, TNF-α, K10, adiponectin receptor 1 (AdipoR1), and adiponectin receptor 2 (AdipoR2) protein expression levels using the WBlot technique: First, the protein concentrations of corneoconjunctival tissue were measured with a Lowry kit. About 30 µg of the protein samples was loaded into each wells of Sodium Dodecyl Sulfate Polyacrylamide Gel Electrophoresis (SDS-PAGE), later, the protein samples of the corneoconjunctival tissue were run on 12% gel via the SDS-PAGE and carried to a nitrocellulose membrane. The samples were then incubated overnight at 4 °C with primary antibodies against VEGF (sc-7269, Santa Cruz-Germany), TNF-α (ab8348, Abcam-UK), K10 (NBP1-97795, Novus Bio-USA), AdipoR1 (ab126611, Abcam-U.K.), AdipoR2 (ab77612, Abcam-U.K.), and beta-actin (sc-47778, Santa Cruz-Germany) (dilution: 1/500 for all antibodies).

After, the protein samples were incubated by the HRP-conjugated secondary antibody (1/1000) for 60 min at room temperature, the nitrocellulose membrane was colored with DAB and the protein levels calculated with an image program (Image J; National Institutes of Health, Bethesda, MD, USA)[3,2,28].

Tissue fixation and processing: After the mice were decapitated, their left and right eyes were removed for WBlot and IHC, fixed in 10% neutral buffered formaldehyde, sectioned in the vertical plane adjacent to the optic nerve, and embedded in paraffin. Serial sections in 5 µm thickness including the cornea, retina and optic nerve were cut.

IHC analysis: The paraffin embedded sections were deparaffinized in xylene and dehydrated using a series of graded alcohol. UltraVision™ ONE Detection System: HRP Polymer/ AEC Chromogen (ThermoFisher Scientific, Rockford, IL, USA) was used according to the manufacturer's protocol. Briefly; antigen retrieval was accomplished by microwaving the sections for 15 min in Citrate Buffer at pH6, then allowed to cool for 20 min. The sections were washed in PBS and primary antibodies were applied after Hydrogen Peroxide Block (5 min) and Ultra-V Block (5 min). The sections were incubated in primary antibodies,including VEGF (1/100, sc-7269), TNF-α (1/100, ab8348), K10 (1/100, NBP1-97795), AdipoR1 (1:20, ab126611), AdipoR2 (1:250, ab77612). Then incubation with primary antibodies against immunodetection was performed for 60 min at 37 ˚C with biotinylated goat anti–polyvalent, followed by peroxidase-labeled streptavidin using a labeled streptavidin biotin kit with a 3- Amino-9-Ethylcarbazol(AEC) (ThermoFisher Scientific, Rockford, IL, USA), as the chromogen substrate. The sections were counterstained with Gill's hematoxylin, and coverslips were attached using aqueous mounting media. The intensity and prevalence of the IHC staining was scored on a scale of 0 to +3 (0: absent, +1: weak, +2: medium, +3: strong). Scoring was done for each mouse,individually.

The TUNEL method: Sections were stained using In-Situ Cell Death Detection POD apoptosis kit (Boehringer Mannheim, Mannheim, Germany) following recommended standard procedures. After the tissue sections were taken on positively charged slides at a thickness of 5 µm, they were left to dry overnight in a 60 °C oven, deparaffinized in xylol, and dehydrated in serial alcohols. After the contours of the sections were drawn with a bounding pencil, they were kept with a 1:500 dilution of Protinase K solution for 7 min at room temperature. To stop endogenous peroxidase activity, 5 min of a blockage in 3% H_2O_2 prepared in methanol was applied. Then, each section was washed with 13 µL/cm^2 of equilibration buffer solution for 6 min at room temperature and covered with a plastic coverslip, then left in 100 µL terminal deoxynucleotidyl transferase (TdT) enzyme solution at 37 °C for 1 hour before being transferred to protein blocking serum for 10 min to prevent non-antigenic binding. All the tissue sections were incubated with anti-digoxigenin conjugate for 30 min at room temperature. They were washed 3 times with PBS for 5 min after each procedure, except for the incubation step with the protein blocking serum. DAB was used as the chromogen. For contrast staining, Gill's hematoxylin was used. Finally, the slides were covered with water-based adhesive (Bio-Optica, Milan, Italy). TUNEL staining was scored using the same scoring that was used in the IHC method described earlier.

Statistical analysis: SPSS 13.0 (SPSS Inc., Chicago, IL, USA) version was used for the statistical analysis of clinical parametric tests. An independent statistical analysis was applied to each test. Friedman test, used for non-parametric and repeated measurements, was applied to determine the difference between the different measurement times of a group for a specific test. In a group with significant differences, the Wilcoxon test was used to determine if there was a difference between the measurement times. The difference between the groups at each measurement time was assessed using Tukey's

test in one-way analysis of variance (ANOVA). Statistical results, set to $P < 0.05$ or $P < 0.001$, were accepted as significant.

The IBM SPSS Statistics 20.0 package program was used for statistical analysis of the WBlot, IHC, and TUNEL techniques. Group variability was tested with one-way ANOVA; post-hoc, Duncan, and Games-Howell tests were used for WBlot analysis; Tukey's test was used for the IHC and TUNEL analyses. Statistical results were accepted as significant at $P < 0.05$. For the reliability of the statistics, the measurements were repeated at least 3 times in the WBlot analysis.

Results

EAPPTT: For the EAPPTT parameter, the difference between all the groups was significant at all the measurement times ($P < 0.001$; Table 1) except at baseline ($P > 0.05$; Table 1). On the 15th day, the first measurement after BEC application, the highest aqueous tear production rate was recorded in CG, and the difference between this group and all the other groups was significant ($P < 0.05$; Table 1); however, the differences in the EAPPTT results between all the groups, except the CG, were insignificant ($P > 0.05$; Table 1). At the last measurement time of the study (30th day), the mean tear production rate in the treatment groups, ranging from highest to lowest, were: BAF35, BAF50, BAF100, and BAF20, although the difference was not statistically significant ($P > 0.05$; Table 1).

TBUT: For all measurement times, except baseline the difference between groups was statistically significant ($P < 0.001$; Table 2). On the 15th day, the highest mean TBUT mean (6.99±0.48 sec) was recorded in the CG subjects and the lowest TBUT was recorded in the DE group. The differences between all the groups on the 30th day, the last measurement time of the study, were found to be statistically significant ($P < 0.05$; Table 2). Among the treatment groups, it was determined that the BAF50 group had longest TBUT values and the BAF20 group had the shortest TBUT values.

Corneal fluorescein staining test: The baseline score for all the groups was 0 ($P > 0.05$; Table 3). For the other measurement times, a significant difference ($P < 0.001$; Table 3) was observed between the groups. On the 15th day of measurements, the difference between all the groups, except CG, was statistically insignificant ($P > 0.05$; Table 3). In the last measurement time (the 30th day), the lowest mean scores among the treatment groups were recorded in BAF35, BAF50, and BAF100 groups, with no statistically significant difference between them($P > 0.05$; Table 3). On the 30th day, the highest mean score among these groups was recorded in the BAF20 group.

WBlot analysis: VEGF and TNF-α inflammatory cytokine expression levels were measured in the highest DE group and the lowest in the CG and BAF35 groups, and these groups showed the significant differences with the other groups ($P < 0.05$; Fig. 1A,B,C). For K10, the highest levels were found in the DE, BAF20 and BAF100 groups ($P < 0.05$), and the lowest levels in the CG and BAF35 groups ($P < 0.05$; 1A,D). AdipoR1 and AdipoR2 protein expression levels determined higher in DE group in comparison to all the groups ($P < 0.05$; Fig. 1A,E,F). Compared to all other groups, the lowest AdipoR1 expression levels are in the CG group; the lowest AdipoR2 levels were measured in CG and BAF35 groups ($P < 0.05$; Fig. 1A,E,F).

IHC analysis and TUNEL method: For VEGF, it was found that immunoreactivity was evident in the corneal epithelium of the DE group (Fig. 2Aa). It was found that immunoreactivity was low in BAF50 and BAF100 groups along with BAF35 (Fig. 2Ab) in treatment groups, but not in CG (Fig. 2Ac). Immunoreactivity for TNF-a was found to be evident in the corneal epithelium and subepithelial corneal stromal cells of the DE group (Fig. 2Ba). In the treatment groups, immunoreactivity was lower in BAF35 (Fig.

Table 1. Statistical analysis of EAPPTT data according to measurement times and group variables (Mean ± standard deviation). *Baseline values of the study, a-e: There is a significant difference between groups containing different letters in the same column. ($P < 0.05$), ANOVA-Posthoc, Tukey test were used. A-F: The differences between groups that contain different letters on the same line are significant. ($P < 0.05$). Friedman was used for non-parametric tests and Wilcoxon test for intra-group comparisons. (n=10x 6 group)

Groups	Measurement Times							---*P*---
	Baseline* (mm/min)	15th day (mm/min)	18th day (mm/min)	22nd day (mm/min)	25th day (mm/min)	28th day (mm/min)	30th day (mm/min)	
CG	4.59±0.32	$4.74±0.37^{a}$	$4.79±0.15^{a}$	$4.67±0.26^{a}$	$4.61±0.40^{a}$	$4.39±0.25^{a}$	$4.55±0.41^{a}$	0.066
DE	$4.79±0.41^{A}$	$2.47±0.23^{Bb}$	$2.45±0.34^{Bd}$	$2.41±0.20^{Bd}$	$2.37±0.30^{Be}$	$2.42±0.32^{Be}$	$2.54±0.33^{Bd}$	0.001
BAF20	$4.50±0.36^{A}$	$2.39±0.27^{Cb}$	$2.94±0.20^{Bc}$	$2.97±0.20^{Bc}$	$3.04±0.17^{Bd}$	$3.07±0.19^{Bd}$	$3.07±0.16^{Bc}$	0.001
BAF35	$4.60±0.29^{A}$	$2.47±0.26^{Eb}$	$3.30±0.19^{Db}$	$3.34±0.21^{Db}$	$3.68±0.22^{Cb}$	$4.05±0.15^{Bb}$	$4.08±0.13^{Bb}$	0.001
BAF50	$4.59±0.31^{A}$	$2.42±0.28^{Fb}$	$2.95±0.19^{Ec}$	$3.15±0.13^{Dbc}$	$3.14±0.09^{DEcd}$	$3.52±0.19^{Cc}$	$3.95±0.18^{Bb}$	0.001
BAF100	$4.44±0.29^{A}$	$2.43±0.19^{Fb}$	$2.79±0.19^{Ec}$	$3.18±0.15^{Dbc}$	$3.39±0.12^{Cbc}$	$3.46±0.13^{Cc}$	$3.94±0.15^{Bb}$	0.001
---*P*---	0.292	0.001	0.001	0.001	0.001	0.001	0.001	

Table 2. Statistical analysis of TBUT data according to measurement times and group variables (Mean ± standard deviation). *Baseline values of the study, a-f: There is a significant difference between groups containing different letters in the same column. ($P < 0.05$), ANOVA-Posthoc, Tukey test were used. A-F: The differences between groups that contain different letters on the same line are significant. ($P < 0.05$). Friedman was used for non-parametric tests and Wilcoxon test for intra-group comparisons. (n=10x 6 group)

Groups	Measurement Times							---*P*---
	Baseline* (sec)	15th day (sec)	18th day (sec)	22nd day (sec)	25th day (sec)	28th day (sec)	30th day (sec)	
CG	7.25±0.44	$6.99±0.48^{a}$	$7.21±0.30^{a}$	$6.93±0.22^{a}$	$6.81±0.30^{a}$	$6.89±0.38^{a}$	$6.96±0.29^{a}$	0.161
DE	$6.99±0.33^{A}$	$2.15±0.32^{Be}$	$2.04±0.17^{Be}$	$2.08±0.29^{Be}$	$2.02±0.17^{Bd}$	$2.13±0.20^{Be}$	$2.18±0.26^{Bf}$	0.001
BAF20	$7.37±0.25^{A}$	$2.49±0.30^{Dbc}$	$3.53±0.22^{Cd}$	$4.39±0.24^{Bd}$	$4.59±0.24^{Bc}$	$4.48±0.29^{Bd}$	$4.49±0.18^{Be}$	0.001
BAF35	$7.19±0.21^{A}$	$2.69±0.21^{Eb}$	$3.92±0.20^{Dc}$	$4.98±0.25^{Cbc}$	$5.27±0.22^{Cb}$	$5.40±0.23^{BCc}$	$5.58±0.34^{Bc}$	0.001
BAF50	$7.27±0.41^{A}$	$2.17±0.29^{Fc}$	$4.29±0.28^{Eb}$	$5.02±0.29^{Db}$	$5.25±0.29^{Cb}$	$6.42±0.31^{Bb}$	$6.54±0.17^{Bb}$	0.001
BAF100	$7.30±0.38^{A}$	$2.62±0.27^{Eb}$	$4.29±0.32^{Db}$	$4.65±0.30^{Ccd}$	$4.55±0.40^{CDc}$	$4.69±0.51^{Cd}$	$4.99±0.33^{Bd}$	0.001
---*P*---	0.231	0.001	0.001	0.001	0.001	0.001	0.001	

Table 3. Statistical analysis of corneal fluorescein staining test scores according to measurement times and group variables (Mean ± standard deviation). *Baseline values of the study, a-d: There is a significant difference between groups containing different letters in the same column. ($P < 0.05$), ANOVA-Posthoc, Tukey test were used. A-G: The differences between groups that contain different letters on the same line are significant. ($P < 0.05$). Friedman was used for non-parametric tests and Wilcoxon test for intra-group comparisons. (n=10x 6 group)

Groups	Measurement Times							---*P*---
	Baseline* (score)	15th day (score)	18th day (score)	22nd day (score)	25th day (score)	28th day (score)	30th day (score)	
CG	0	0^{a}	0^{a}	0^{a}	0^{a}	0^{a}	0^{a}	------
DE	0^{A}	$3.55±0.37^{Cb}$	$3.45±0.37^{Cc}$	$3.45±0.37^{Cc}$	$3.45±0.37^{Cc}$	$3.25±0.26^{Bd}$	$3.10±0.21^{Bd}$	0.001
BAF20	0^{A}	$3.65±0.34^{Fb}$	$3.10±0.21^{Ebc}$	$2.80±0.26^{Db}$	$2.30±0.26^{Cb}$	$2.15±0.24^{Cc}$	$1.90±0.21^{Bc}$	0.001
BAF35	0^{A}	$3.60±0.39^{Gb}$	$3.10±0.32^{Fbc}$	$2.40±0.39^{Eb}$	$2.15±0.34^{Db}$	$1.50±0.41^{Cb}$	$0.75±0.59^{Bb}$	0.001
BAF50	0^{A}	$3.61±0.32^{Gb}$	$2.78±0.48^{Fb}$	$2.39±0.39^{Eb}$	$1.83±0.41^{Db}$	$1.22±0.48^{Cb}$	$0.50±0.41^{Bb}$	0.001
BAF100	0^{A}	$3.40±0.39^{Gb}$	$2.90±0.21^{Fb}$	$2.55±0.28^{Eb}$	$1.95±0.44^{Db}$	$1.60±0.52^{Cb}$	$0.55±0.37^{Bb}$	0.001
---*P*---	------	0.001	0.001	0.001	0.001	0.001	0.001	

2Bb) and BAF50 and BAF100. In CG, there was no immunoreactivity (Fig. 2Bc). For K10, immunoreactivity was most prominently detected in the corneal epithelium of the DE group (Fig. 2Ca). Immunoreactivity was found to be less pronounced in BAF50 (Fig. 2Cb) and BAF35 and BAF100. In CG, there was no immunoreactivity (Fig. 2Cc). Immunoreactivity for AdipoR1 was evident detected in the corneal epithelium of the DE group (Fig. 2Da). Immunoreactivity was less pronounced in the BAF50 group with BAF35 (Fig. 2Db). There was no AdipoR1 immunoreactivity in CG (Fig. 2Dc). Immunoreactivity for AdipoR2 was evident in the corneal epithelium of the DE group (Fig. 2Ea). It was found less in BAF20 and BAF35 groups with BAF50 (Fig. 2Eb). There was no AdipoR2 immunoreactivity in CG (Fig. 2Ec). In TUNEL staining, the number of apoptotic cells in the corneal epithelium of the DE group was found to be high (Fig. 2Fa). While the number of apoptotic cells was less common in BAF50 (Fig. 2Fb) and other treatment groups, it was not detected in CG (Fig. 2Fc).When all groups were evaluated according to the severity scores of the immunoreactive cells; for VEGF, the immunoreactive cell score was measured at the highest DE ($P < 0.05$) and the lowest at CG($P < 0.05$). In the treatment groups, the severity score of all the groups except for BAF20 was low (Fig. 3A). For TNF-α ve K10, the immunoreactive cell score was highest in the DE group($P < 0.05$) and the lowest in all other groups except BAF20 (Fig. 3B,C). For AdipoR1, the immunoreactive cell score was highest in the DE group ($P < 0.05$) and lowest in the CG, BAF35 and BAF50 groups (Fig. 3D). For AdipoR2, the immunoreactive cell score was highest in the DE group($P < 0.05$)and lowest in all other groups except BAF100 (Fig. 3E). For TUNEL, the immunoreactive cell score was highest in the DE group($P < 0.05$), lowest in the CG group($P < 0.05$), and low in all treatment groups with no statistically significant difference ($P > 0.05$) between them (Fig. 3F).

Discussion

DE is an complex ocular disorder characterized by excessive evaporation of the aqueous and alteration of the mucin components of PTF due to increased tear osmolarity, corneal and conjunctival epithelial damage, squamous metaplasia, and dysfunction or inflammation of the ocular surface and the tear glands[19,52,55,57]. To date, many experimental DE models have been established to investigate its complex pathogenesis and realize novel and effective treatment options[1,4,5,8,10,21,37,50]. Xiong *et al*[56] suggested that, although these models provide important data about the disease, each of them has its own characteristics and limitations; therefore, they do not fully reflect the complex etiopathogenesis and chronic form of DE. In their DE rabbit model, these investigators used BEC, a preservative constituent of ophthalmic preparations, as the DE inductive agent, which is well-known to rapidly and progressively destabilize PTF via altering its lipid and mucin layers. They found that BEC can reduce the amount of aqueous tear production and conjunctival goblet cells and increase corneal fluorescein and Rose Bengal staining areas in subjects. Many in vivo studies performed using mice[24,36], rats[41], cats[6] and rabbits[56] have shown that BEC also induces corneal and conjunctival inflammatory cell infiltration, excessive release of pre-inflammatory mediators, PGF instability, conjunctival goblet cell loss, corneal epithelial desquamation, erosions, ulceration, and corneal neovascularization. Considering its negative effects on the ocular surface, many researchers[19,36,55,56,59] have recently used BEC to establish a successful DE model in different animal species. The present study established murine DE model by topically applying 5 μL 0.2% BEC to both eyes of the subjects for 14 days. At the end of this period, the average tear production rate decreased, the TBUT shortened and corneal fluorescein staining scores increased significantly in comparison to the baseline values

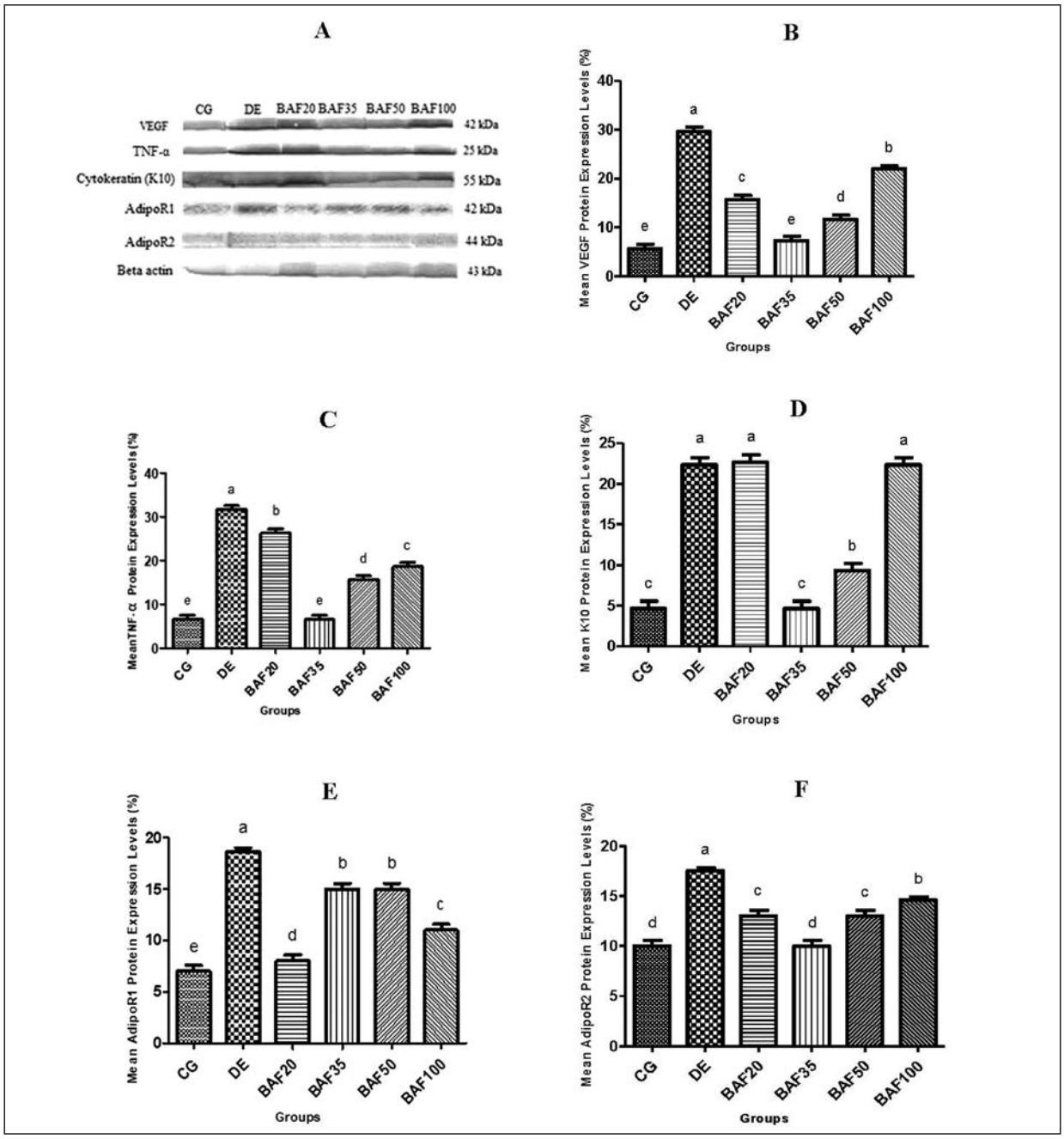

Fig. 1. Western blotting mean protein expression results (CG: Control group, DE: Dry Eye group). **A.** VEGF, **B.** TNF-α, **C.** K10, **D.** AdipoR1, **E.** AdipoR2, **F.** Western blotting protein bands. *a-e: Differences between groups with different letters are statistically significant ($P < 0.05$). One-Way ANOVA Post Hoc Duncan Test. (n = 3 x 6 groups, mean ± standard deviation). The protein expression levels in y-axis defined as percent of control.

in all subjects except for those in the CG having no BEC. It was also observed that all these abnormalities continued in the DE group until the end of the study. According to WBlot and IHC analyses of the corneal and conjunctival tissues obtained from all the group subjects at the end of the study, the levels of inflammatory cytokines, such as TNF-α and VEGF, and K10, markers of squamous metaplasia, and levels of AdipoR1 and AdipoR2, indicators of inflammatory

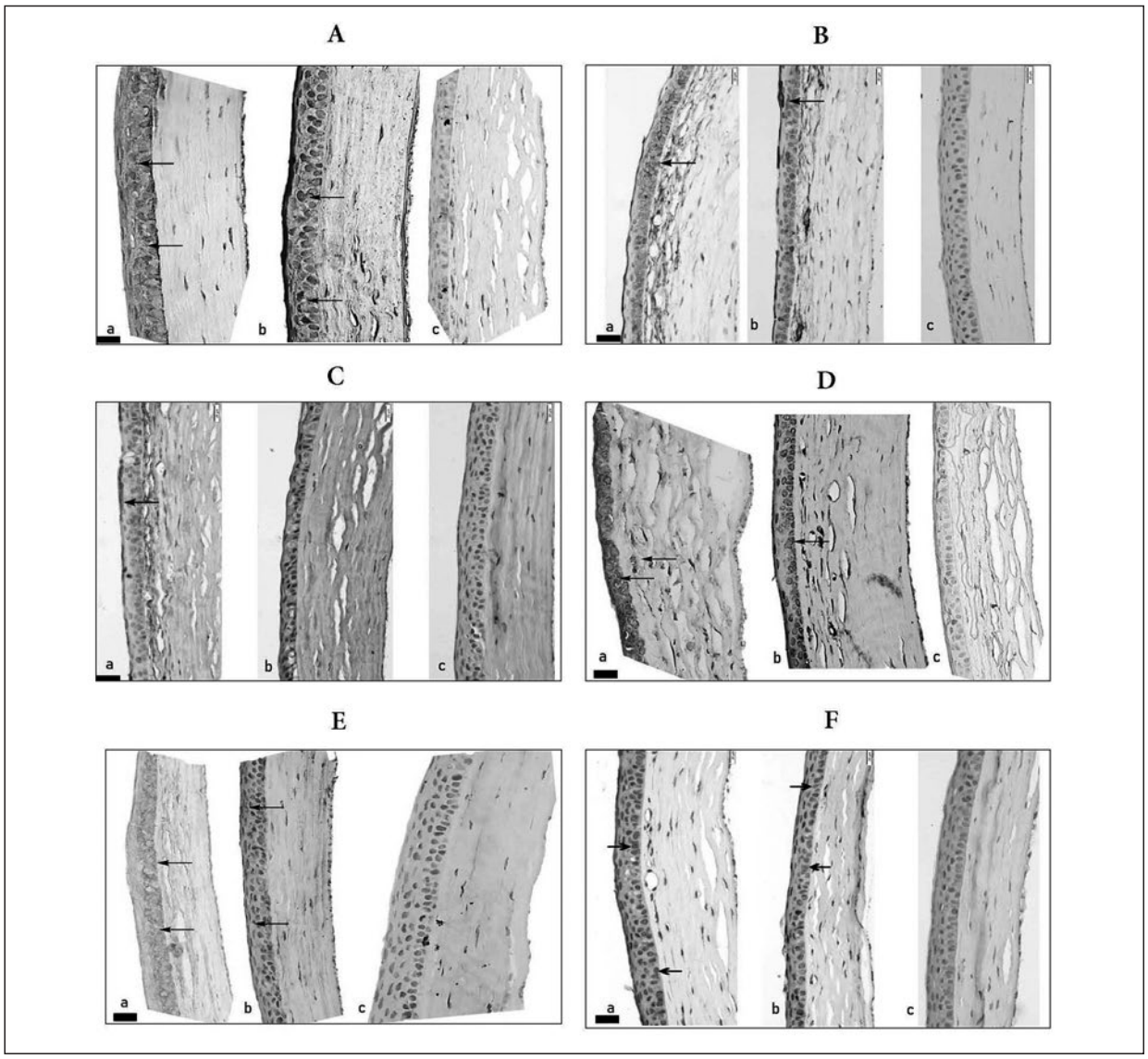

Fig. 2. IHC for immunoreactive cells, TUNEL method. A. VEGF (a) Increased immunoreactivity in corneal epithelium (arrows, mouse no: 1) in DE group, (b) Decreased immunoreactivity of corneal epithelium (arrows, mouse no: 3) in BAF35 group, (c) no immunreactivity in CG (mouse no: 4). **B. TNF-α**(a) Increased immunoreactivity in corneal epithelium (arrow, mouse no: 2) in DE group, (b) Decreased immunoreactivity of corneal epithelium (arrow, mouse no: 4) in BAF35 group, (c) No immunoreactivity in CG (mouse no: 3). **C. K10** (a) Increased immunoreactivity in corneal epithelium (arrow, mouse no: 3) in DE group, (b) Decreased immunoreactivity of corneal epithelium (mouse no: 4) in BAF50 group, (c) No immunoreactivity in CG (mouse no: 2). **D. AdipoR1** (a) Increased immunoreactivity (arrows, mouse no: 1) in DE group, (b) Decreased immunoreactivity (arrow, mouse no: 2) in BAF35 group, (c) No immunoreactivity in CG (mouse no: 5). **E. AdipoR2** (a) Increased immunoreactivity (arrows, mouse no: 5) in DE group (b) Decreased immunoreactive cells (arrows, mouse no: 5) in BAF50 group (c) No immunoreactivity in CG group (mouse no: 3). Immunoperoxidase staining, 400X, Bar:20 μm. **F. TUNEL method** (a) Increased apoptotic cells (arrows, mouse no: 4) in DE group, (b) Decreased apoptotic cells (arrows, mouse no: 3) in BAF50 group, (c) No apoptotic cells (mouse no: 4) CG group. TUNEL staining, 400X, Bars: 20 μm.

reaction, increased in the DE group. When all these parameters are evaluated together, it was concluded that BEC produced an effect similar to DE in both the molecular and clinical levels.

A decrease in the aqueous tear production rate, the most prominent clinical symptom of DE, triggers many inflammatory eye diseases, including DE, by activating the inflammatory process[15,35,38,46]. In recent years, EAPPTT has been used to measure the amount of aqueous tear

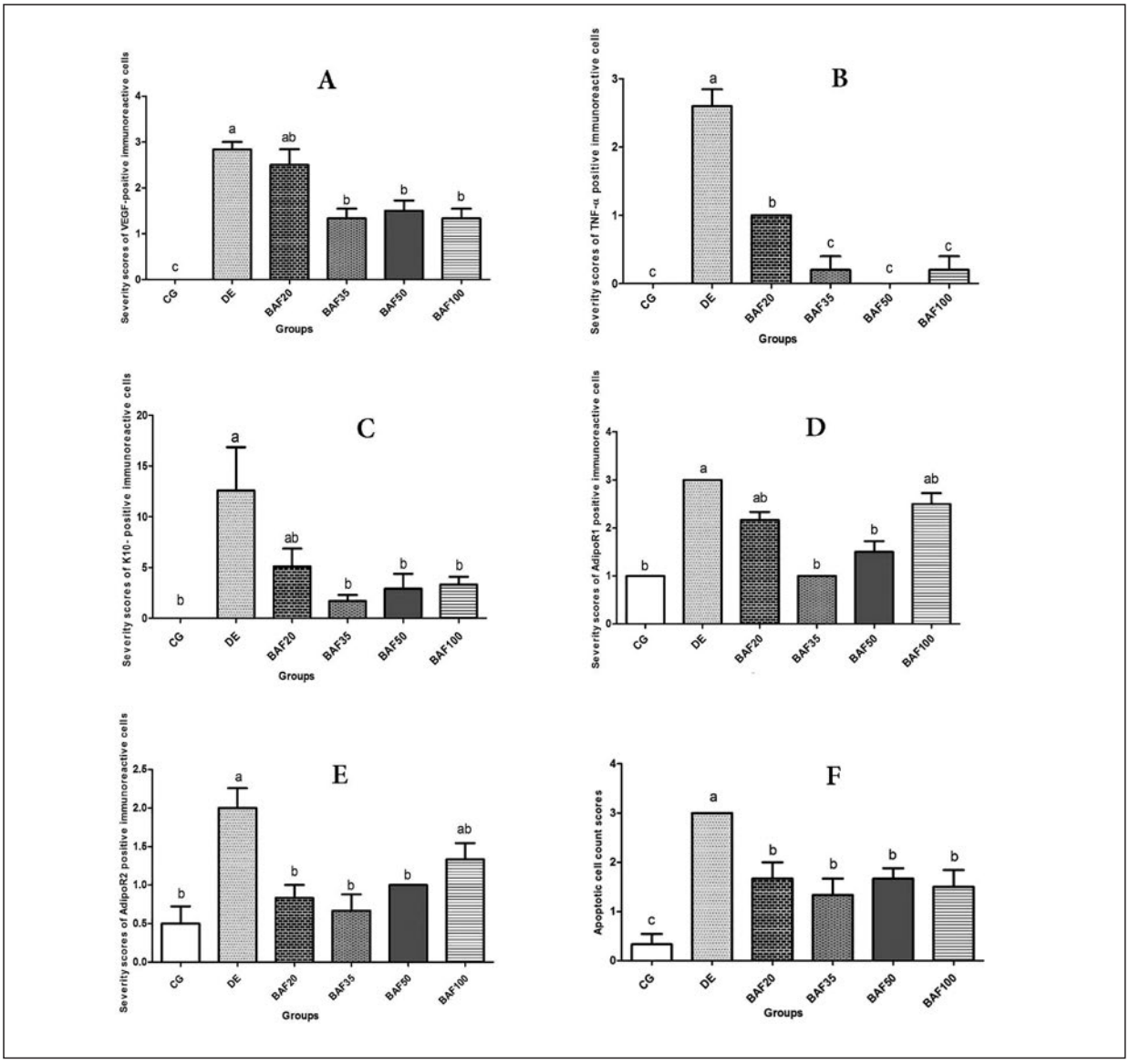

Fig. 3. Statistical bar graph of severity scores of immunoreactive cells in all groups (CG: Control group, DE: Dry eye group). **A.** VEGF, **B.** TNF-α, **C.** K10, **D.** AdipoR1, **E.** AdipoR2, **F.** TUNEL. *a-c: The difference between the groups with the different letters in the columns is significant ($P < 0.05$). (n=3 x 6 groups, mean ± standard deviation).

production in experimental studies using small laboratory and exotic animals[29,30]. This test was also used in the present study. Mean EAPPTT recorded in the initial measurements (baseline) of all subjects showed a statistically significant decrease tear rate in all the experimental groups in comparison to the tear rate at the time (14 days) of the first measurement after BEC administration. These data show that BEC causes a significant reduction in aqueous tear production. This reducing trend, which continued until the end of the study, especially in DE group, indicates that BEC suppresses the amount of aqueous tear production as long as it is applied. In murine DE models, where DE was induced twice daily with 0.2% BEC for 14 days[59] and with 0.1% BEC for 10 days[55], and where phenol red cotton thread test (PRTT) was used to measure aqueous tear production, this agent was found to significantly reduce aqueous tear production. Similar results

have been obtained in other DE model studies using BEC[23,36,54]. In the present study, when the treatment groups were evaluated according to the aqueous tear production parameter, it was found that the mean EAPPTT increased continuously for all the groups, except for the BAF20 group, at all measurement times after 15 days, and the difference between these groups at the last measurement (30th day) was not statistically significant. In a DE model investigating the therapeutic effects of 3 different concentrations of human amniotic fluid (20%, 50% and 100%), it was reported that all concentrations significantly increased aqueous tear production within 2 weeks; however the best result was obtained in amniotic fluid concentrations of 50% and 100%[45]. A similar result was obtained in another study using pure HAF; that study reported that pure HAF significantly decreased the corneal fluorescein score[44]. In the present study, as in the HAF study, the moderate and high concentrations of BAF (35%, 50%, and 100%) were found to have the most beneficial effect on the amount of aqueous tear production.

Evaluation of PTF stability is important, especially in revealing mucin and lipid tear deficiencies and determining dysfunction of meibomian gland[47,52]. In many DE model studies[11,19,32,36,51,54,55,59] tear film stability has been evaluated using TBUT. In a DE model in which 0.2% BEC was administered topically for 7 days in mouse eyes, it was found that TBUT gradually decreased in the experimental group in comparison to the CG, and the difference between these two groups was statistically significant[36]. Similar results were obtained in other DE model studies where 0.1% BEC was applied topically for 10 days[55] and 0.2% BEC for 14 days[59]. In the present study, mean TBUT was recorded as 7.00–7.37 sec in the baseline measurement in all the subjects, which decreased to 2.15–2.69 sec at the first measurement time after 14 days of BEC application. These data show that BEC impairs PTF stability in subjects. Mean TBUT measured on day 15 in all treatment groups was observed to be almost twice as long on day 30, the last measurement time of the study. Xiao *et al.*[55] found that the human amniotic membrane prolongs TBUT in aBEC induced DE model. Our study found beneficial effect on TBUT in all groups, with the longest TBUT value in the BAF50 group.

The corneal fluorescein staining test is routinely used to determine epithelial damage, PGF quality and ocular surface abnormalities[39]. Many DE studies on animals have reported that DE causes tear film instability, ocular inflammation, conjunctival goblet cell loss, and corneal neovascularization as well as corneal epithelial cell shedding and corneal erosions and ulceration[19,36,56,59]. Xiao *et al.*[54] determined that the corneal fluorescein staining scores increased in the first measurements of the subjects received 0.2% BEC twice a day for 14 days, the scores gradually started to decrease after BEC administration was discontinued. Using the same model, our study found that the corneal fluorescein staining score significantly increased in all the experimental groups at the first measurement time after administering BEC for 14 days in comparison to the baseline measurement. After stopping the BEC application and starting the BAF treatment, the corneal fluorescein staining scores decreased continuously until the end of the study in all treatment groups except for the BAF20 group. In the terms of the last measurement, the difference in the corneal fluorescein staining scores between the BAF35, BAF50, and BAF100 groups was not significant. Similar to our results, Quinto *et al.*[45] found that moderate and high density human amniotic fluid reduced the corneal fluorescein staining scores more effectively than a20% of BAF.

Ocular surface inflammation plays a key role both as a cause and a result of the pathogenesis of the DE cycle[7,36,59]. Experimental studies have revealed inflammatory cell infiltrations and increased levels of inflammatory cytokine and chemokine (IL-1α-β, TNF-α, VEGF) in the lacrimal tissues and ocular surface epithelium of DE

patients[7,13,59,60]. Recently, many researchers who recognized the importance of the inflammatory process on DE pathogenesis have focused on measuring the levels of inflammatory cytokines and chemokine in the ocular tissues of the subjects using different techniques[19,31,58]. In the present study, the WBlot and IHC analyses showed that the DE group had the highest VEGF and TNF-α levels, suggesting that BEC induces an inflammatory reaction in corneoconjunctival tissues. As a matter of fact, the lowest VEGF and TNF-α levels in the treatment groups were recorded in the BAF35 group in the WBlot analysis and in the BAF35, BAF50, and BAF100 groups in the IHC analysis. These data from the treatment groups indicate that moderate and high concentrations of BAF have a positive effect on the inflammatory process of DE. It has also been suggested[19] that this increase in the concentrations of the cytokines may accelerate the development of squamous metaplasia via inflammatory reaction. Squamous metaplasia, conversion of corneal epithelial cells to keratinizing cells or non-keratinized epithelium into squamous epithelium, is considered to be one of the important symptoms of chronic inflammatory diseases, such as DE[19,31,36]. The presence of squamous metaplasia is demonstrated by increases in the level of K10, an epidermis-specific cytokeratin[19,55]. Recent DE model studies using different measurement techniques[19,55,59] showed that the K10 levels were significantly higher in the corneal epithelium of the DE groups comparison to the controls. In the present study, the highest K10 levels in the corneoconjunctival tissue were recorded in DE, BAF20, and BAF100 groups using the WBlot technique and in the DE and BAF20 groups using IHC staining. As reported in previous studies[36,55,59] the results indicate that BEC-induced DE causes squamous metaplasia in the corneal epithelium of the subjects. In the present study, the lowest K10 levels were measured in the CG and the BAF35 groups according to WBlot analysis and in the BAF35, BAF50, and BAF100 groups according to IHC analysis. When the results of both analyses was evaluated together, the K10 levels were found to decrease significantly in all the treatment groups, except the BAF20 group.

Adiponectin, a protein that secrets from adipose tissues and is abundant in plasma, has anti-inflammatory, anti-diabetic, and anti-angiogenic properties in different tissues[33,34]. From this protein, three different receptors have been identified: AdipoR1, AdipoR2, and T-cadherin[20,34]. Katsiougiannis *et al.*[20] reported that inflammation accelerates adipose and fibrotic tissue formation in the lacrimal glands and ocular tissue; and this suggests that adipocytes may be an important marker in the defense or repair repertoire of these tissues. In the present study, the WBlot and IHC analyses showed that the DE group had the highest AdipoR1 and AdipoR2 levels, which supports the claims of Katsiougiannis *et al.*[20] that adipocyte density increased in cases of inflammation. When the WBlot and IHC analyses were evaluated together, the AdipoR1 and AdipoR2 levels were lower in the BAF treatment groups than the DE group. These results indicate that BEC has an inflammatory effect on the ocular surface and that different concentrations of BAF suppress this inflammatory process to varying degrees.

It is suggested that the inflammatory process that plays a key role in DE pathogenesis and the subsequently development of squamous metaplasia induces epithelial apoptosis[19,36]. Apoptosis positive cells have been reported in the cornea, the conjunctiva, and the lacrimal glands using the TUNEL method[19,31,55]. Some studies[36,42] have reported that a high concentration of preservative agents, such as BEC, cause necrosis while low concentrations cause apoptosis. In the present study, in all groups, apositive staining response was obtained in the epithelial and stromal layers of the cornea with the highest apoptotic cell score in the DE group and the lowest score in CG; no significant difference in the apoptotic cell score was found between the treatment groups. Moreover, the apoptotic cell

score was lower in the BAF treatment groups than the DE group. Similar results have also been reported in previous studies[19,36,55], which found that low BEC concentrations may lead to epithelial apoptosis on the ocular surface. Furthermore, the efficacy of all the BAF concentrations against epithelial apoptosis in which we compared the therapeutic effects supports the view expressed Lin *et al.*[36] that suppression of apoptosis is important in the treatment of ocular surface disorders.

In the present study, all the parameters, including the clinical tests and observations as well as the WBlot, IHC, and TUNEL analyses, demonstrate that moderate to high concentrations of BAF had positive effects on both the molecular and clinical signs of BEC- induced DE. The diagnostic methods used in this study were designed by considering the relationship between the clinical forms of DE and pathogenesis this condition. In two previous DE models[44,45] in which the therapeutic effect of HAF was investigated, the diagnosis was largely established based on the results of clinical tests; however, in addition to these tests, the present study used specific complementary molecular tests, such as IHC, WBlot, and TUNEL, to implement an inclusive diagnostic strategy to investigate the therapeutic effect of BAF, expecting it to be an alternative biological agent to HAF. This approach allowed the results obtained from each measurement technique to be interrelated and supportive, thus enabling a broader evaluation of the study.

Acknowledgements

This study was financially supported by The Scientific and Technological Research Council of Turkey (TUBITAK). (Project number: 116O927). The data of this study were presented as an oral presentation at the 2nd International Veterinary Surgery Congress of Turkey.

References

1) Altinors DD, Bozbeyoglu S, Karabay G, Akova YA. Evaluation of ocular surface changes in a rabbit dry eye model using a modified impression cytology technique. Curr Eye Res 32, 301-307, 2007.
2) Aslan A, Gok O, Erman O, Kuloglu T. Ellagic acid impedes carbontetrachloride- induced liver damage in rats through suppression of NF-kB, Bcl-2 and regulating Nrf-2 and caspase pathway. Biomed Pharmacother 105, 662-669, 2018.
3) Aslan A. The effects of different essential fruit juice and their combination on Saccharomyces cerevisiae cell growth. Prog Nutr 17, 36-40, 2015.
4) Barabino S, Dana MR. Animal Models of dry eye: A critical Assessment of Opportunities and Limitations. Invest Ophthalmol Vis Sci 45, 1641-1646, 2004.
5) Barabino S, Shen L, Chen L, Rashid S, Rolando M, Dana MR. The controlled- environment chamber: a new mouse model of dry eye. Invest Ophthalmol Vis Sci 46, 2766- 2771, 2005.
6) Bates N, Edwards N. Benzalkonium chloride exposure in cats: a retrospective analysis of 245 cases reported to the Veterinary Poisons Information Service (VPIS). Vet Rec 176, 229, 2015.
7) Brignole F, Pisella PJ, Goldschild M, De Saint Jean M, Goguel A, Baudouin C. Flow cytometric analysis of inflammatory markers in conjunctival epithelial cells of patients with dry eyes. Invest Ophthalmol Vis Sci 41, 1356-1363, 2000.
8) Burgalassi S, Panichi L, Chetoni P, Saettone MF, Boldrini E. Development of a simple dry eye model in the albino rabbit and evaluation of some tear substitutes. Ophthalmic Res 31, 229-235, 1999.
9) Calonge M. The Treatment of Dry Eye. Surv Ophthalmol 45, 227-239, 2001.
10) Chen W, Zhang X, Zhang J, Chen J, Wang S, Wang Q, Qu J. A murine model of dry

eye induced by an intelligently controlled environmental system. Invest Ophthalmol Vis Sci 49, 1386-1391, 2008.

11) Choi JH, Kim JH, Li Z, Oh HJ, Ahn KY, Yoon KC. Efficacy of the mineral oil and hyaluronic acid mixture eye drops in murine dry eye. Korean J Ophthalmol 29, 131-137, 2015.

12) Esmaeili A, Abbasian B, Kazemini H, Adibi S. Effect of bovine amniotic fluid on intra-abdominal adhesion in male rats. Int J Surg 8,639-42, 2010.

13) Fabiani C, Barabino S, Rashid S, Dana MR. Corneal epithelial proliferation and thickness in a mouse model of dry eye. Exp Eye Res 89, 166-171, 2009.

14) Foulks GN. Pharmacological management of dry eye in the elderly patient. Drugs Aging 25, 105-118, 2008. 15)Gayton JL. Etiology, prevalance, and treatment of dry eye disease. Clin Ophthalmol 3, 405-412, 2009.

15) Gayton JL. Etiology, prevalance, and treatment of dry eye disease. Clin Ophthalmol 3, 405-412, 2009.

16) Gonenci R, Altug ME, Koc A, Yalcin A. Effects of Bovine Amniotic Fluid on Acute Corneal Alkali Burns in the Rat. J Anim Vet Adv 8, 617-623, 2009.

17) Gumus K, Cavanagh DH. The role of inflammation and antiinflammation therapies in keratoconjunctivitis sicca. Clin Ophthalmol 3, 57-67, 2009.

18) Herretes S, Suwan-Apichon O, Pirouzmanesh A, Reyes JM, Broman AT, Cano M, Gehlbach PL, Gurewitsch ED, Duh EJ, Behrens A. Use of topical human amniotic fluid in the treatment of acute ocular alkali injuries in mice. Am J Ophthalmol 142, 271-278, 2006.

19) Kang SW, Kim KA, Lee CH, Yang SJ, Kang TK, Jung JH, Kim TJ, Oh SR, Jung SH. A standardized extract of Rhynchosia volubilis Lour. exerts a protective effect on benzalkonium chloride-induced mouse dry eye model. J Ethnopharmacol 215, 91-100, 2018.

20) Katsiougiannis S, Kapsogeorgou EK, Manoussakis MN, Skopouli FN. Salivary gland epithelial cells: a new source of the immunoregulatory hormone adiponectin. Arthritis Rheum 54, 2295-2299, 2006.

21) Kilic S, Kulualp K. Efficacy of Several Therapeutic Agents in a Murine Model of Dry Eye Syndrome. Comp Med 66, 112-118, 2016.

22) Kilic S, Kulualp K. Tear Production Rate in a Mouse Model of Dry Eye According to the Phenol Red Thread and Endodontic Absorbent Paper Point Tear Tests. Comp Med 66, 112-118, 2016.

23) Kim KA, Hyun LC, Jung SH, Yang SJ. The leaves of Diospyros kaki exert beneficial effects on a benzalkonium chloride-induced murine dry eye model. Mol Vis 22, 284-293, 2016.

24) Kim YH, Jung JC, Jung SY, Yu S, Lee KW, Park YJ. Comparison of the Efficacy of Fluorometholone With and Without Benzalkonium Chloride in Ocular Surface Disease. Cornea 35, 234-42, 2016.

25) Kulualp K, Kilic S. Evaluation of the effects of different therapeutic agents on experimental dry eye (DE) for the purposes of ocular surface impairment in mice. J Anim Vet Adv 11, 1555–1563, 2012.

26) Kumar A, Chandra RV, Reddy AA, Reddy BH, Reddy C, Naveen A. Evaluation of clinical, antiinflammatory and antiinfective properties of amniotic membrane used for guided tissue regeneration: A randomized controlled trial. Dent Res J (Isfahan) 12, 127-135, 2015.

27) Kymionis GD, Bouzoukis DI, Diakonis VF, Siganos C. Treatment of chronic dry eye: focus on cyclosporine. Clin Ophthalmol 2, 829-836, 2008.

28) Laemmli UK. Cleavage of structural proteins during the assembly of the head of bacteriophage T4. Nature 227, 680-685, 1970.

29) Lange RR, Lima L, Montiani-Ferreira F. Measurement of tear production in black-tufted marmosets (Callithrix penicillata) using 3 different methods: modified Schirmer's I, phenol red thread, and standardized endodontic absorbent paper points. Vet Ophthalmol 15, 376–382, 2012.

30) Lange RR, Lima L, Przydzimirski AC, Montiani-Ferreira F. Reference values for the production of the aqueous fraction of the tear film measured by the standardized endodontic absorbent paper point test in different exotic and laboratory animal species. Vet Ophthalmol 17, 41–45, 2014.

31) Li J, Tan G, Ding X, Wang Y, Wu A, Yang Q, Ye L, Shao Y. A mouse dry eye model induced by topical administration of the air pollutant particulate matter 10. Biomed Pharmacother 96, 524-534, 2017.

32) Li Y, Cui L, Lee HS, Kang YS, Choi W, Yoon KC. Comparison of 0.3% Hypotonic and Isotonic Sodium Hyaluronate Eye Drops in the Treatment of Experimental Dry Eye. Curr Eye Res 42, 1108-1114, 2017.

33) Li Z, Cui L, Yang JM, Lee HS, Choi JS, Woo JM, Lim SK, Yoon KC. The Wound Healing Effects of Adiponectin Eye Drops after Corneal Alkali Burn. Curr Eye Res 41, 1424- 1432, 2016.

34) Li Z, Woo JM, Chung SW, Kwon MY, Choi JS, Oh HJ, Yoon KC. Therapeutic effect of topical adiponectin in a mouse model of desiccating stress-induced dry eye. Invest. Ophthalmol Vis Sci 54, 155-162, 2013.

35) Lima L, Lange RR, Turner-Giannico A, Montiani-Ferreira F. Evaluation of standardized endodontic paper point tear test in New Zealand white rabbits and comparison between corneal sensitivity followed tear tests. Vet Ophthalmol 1, 119-124, 2015.

36) Lin Z, Liu X, Zhou T, Wang Y, Bai L, He H, Liu Z. A mouse dry eye model induced by topical administration of benzalkonium chloride. Mol Vis 17, 257-264, 2011.

37) Maitchouk DY, Beuerman RW, Ohta T, Stern M, Varnell RJ. Tear production after unilateral removal of the main lacrimal gland in squirrel monkeys. Arch Ophthalmol 118, 246-252, 2000.

38) McCabe E, Narayanan S. Advancements in anti-inflammatory therapy for dry eye syndrome. Optometry 80, 555-566, 2009.

39) Messmer EM. The pathophysiology, diagnosis, and treatment of dry eye disease. Dtsch Arztebl Int 112, 71-81, 2015.

40) Oriá AP, Oliveira AV, Pinna MH, Martins Filho EF, Estrela-Lima A, Peixoto TC, Silva RM, Santana FO, Meneses ÍD, Requião KG, Ofri R. Ophthalmic diagnostic tests, orbital anatomy, and adnexal histology of the broad-snouted caiman (Caiman latirostris). Vet Ophthalmol 1, 30-39, 2015.

41) Pauly A, Labbe A, Baudouin C, Liang H, Warnet JM, Brignole-Baudouin F. In vivo confocal microscopic grading system for standardized corneal evaluation: application to toxic-induced damage in rat. Curr Eye Res 33, 826-838, 2008.

42) Pauly A, Brignole-Baudouin F, Labbé A, Liang H, Warnet JM, Baudouin C. New tools for the evaluation of toxic ocular surface changes in the rat. Invest Ophthalmol Vis Sci 48, 5473-5483, 2007.

43) Pinto-Fraga J, López-de la Rosa A, Blázquez Arauzo F, Urbano Rodríguez R, González-García MJ. Efficacy and Safety of 0.2% Hyaluronic Acid in the Management of Dry Eye Disease. Eye Contact Lens 43, 57-63, 2016.

44) Quinto GG, Camacho W, Castro-Combs J, Li L, Martins SA, Wittmann P, Campos M, Behrens A. Effects of topical human amniotic fluid and human serum in a mouse model of keratoconjunctivitis sicca. Cornea 31, 424-430, 2012.

45) Quinto GG, Castro-Combs J, Li L, Gupta N, Campos M, Behrens A. Outcomes of different concentrations of human amniotic fluid in a keratoconjunctivitis sicca-induced mouse model. Int Ophthalmol 36, 643-650, 2016.

46) Rolando M, Zierhut M. The ocular surface and tear film and their dysfunction in dry eye disease. Surv Ophthalmol 2, 203-210, 2001.

47) Savini G, Prabhawasat P, Kojima T, Grueterich M, Espana E, Goto E. The challenge of dry eye diagnosis. Clin Ophthalmol 2, 31-55, 2008.

48) She Y, Li J, Xiao B, Lu H, Liu H, Simmons PA, Vehige JG, Chen W. Evaluation of a Novel Artificial Tear in the Prevention and

Treatment of Dry Eye in an Animal Model. J Ocul Pharmacol Ther 31, 525-30, 2015.
49) Skalicky SE, Petsoglou C, Gurbaxani A, Fraser CL, McCluskey P. New agents for treating dry eye syndrome. Curr Allergy Asthma Rep 13, 322-328, 2013.
50) Sullivan DA, Allansmith MR. Hormonal modulation of tear volume in the rat. Exp Eye Res 42, 131-139, 1986.
51) Sung MS, Li Z, Cui L, Choi JS, Choi W, Park MJ, Park SH, Yoon KC. Effect of Topical 5-Aminoimidazole-4-carboxamide-1-β-d-Ribofuranoside in a Mouse Model of Experimental Dry Eye. Invest Ophthalmol Vis Sci 56, 3149-3158, 2015.
52) Tavares Fde P, Fernandes RS, Bernardes TF, Bonfioli AA, Soares EJ. Dry eye disease. Semin Ophthalmol 25, 84-93,2010.
53) Urzua CA, Vasquez DH, Huidobro A, Hernandez H, Alfaro J. Randomized double-blind clinical trial of autologous serum versus artificial tears in dry eye syndrome. Curr Eye Res 37, 684-888, 2012.
54) Xiao X, He H, Lin Z, Luo P, He H, Zhou T, Zhou Y, Liu Z. Therapeutic effects of epidermal growth factor on benzalkonium chloride-induced dry eye in a mouse model. Invest Ophthalmol Vis Sci 53, 191-197, 2012.
55) Xiao X, Luo P, Zhao H, Chen J, He H, Xu Y, Lin Z, Zhou Y, Xu J, Liu Z. Amniotic membrane extract ameliorates benzalkonium chloride-induced dry eye in a murine model. Exp Eye Res 115, 31-40, 2013.
56) Xiong C, Chen D, Liu J, Liu B, Li N, Zhou Y, Liang X, Ma P, Ye C, Ge J, Wang Z. A rabbit dry eye model induced by topical medication of a preservative benzalkonium chloride. Invest Ophthalmol Vis Sci 49, 1850-1856, 2008.
57) Yagci A, Gurdal C. The role and treatment of inflammation in dry eye disease. Int Ophthalmol 34, 1291-1301, 2014.
58) Yang QC, Bao J, Li C, Tan G, Wu AH, Ye L, Ye LH, Zhou Q, Shao Y. A murine model of dry eye induced by topical administration of erlotinib eye drops. Int J Mol Med 41, 1427-1436, 2018.
59) Zhang Z, Yang WZ, Zhu ZZ, Hu QQ, Chen YF, He H, Chen YX, Liu ZG. Therapeutic effects of topical doxycycline in a benzalkonium chloride-induced mouse dry eye model. Invest Ophthalmol Vis Sci 55, 2963-2974, 2014.
60) Zhu L, Shen J, Zhang C, Park CY, Kohanim S, Yew M, Parker JS, Chuck RS. Inflammatory cytokine expression on the ocular surface in the Botulinum toxin B induced murine dry eye model. Mol Vis 15, 250-258, 2009.

Japanese Journal of Veterinary Research 68(3): 187-195, 2020

JJVR

REGULAR PAPER Experimental Research

Cold Exposure Increases Circulating miR-122 Levels via UCP1-Dependent Mechanism in Mice

Jussiaea Valente Bariuan[1)], Yuko Okamatsu-Ogura[1,*)], Ayumi Tsubota[1)], Shinya Matsuoka[1)], Masayuki Saito[1)] and Kazuhiro Kimura[1)]

[1)] *Laboratory of Biochemistry, Faculty of Veterinary Medicine, Hokkaido University, Sapporo 060-0818, Japan*

Received for publication, February 27, 2020; accepted, May 21, 2020

Abstract

MicroRNA(miR)-122 is highly expressed in liver and secreted into blood, which is reported to enter other tissues to modulate lipid metabolism. Brown adipose tissue (BAT) is responsible for nonshivering thermogenesis required for body temperature maintenance in cold environments. Since BAT activity is deeply related to lipid metabolism, there may be metabolic crosstalk between the liver and BAT through miR-122. In this study, we examined the effect of cold exposure on circulating miR-122 (cir-miR-122) levels in mice. Cold exposure significantly increased the expressions of Uncoupling protein 1 *(Ucp1)*, a key molecule for thermogenesis, indicating the activation of BAT. Cold exposure significantly increased cir-miR-122 level but caused no change in miR-122 and its precursor levels in the liver. In contrast, cold exposure significantly decreased miR-122 level in the muscle, but not in BAT, suggesting that increased cir-miR-122 was due to the enhancement of its secretion from the muscle. To examine whether BAT thermogenesis was a prerequisite for increased cir-miR-122 and decreased miR-122 level in the muscle, effect of cold exposure was examined in UCP1-KO mice. While the expressions of thermogenesis-related genes in BAT, except for that of *Ucp1*, was increased after cold exposure, no significant changes were observed in cir-miR-122 and muscle miR-122 level in UCP1-KO mice. These results suggest that cold-induced activation of BAT thermogenesis increased cir-miR-122 through the secretion from muscle, although further study is required to find the missing link between BAT thermogenesis and miRNA secretion from the muscle.

Key Words: brown adipose tissue, cold exposure, miRNA, skeletal muscle, uncoupling protein 1

Introduction

Mammals have two types of adipose tissue [8,12)]. White adipose tissue (WAT) stores energy as triglyceride and releases fatty acids when required. Brown adipose tissue (BAT) is a specialized tissue for non-shivering thermogenesis which depends on uncoupling protein 1 (UCP1), a mitochondrial protein specifically expressed in brown adipocytes. BAT thermogenesis plays an important role in the regulation of body temperature especially in a cold environment. Cold stimulation activates sympathetic nervous system (SNS), and norepinephrine (NE) released from nerve endings activates the ß-adrenergic receptor (ß-AR), particularly ß3-AR which is predominantly expressed in adipocytes, and induces lipolysis in both white and brown adipocytes. In brown adipocytes, liberated fatty acids (FAs) activate thermogenic activity of

* Corresponding author: Yuko Okamatsu-Ogura, DVM, PhD Laboratory of Biochemistry, Faculty of Veterinary Medicine, Hokkaido University, Sapporo 060- 0818, Japan
Tel.: +81-11-706-5205 Fax: +81-11-757-0703 E-mail: y-okamatsu@vetmed.hokudai.ac.jp
doi: 10.14943/jjvr.68.3.187

UCP1 and are simultaneously used as substrates for thermogenesis [17]. FAs released from white adipocytes are also used in brown adipocytes for thermogenesis [8]. The indispensable role of BAT-UCP1 thermogenesis in the regulation of body temperature is evidenced by the fact that the mice deficient in UCP1 are unable to maintain body temperature in a cold environment [15].

MicroRNAs (miRNAs) are short, endogenous non-coding RNAs that inhibit gene expression by targeting mRNAs for translational repression or cleavage [22,26]. Several miRNA have been reported to regulate brown adipogenesis [24,28,31]. miRNAs exist not only inside of cells but also in a variety of body fluids by binding to lipids or proteins or being packed in exosome, a small extracellular vesicle stably existing in fluid [19,22]. miRNA transported to other cells, can exhibit their effects in a paracrine and endocrine-like manner [13,32]. Brown adipocytes are reported to secrete miR-92a, and the serum level of exosomal miR-92a is correlated with BAT activity in both humans and mice [10].

miR-122 is miRNA expressed abundantly in liver that are found in high levels in the circulation. As such, circulating miR-122 is used as a biomarker for variety of liver pathologic conditions [4]. Intracellular miR-122 plays a pivotal role in regulation of lipid metabolism through the direct targeting of the genes involved in triglyceride (TG) synthesis, such as *Agpat1* [21] and *Dgat1* [9], or the indirect unknown mechanism. Liver-specific knockout of miR-122 mice shows TG accumulation in liver, due to the enhancement of TG synthesis and decreased secretion [21]. On the other hand, expression and secretion of hepatic miR-122 is regulated by FAs. Chai et al., revealed that injection of ß3-AR agonist activated lipolysis in WAT, and mobilized FAs to act on liver to increase the expression and secretion of miR-122 [9]. Thus, it is likely that adipose tissue is involved in the regulation of circulating miR-122 level through FAs. Although ß3-AR agonist simultaneously induces BAT thermogenesis, the role of BAT in miR-122 metabolism has not been examined. It was also shown that the circulating miR-122 entered other tissues including muscle, and reduced triglyceride storage by targeting mRNAs of enzymes involved in the triglyceride synthesis [9].

As mentioned above, BAT uses fatty acids for thermogenesis. It is also reported that BAT activation resulted in the clearance of plasma triglyceride and cholesterol [5-7]. Since the BAT activity is deeply related with lipid metabolism, it is possible that there is metabolic organ crosstalk between the liver and BAT through miR-122. In this study we analyzed circulating miR-122 in mice with activation of BAT thermogenesis by cold exposure.

Materials and Methods

Animals

The experimental procedures and care of animals were approved by the Animal Care and Use Committee of Hokkaido University. All experiments using mice were conducted in an animal facility approved by the Association for Assessment and Accreditation of Laboratory Animal Care (AAALAC) International. UCP1-KO (*Ucp1*$^{-/-}$) mice were kindly provided by Dr. L. Kozak (Pennington Biomedical Research Center, Baton Rouge, LA, U.S.A) All wild-type (WT; *Ucp1*$^{+/+}$) mice were C57BL/6J strain. Male C57BL/6J mice were purchased from Japan SLC Inc. (Hamamatsu, Japan). Mice were bred and housed in plastic cages placed in a room temperature controlled to 23±2°C with a 12:12 hr light: dark cycle and given free access to laboratory chow (Oriental Yeast, Tokyo, Japan).

Mice of 12- to 13-week old were individually caged and placed in a room with a temperature of 10±2°C or 23±2°C for 4 hr before the sampling. We chose mild cold condition because of the cold intolerant phenotype of UCP1-KO mice [15]. The duration of cold exposure treatment was determined in the reference to the previous report where the effect of ß3-AR agonist on cir-miR-122 was examined [9]. The mice were anesthetized by intraperitoneal injection of ketamine (75 mg/

kg; Ketalar, Daiichi-Sankyo, Tokyo, Japan) and medetomidine (1 mg/kg; Domitor, Zenoaq, Fukushima, Japan) before blood sampling from the jugular vein. Ethylenediaminetetraacetic acid (EDTA) was used as an anticoagulant for the blood samples. Euthanasia via cervical dislocation was conducted and organs including the liver, interscapular BAT (iBAT), gastrocnemius muscle were quickly taken and transferred into RNAlater storage solution (Life Technologies, Carlsbad, CA, U.S.A) for miRNA analysis.

Blood samples were centrifuged at 2000 rpm for 30 min to harvest the plasma. Samples that were still cloudy after 30 min of centrifuge were centrifuged at 3000 rpm for an additional 30 min before storage. Samples were stored at -80°C until use.

Extraction of miRNA and total RNA

Extraction of miRNA from plasma and tissue was achieved using miRNeasy kit (QIAGEN, Hilden Germany). For plasma samples, 100 µL of QIAzol reagent (QIAGEN) was added to 20 µL of isolated plasma and incubated for 5 min at room temperature. After the addition of 10 µL of 1 nM Cel-miR-39-3p spike-in (QIAGEN) and 20 µL of chloroform, samples were centrifuged at 12,000 x g for 15 min at 4 °C. For tissue samples, 10-20 mg of tissues stored in RNAlater were placed in a tube and 1 mL of QIAzol reagent was added. The samples were then homogenized using Mixer Mill 300 (Retsch, Haan, Germany), for 1 min and centrifuged after at 12,000 x g for 15 min at 4 °C. The upper aqueous phase of each sample, both plasma and tissue, was carefully transferred to a fresh tube, and 1.5 volumes of ethanol was added. Each sample was then applied directly to columns and after washing, miRNA was eluted in 12 and 40 µl of nuclease-free water for plasma and tissue samples, respectively. The quantity of miRNA was measured with Qubit microRNA assay kit (Thermo Fisher Scientific, Eugene, OR, U.S.A) reagents using a Qubit 3.0 Fluorometer (Thermo Fisher Scientific). Extraction of total RNA from tissue was achieved using TRIzol (Thermo Fisher Scientific) according to the manufacturer's instructions.

Real-time PCR

The extracted miRNA was reverse transcribed using a miR-X miRNA First Strand Synthesis kit (Clontech, Palo Alto, CA, U.S.A). Briefly, 1.5 µl of miRNA, with concentrations ranging from 0.4 to 0.6 ng/µL, was mixed with an mRQ enzyme and incubated at 37 °C for 1 h and then at 85 °C for 5 min. After the addition of 100 µl of ultrapure water, 2 µl of the sample was used for real-time PCR. For mRNA analysis, total RNA (2 µg) was reverse-transcribed using a 15-mer oligo(dT) adaptor primer and M-MLV reverse transcriptase (Promega, Madison, WI, U.S.A).

Real-time PCR was performed on a fluorescence thermal cycler (Light Cycler system, Roche Diagnostics, Mannheim, Germany) with FastStart Essential DNA Green Master (Roche Diagnostics), and primers specific to each miRNA or mRNA. For miRNA analysis, mRQ3' primer supplied by miRX miRNA First Strand Synthesis kit (Clontech) and miRNA-specific primer prepared according to the kit manual were used. Other primers used in the study are listed in Table 1.

Expressions of miRNA were normalized to Cel-miR-39-3p or small nuclear RNA U6 *(snRU6)* as reference. Expressions of mRNA were normalized to the expression levels of *Actb*.

Plasma non-esterified fatty acid (NEFA) and exosomal CD63 measurement

Plasma NEFA concentration was assayed using a NEFA C kit (Wako, Osaka, Japan) following the manufacturer's instructions.

Exosome level was measured using PS Capture Exosome ELISA Kit Anti Mouse IgG POD (Wako) according to the manufacturer's instructions with a slight modification. Briefly, plasma samples were incubated with stirring at room temperature for 2 hr in the Exosome Capture 96 Well Plate. After washing, anti-mouse CD63 monoclonal antibody (Biolegend,

Table 1. Primer sequences for quantitative real-time PCR.

Gene name (gene symbol): NCBI Reference Sequence number, Product size Forward, and reverse primer sequence
Small nuclear U6 (snRU6): XR_003953346.1, 107 bp
5' – CTCGCTTCGGCAGCACA - 3', 5' – AACGCTTCACGAATTTGCGT – 3'
Actin beta (Actb): NM_007393.5, 234 bp
5' – TCG TTA CCA CAG GCA TTG TGA T - 3', 5' – TGC TCG AAG TCT AGA GCA AC – 3'
Uncoupling protein 1 (Ucp1): NM_009463.3, 197 bp
5' – GTG AAG GTC AGA ATG CAA GC - 3', 5' – AGG GCC CCC TTC ATG AGG TC – 3'
Iodothyronine deiodinase 2 (Dio2): NM_010050.4, 130bp
5' – CAG TGT GGT GCA CGT CTC CAA TC – 3', 5' – TGA ACC AAA GTT GAC CAC CAG – 3'
Fibroblast growth factor 21 (Fgf21): NM_020013.4, 154bp
5' – CTG CTG GGG GTC TAC CAA G – 3', 5' – CTG CGC CTA CCA CTG TTC C – 3'
PR domain containing 16 (Prdm16): XM_006539175.4, 180bp
5' – GAC ATT CCA ATC CCA CCA GA – 3', 5' – CAC CTC TGT ATC CGT CAG CA – 3'
Cell death-inducing DNA fragmentation factor alpha (Cidea): NM_007702.2, 222bp
5' – CTT ATC AGC AAG ACT CTG GAT G – 3', 5' – GAA GGT GAC TCT GGC TAT TC – 3'
Cytochrome c oxidase subunit 4 (Cox4): NM_009941.3, 252 bp
5' – TGA GCC TGA TTG GCA AGA GA – 3', 5' – CGA AGC TCT CGT TAA ACT GG – 3'
Epithelial V-like antigen 1 (Eva1): NM_007962.4, 111bp
5' – CCA CTT CTC CTG AGT TTA CAG C – 3', 5' – GCA TTT TAA CCG AAC ATC TGT CC – 3'

CA, U.S.A) was added and incubated at room temperature for 1 hr. The plate was washed again and HRP-conjugated anti-mouse IgG was added and allowed to incubate with shaking at room temperature for 1 hr. The plate was washed again before reacting with TMB Solution at room temperature for 30 min. Stop Solution was added and absorbance was measured at 450 nm.

Data analysis

Statistical analyses were performed using the SPSS Statistics Version 23 software package from IBM (Chicago, IL, U.S.A). Differences between the treatment groups were analyzed by Student's t-test. P-values < 0.05 were considered to be statistically significant.

Results

First, we exposed mice to a cold temperature of 10°C for 4 hr and examined the gene expression in BAT. Cold exposure significantly increased the expression of the BAT marker, *Ucp1*, by 2-fold (Fig.1), indicating the activation of BAT. As reported previously [14], the expressions of *Dio2* and *Fgf21* were also significantly increased by cold exposure. The change in the expressions of other genes related to BAT thermogenic function including *Prdm16*, *Cidea*, and *Eva1* was negligible in this condition.

Next, we examined the effect of cold exposure on cir-miR-122. Cir-miR-122 levels of cold exposed mice increased by 3-fold compared to the control mice kept at 23°C (Fig 2A). However, cold exposure did not alter the plasma NEFA concentration (Fig 2B) and exosome level (Fig 2C). These results indicate that cold exposure increased cir-miR-122 was not due to plasma fatty acid level changes.

To identify the source of cir-miR-122 in cold-exposed mice, hepatic content of miR-122 was measured. Cold exposure did not show any changes in both hepatic miR-122 (Fig 3A) and

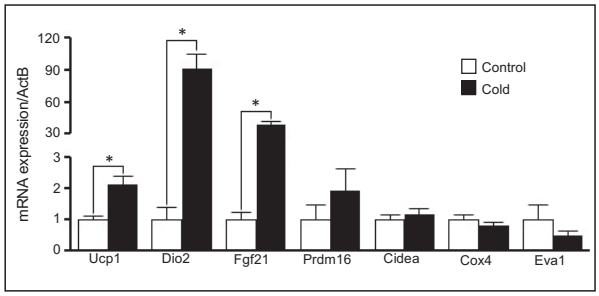

Fig. 1. Effect of cold exposure on thermogenic gene expressions in BAT of wild-type mice.

Wild-type mice were exposed to 23°C (Control) or 10°C (Cold) for 4 hr. Expressions of thermogenic genes in BAT were measured by real-time PCR. Data were normalized to *ActB* expression and expressed relative to the value of control group. Values are expressed as means ± SE (n=11 for control and n=8 for cold group). **P* < 0.05, Student's t-test.

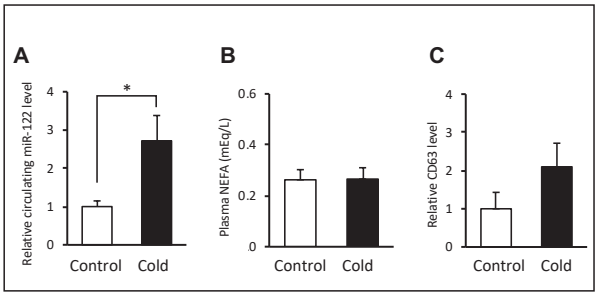

Fig. 2. miR-122 levels, NEFA concentration, and CD63 levels in the circulation of wild-type mice after cold exposure.

Mice were exposed to 23°C (Control) or 10°C (Cold) for 4 hr. Blood was taken from the jugular vein, and plasma miR122 levels (A), NEFA concentrations (B), and CD63 levels (C) were measured. Circulating miR-122 levels were measured by real-time PCR and normalized to the levels of spike-in cel-miR-39a. Values are expressed as means ± SE (n=11 for control and n=8 for cold group). Values are expressed as means ± SE. **P* < 0.05, Student's t-test.

pre-miR-122 levels (Fig 3B), suggesting that the increase in cir-miR-122 induced by cold exposure was unlikely due to the production nor the secretion from the liver. To examine the involvement of other tissues, iBAT and skeletal muscle were analyzed. The miR-122 level was not affected in iBAT (Fig 3C), but significantly decreased in muscle (Fig 3D).

UCP1-KO mice were used to directly examine the relation between the cold-induced BAT thermogenesis and the change in cir-miR-122 levels. Cold exposure for 4 hr in UCP1-KO mice caused significant increase in the expression of *Dio2* and *Cidea*, and not in *Fgf21*, *Prdm16*, and *Eva1*, although there was a tendency of increase (Fig.4A). These results indicate the cold exposure was sufficient in inducing the SNS-NE-ß-AR pathway for BAT thermogenesis in UCP1-KO mice [14]. In contrast to the response of WT mice, cold exposure did not change cir-miR-122 level, as well as plasma NEFA concentration and exosome level, in UCP1-KO mice (Fig 4B-D). Hepatic miR-122 level also failed to show any change in cold-exposed UCP1-KO mice (Fig 4E). MiR-122 level in BAT and skeletal muscle also did not change after cold exposure in UCP1-KO mice (Fig 4 F-G).

Discussion

In this study, we examined the effect of cold exposure on the cir-miR-122 levels in mice. Previously, it was reported that the injection of ß3-AR agonist CL316,243 increased expression and secretion of hepatic miR-122 and therefore cir-miR-122, through its action on WAT to mobilize FAs in circulation [9]. In addition to WAT lipolysis, ß3-AR agonist also induces BAT thermogenesis, however, the role of BAT in miR-122 metabolism has not been examined. Cold exposure is a potent physiological stimuli to induce BAT thermogenesis: it activates SNS, which leads to the stimulation of ß3-AR in BAT and WAT, as well as other types of adrenoceptor in many tissues. We found that cold exposure at 10°C for 4 hr resulted in a modest increase in cir-miR-122, without alteration of the plasma NEFA concentration. Thus, the increases in cir-miR-122 after cold exposure is likely independent of the effect of FAs on liver. In agreement with this idea, hepatic miR-122 level showed no change upon cold exposure. Although liver is known as a major source of cir-miR-122, it is plausible that the cold-induced elevation of cir-miR-122 may be not through the secretion from liver.

Since the cold exposure induces shivering and

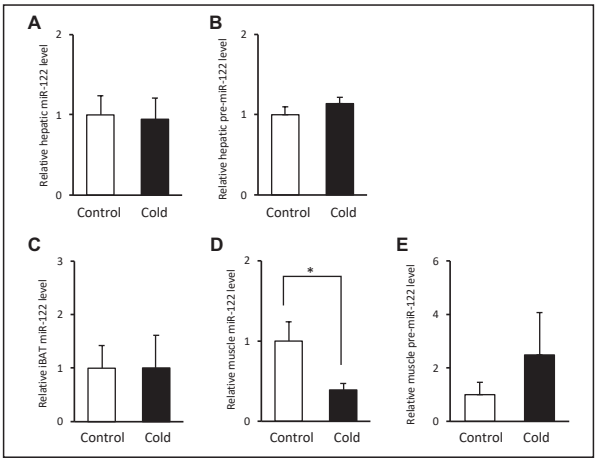

Fig. 3. Content of miR-122 and pre-miR-122 in tissues of wild-type mice after cold exposure.

Mice were exposed to 23°C (Control) or 10°C (Cold) for 4 hr. Tissue samples were taken and miR-122 levels in liver (A), gastrocnemius muscle (C) and BAT (D) (n=11 for control and n=8 for cold group) and pre-miR-122 in liver (B) (n=4 for control and cold groups) were measured by real-time PCR. Data were normalized to the levels of small nuclear RNA U6. Values are expressed as means ± SE. *$P < 0.05$, Student's t-test.

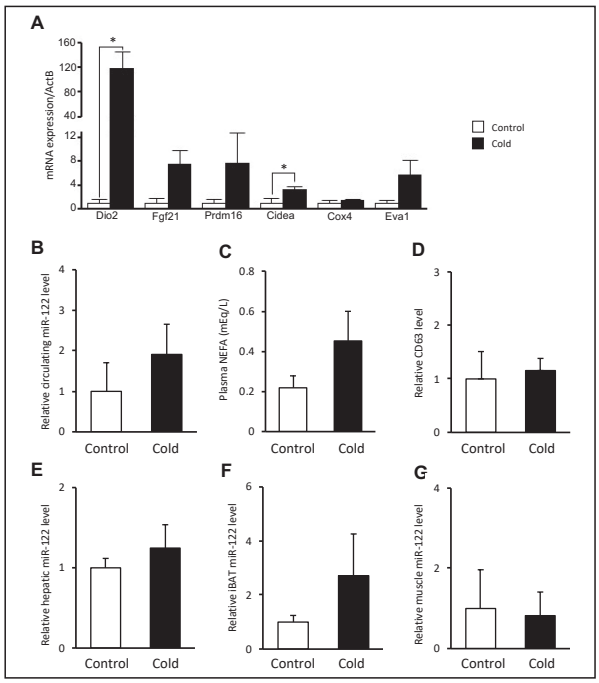

Fig. 4. Effect of cold exposure on gene expressions, plasma parameters, and tissue miR-122 levels in UCP1-KO mice.

UCP1-KO mice were exposed to 23°C (Control) or 10°C (Cold) for 4 hr. Expressions of thermogenic genes in BAT were measured by real-time PCR (A). Plasma miR-122 levels (B), NEFA concentrations (C) (n=6 for control and n=4 for cold group), and CD63 levels (D) (n=4 for control and cold groups) were measured. The miR-122 levels in liver (E), BAT (F), and gastrocnemius muscle (G) were also measured (n=6 for control and n=4 for cold group). Values are expressed as means ± SE. *$P < 0.05$, Student's t-test.

non-shivering thermogenesis [2,3,8], we examined the involvement of their responsible tissues, BAT and skeletal muscle, as a source of miR-122 upon cold exposure. miR-122 levels in BAT did not show any significant change after the cold exposure, whereas those in muscle were significantly decreased in the cold-exposed mice compared to the control mice. These results suggest that the release of miR-122 from muscle may contribute to the increase in cir-miR-122. It has been reported that skeletal muscle release various kinds of exosomal miRNAs that function in a paracrine or endocrine manner. For example, exosomal miRNAs derived from myotube were reported to downregulate Sirtuin1 (Sirt1) expression in myoblasts and affect their differentiation [18]. In addition, muscle-derived microRNAs that affect skeletal muscle development [20] or those increased after acute exercise [19] were reported. Thus, it is possible that muscle secretes miRNAs upon cold exposure. Since we found that miR-122 level in muscle is very low compared to that in liver (> 200-fold lower in muscle than that in liver), the physiological significance of this pathway is unknown. However, since skeletal muscle is the largest organ as total mass in whole body than other organs, it may give a significant contribution to circulating level of miR-122. Otherwise, it is also likely that muscle releases miR-122 to the circulation to reduce its intracellular level. In liver, the inhibition of miR-122 is reported to enhance fatty acid oxidation [16], possibly through the increase in the expression of target gene Sirt1 and subsequent activation of AMP-activated protein kinase pathway [25]. Thus, the reduced intracellular level of miR-122 in muscle may result in the increase in fatty acid oxidation, contributing to the effective supply of energy source for shivering thermogenesis.

In contrast to the results in WT mice, cold exposure in UCP1-KO mice did not cause the increase in the cir-miR-122 nor decrease in miR-122 in muscle, indicating that activation of UCP1 thermogenesis in BAT is essential for the release of miR-122 from muscle. It is not clear how the

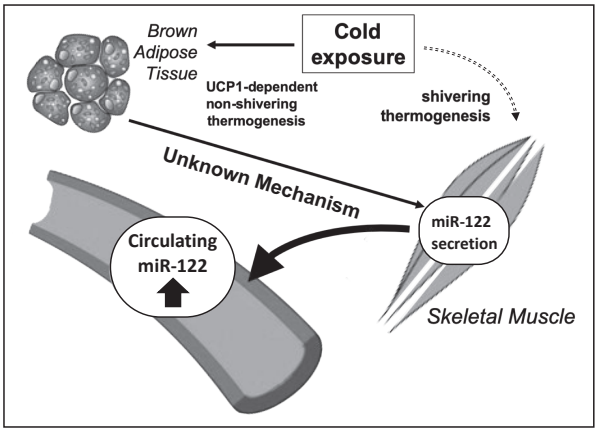

Fig. 5. Scheme of suggested mechanism for cold exposure-induced increase in circulating miR-122.
Cold exposure stimulates UCP1-dependent thermogenesis in BAT. BAT thermogenesis leads to the secretion of miR-122 from skeletal muscle through an unknown mechanism, resulting in the increase in circulating miR-122 (cir-miR-122). Shivering thermogenesis in skeletal muscle is also induced by cold exposure, but results from UCP1-KO mice suggest that it is irrelevant to the cir-miR-122 increase.

status of UCP1 activity in BAT was transmitted to muscle. Recently, it was reported that cold stimulation induces the release of succinate from muscle, and it is subsequently taken up by BAT, activating UCP1 thermogenesis [27]. Although it is unknown if the release of succinate is dependent on BAT activity, it is plausible that there is some inter-organ communication between BAT and muscle. It is also possible that the miR-122 release from muscle did not occur in UCP1-KO mice because of a compensatory phenotypic change for the loss of UCP1. It has been reported that non-shivering thermogenesis in muscle depending on SERCA or sarcolipin compensates the loss of UCP1-dependent thermogenesis in the BAT of UCP1-KO mice [2,3,29,30]. Such compensatory changes of muscle may possibly associate with the lack of the miR-122 release from muscle in UCP1-KO mice.

In summary, we found that cir-miR-122 is increased after cold exposure possibly through the secretion from muscle (Fig. 5). In addition, we found that the cold-induced increase in cir-miR-122 was dependent on UCP1-thermogenesis in BAT. It is not clear how BAT thermogenesis induced miR-122 secretion from muscle, however, there may be some cross talk between BAT and muscle as that reported between BAT and liver [1,11,33]. Further study is required to reveal the precise mechanism for the cold-induced increase in the cir-miR-122.

Acknowledgements

This study was supported by JSPS KAKENHI Grant Numbers 16K15485, 17K08118, 18H02274, and 18J21697.

References

1) Ameka M, Markan KR, Morgan DA, BonDurant LD, Idiga SO, Naber MC, Zhu Z, Zingman LV, Grobe JL, Rahmouni K, Potthoff MJ. Liver derived FGF21 maintains core body temperature during acute cold exposure. Sci Rep 9, 630, 2019.
2) Bal NC, Maurya SK, Sopariwala DH, Sahoo SK, Gupta SC, Shaikh SA, Pant M, Rowland LA, Bombardier E, Goonasekera SA, Tupling AR, Molkentin JD, Periasamy M. Sarcolipin is a newly identified regulator of muscle-based thermogenesis in mammals. Nat Med 18, 1575-1579, 2012.
3) Bal NC, Singh S, Reis FCG, Maurya SK, Pani S, Rowland LA, Periasamy M. Both brown adipose tissue and skeletal muscle thermogenesis processes are activated during mild to severe cold adaptation in mice. J Biol Chem 292, 16616-16625, 2017.
4) Bandiera S, Pfeffer S, Baumert TF, Zeisel MB. miR-122--a key factor and therapeutic target in liver disease. J Hepatol 62, 448-457, 2015.
5) Bartelt A, Bruns OT, Reimer R, Hohenberg H, Ittrich H, Peldschus K, Kaul MG, Tromsdorf UI, Weller H, Waurisch C, Eychmüller A, Gordts PL, Rinninger F, Bruegelmann K, Freund B, Nielsen P, Merkel M, Heeren J. Brown adipose tissue activity controls triglyceride clearance. Nat Med 17, 200-205, 2011.

6) Bartelt A, John L, Schaltenberg N, Berbée JFP, Worthmann A, Cherradi ML, Schlein C, Piepenburg J, Boon MR, Rinninger F, Heine M, Toedter K, Andreas N, Stefan KN, Markus F, Wijers SL, Lichtenbelt WM, Scheja L, Rensen PCN, Heeren J. Thermogenic adipocytes promote HDL turnover and reverse cholesterol transport. Nat Commun 8, 15010, 2017.
7) Berbée JFP, Boon MR, Khedoe PP, Bartelt A, Schlein C, Worthmann A, Kooijman S, Hoeke G, Mol IM, John C, Jung C, Vazirpanah N, Brouwers LP, Gordts PL, Esko JD, Hiemstra PS, Havekes LM, Scheja L, Heeren J, Rensen PC. Brown fat activation reduces hypercholesterolaemia and protects from atherosclerosis development. Nat Commun 6, 6356, 2015.
8) Cannon B and Nedergaard J. Brown adipose tissue: function and physiological significance. Physiol Rev 84, 277-359, 2004.
9) Chai C, Rivkin M, Berkovits L, Simerzin A, Zorde-Khvalevsky E, Rosenberg N, Klein S, Yaish D, Durst R, Shpitzen S, Udi S, Tam J, Heeren J, Worthma A, Galun E. Metabolic circuit involving free fatty acids, microRNA 122, and triglyceride synthesis in Liver and muscle tissues. Gastroenterology 153, 1404-1415, 2017.
10) Chen Y, Buyel JJ, Hanssen MJW, Siegel F, Pan R, Naumann J, Schell M, van derLans A, Schlein C, Froehlich H, Heeren J, Virtanen KA, Lichtenbelt WM, Pfeifer A. Exosomal microRNA miR-92a concentration in serum reflects human brown fat activity. Nat Comm 7, 11420, 2016.
11) Chen Z, Wang GX, Ma SL, Jung DY, Ha H, Altamimi T, Zhao XY, Guo L, Zhang P, Hu CR, Cheng JX, Lopaschuk GD, Kim JK, Lin JD. Nrg4 promotes fuel oxidation and a healthy adipokine profile to ameliorate diet-induced metabolic disorders. Mol Metab 6, 863-872, 2017.
12) Cinti S. The adipose organ at a glance. Dis Model Mech 5, 588-594, 2012.
13) Cortez MA, Bueso-Ramos C, Ferdin J, Lopez-Berestein G, Sood AK, Calin GA. MicroRNAs in body fluids—the mix of hormones and biomarkers. Nat Rev Clin Oncol 8, 467-477, 2011.
14) DeJong JM, Larsson O, Cannon B, Nedergaard J. A stringent validation of mouse adipose tissue identity markers. Am J Physiol. Endocrinol Metab 308, E1085-E105, 2015.
15) Enerback S, Jacobsson A, Simpson EM, Guerra C, Yamashita H, Harper ME, Kozak LP. Mice lacking mitochondrial uncoupling protein are cold-sensitive but not obese. Nature 387, 90-94, 1997.
16) Esau C, Davis S, Murray SF, Yu XX, Pandey SK, Pear M, Watts L, Booten SL, Graham M, McKay R, Subramaniam A, Propp S, Lollo BA, Freier S, Bennett CF, Bhanot S, Monia BP. miR-122 regulation of lipid metabolism revealed by in vivo antisense targeting. Cell Metab 3, 87-98, 2006.
17) Fedorenko A, Lishko PV, Kiszrichok Y. Mechanism of fatty-acid-dependent UCP1 uncoupling in brown fat mitochondria. Cell 151, 400-413, 2012.
18) Forterre A, Jalabert A, Chikh K, Pesenti S, Euthine V, Granjon A, Errazuriz E, Lefai E, Vidal H, Rome S. Myotube-derived exosomal miRNAs downregulate Sirtuin1 in myoblasts during muscle cell differentiation. Cell Cycle 13, 78-89, 2014.
19) Guescini M, Canonico B, Lucertini F, Maggio S, Annibalini G, Barbieri E, Luchetti F, Papa S, Stocchi V. Muscle releases alpha-sarcoglycan positive extracellular vesicles carrying miRNAs in the bloodstream. PloS One 10, e0125094-e0125094, 2015.
20) Horak M, Novak J, Bienertova-Vasku J. Muscle-specific microRNAs in skeletal muscle development. Dev Biol 410, 1-13, 2016.
21) Hsu SH, Wang B, Kota J, Yu J, Costinean S, Kutay H, Yu L, Bai S, La Perle K, Chivukula RR, Mao H, Wei M, Clark KR, Mendell JR, Caligiuri MA, Jacob ST, Mendell JT, Ghoshal

K. Essential metabolic, anti-inflammatory, and anti-tumorigenic functions of miR-122 in liver. J Clin Invest 122(8), 2871-83, 2012.
22) Huang-Doran I, Zhang CY, Vidal-Puig A. Extracellular vesicles: novel mediators of cell communication in metabolic disease. Trends Endocrinol Metab 28, 3-18, 2017.
23) Krol J, Loedige I, Filipowicz W. The widespread regulation of microRNA biogenesis, function and decay. Nat Rev Genet 11, 597-610, 2010.
24) Liu W, Bi P, Shan T, Yang X, Yin H, Wang YX, Liu N, Rudnicki MA, Kuang S. miR-133a regulates adipocyte browning in vivo. PLoS Genet 9, e1003626, 2013.
25) Long JK, Dai W, Zheng YW, Zhao SP. miR-122 promotes hepatic lipogenesis via inhibiting the LKB1/AMPK pathway by targeting Sirt1 in non-alcoholic fatty liver disease. Mol Med 25(1), 2, 2019.
26) Lorente-Cebrián S, González-Muniesa P, Milagro FI, Martínez JA. MicroRNAs and other non-coding RNAs in adipose tissue and obesity: emerging roles as biomarkers and therapeutic targets. Clin Sci 133, 23-40, 2019.
27) Mills EL, Pierce KA, Jedrychowski MP, Garrity R, Winther S, Vidoni S, Yoneshiro T, Spinelli JB, Lu GZ, Kazak L, Banks AS, Haigis MC, Kajimura S, Murphy MP, Gygi SP, Clish CB, Chouchani ET. Accumulation of succinate controls activation of adipose tissue thermogenesis. Nature 560, 102-106, 2018.
28) Mori M, Nakagami H, Rodriguez-Araujo G, Nimura K, Kaneda Y. Essential role for miR-196a in brown adipogenesis of white fat progenitor cells. PLoS Biol 10, e1001314, 2012.
29) Nowack J, Giroud S, Arnold W, Ruf T. Muscle non-shivering thermogenesis and its role in the evolution of endothermy. Front Physiol 8, 889, 2017.
30) Shabalina IG, Hoeks J, Kramarova TV, Schrauwen P, Cannon B, Nedergaard J. Cold tolerance of UCP1-ablated mice: A skeletal muscle mitochondria switch toward lipid oxidation with marked UCP3 up-regulation not associated with increased basal, fatty acid- or ROS-induced uncoupling or enhanced GDP effects. Biochim Biophys, Acta, Bioenerg 1797, 968–980, 2010.
31) Shamsi F, Zhang H, Tseng YH. MicroRNA regulation of brown adipogenesis and thermogenic energy expenditure. Front Endocrinol 8, 205, 2017.
32) Thomou T, Mori MA, Dreyfuss JM, Konishi M, Sakaguchi M, Wolfrum C, Rao TN, Winnay JN, Garcia-Martin R, Grinspoon SK, Gorden P, Kahn CR. Adipose-derived circulating miRNAs regulate gene expression in other tissues. Nature 542, 450-455, 2017.
33) Villarroya F, Gavaldà-Navarro A, Peyrou M, Villarroya J, Giralt M. The lives and times of brown adipokines. Trends in Endocrin Met 28, 855–867, 2017.

Japanese Journal of Veterinary Research 68(3): 197-202, 2020

JJVR

SHORT COMMUNICATION Regional Study

Isolation of methicillin-resistant *Staphylococcus aureus* ST398 from pigs in Japan

Yoshimasa Sasaki[1, 2, 3, *], Tetsuo Asai[2], Mika Haruna[3], Tsuyoshi Sekizuka[4], Makoto Kuroda[4] and Yukiko Yamada[3]

[1]Division of Biomedical Food Research, National Institute of Health Sciences, 3-25-26, Tonomachi, Kawasaki-ku, Kawasaki, Kanagawa 210-9501, Japan

[2]Department of Applied Veterinary Science, the United Graduate School of Veterinary Science, Gifu University, 1-1, Yanagido, Gifu 501-1193, Japan

[3]Food Safety and Consumer Affairs Bureau, Ministry of Agriculture, Forestry and Fisheries, 1-2-1, Kasumigaseki, Chiyoda-ku, Tokyo 100-8950, Japan

[4]Laboratory of Bacterial Genomics, Pathogen Genomics Center, National Institute of Infectious Diseases, 1-23-1 Toyama, Shinjuku-ku, Tokyo 162-8640, Japan

Received for publication, October 7, 2019; accepted, March 28, 2020

Abstract

Methicillin-resistant *Staphylococcus aureus* (MRSA) is a major concern for public health. Recent decades have seen the emergence and worldwide spread of livestock-associated MRSA, particularly sequence type (ST) 398, in pigs. Two investigations were conducted to confirm the presence of MRSA ST398 in domestic Japanese pigs. In the first investigation, nasal swabs were collected from 500 pigs on 50 pig farms between August 2012 and February 2013. MRSA ST398 was isolated from four pigs from a farm. In the second investigation, nasal swabs were collected from 480 pigs on 24 pig farms between November 2013 and March 2014. MRSA ST398 was isolated from 54 pigs on five farms. These results indicate that MRSA ST398 has become established in domestic Japanese pigs.

Key Words: MRSA, ST398, pig

Transmission of methicillin-resistant *Staphylococcus aureus* (MRSA) between pigs and humans in European countries was first reported in 2005[2, 26]. In a Dutch hospital located in a pig-dense area, a three-fold increase in MRSA incidence was observed over a few years[25]. These reports suggested that pig farming was a risk factor for MRSA carriage in the families of farmers and of their neighbours. Since then numerous studies of MRSA in pigs have been conducted in many countries, showing that some sequence type (ST) clonal lineages of MRSA, such as ST5, ST9, ST97, and ST398 are present in pigs[1, 8, 16, 20, 22]. These lineages can cause human MRSA infections[2, 6,12, 15, 18], are called livestock-associated MRSA (LA-MRSA) and are of great concern in human and veterinary medicine. Most LA-MRSA isolates from pigs belong to ST398[8, 16, 22].

Despite the prevalence of this MRSA ST in other regions, there had been no evidence of it in pigs in Japan. In Japan, approximately one thousand pigs are imported annually[19], all of which are required to undergo quarantine

* Corresponding author: Yoshimasa Sasaki, D.V.M., Ph.D., Division of Biomedical Food Research, National Institute of Health Sciences, 3-25-26, Tonomachi, Kawasaki-ku, Kawasaki, Kanagawa 210-9501, Japan
Phone: +81-44-270-6566; Fax: +81-44-270-6569 E-mail: ysasaki@nihs.go.jp
doi: 10.14943/jjvr.68.3.197

inspections prior to import. However, carriage of MRSA is not inspected because it is not a targeted infectious disease according to the Domestic Animal Infectious Disease Control Law. If pigs infected with MRSA are imported, MRSA could be introduced and spread among domestic pig farms. Evidence of this can be seen in Republic of Korea, which imports breeding pigs from Canada, Denmark and the USA, where MRSA ST398 was isolated from pigs in 2008[16]. According to e-Stat, which is a portal site for the Japanese Government Statistics (https://www.e-stat.go.jp), Japan has imported live pigs from these three countries for breeding purposes. To determine whether MRSA ST398 was present in domestic Japanese pig farms, we conducted two surveys of a large number of pig farms in geographically disparate regions in Japan.

In the first investigation, veterinarians visited a total of 50 pig farms (48 farrow-to-finish and 2 finishing farms) in four regions (ten in Tohoku, 23 in Kanto, seven in Tokai region on Honshu; and ten in Kyushu) between August 2012 and February 2013. These four regions are the main pork producing regions in Japan: accommodating more than 80% of the pigs in the whole country[19]. All farms participated voluntarily on condition of anonymity. On each farm, ten animals (6–29 weeks of age) were selected by veterinarians, totalling 500 pigs. A nasal swab sample was collected from each animal using a BBL CultureSwab Plus Amies Gel with Charcoal, Single Swab (Becton Dickinson, MD, USA). Samples were delivered under refrigeration to the Research Institute for Animal Science in Biochemistry and Toxicology (Kanagawa, Japan) within 24 hr. MRSA isolation was conducted within 48 hr of sampling according to the protocol recommended by the baseline survey on the prevalence of MRSA in holdings with breeding pigs in the EU[24]. In brief, the tip of each nasal swab was added to a tube containing 9 ml of Mueller Hinton broth (Becton Dickinson) containing 6.5% NaCl; the cultures were then incubated for 24 hr at 37 °C. After incubation, 1 ml of the enrichment culture was added to 10 ml tryptic soy broth (Becton Dickinson) containing 3.5 mg/l cefoxitin (Sigma-Aldrich, Tokyo, Japan) and 75 mg/l aztreonam (MP Biomedicals, OH, USA), and incubated for 24 hr at 37 °C. The resulting cultures were grown in CHROMagar MRSA medium (CHROMagar, Paris, France) for 24 hr at 37 °C. When suspected MRSA colonies were observed, up to three colonies per sample were isolated and identified using the API Staph system (Sysmex bioMérieux, Tokyo, Japan). One MRSA isolate per sample was subjected to molecular typing and antimicrobial susceptibility testing. Staphylococcal cassette chromosome *mec* (SCC*mec*) typing was performed using multiplex PCR-based amplification as previously described[13]. MRSA isolates were also characterized by *spa* repeat determination[11] and multilocus sequence typing[9]. Presence of genes encoding Panton-Valentine leukocidin toxin (*pvl*) was determined through PCR amplification[17]. *S. aureus* ATCC BAA-1556 was used as a *pvl*-positive control. Minimal inhibitory concentrations (MICs) of ten antimicrobials (ampicillin, chloramphenicol, ciprofloxacin, clindamycin, erythromycin, gentamicin, teicoplanin, tetracycline, oxacillin, and vancomycin) were determined using the broth microdilution method in dried plates (Eiken Chemical) following the guidelines of the Clinical and Laboratory Standards Institute[4, 5]. *S. aureus* ATCC 29213 was used for quality control.

MRSA was isolated from five (1%) pigs aged 5 months on two (4%) of the farms surveyed (farms a and d) (Table), both located in the Kanto region. All five MRSA isolates had the class A *mec* gene complex but were negative for *ccr*, and were classified as atypical. The *pvl* gene was not detected in any of these isolates. One MRSA isolate from "Farm a" was classified as *spa* types t002 and ST5 and was found to be resistant to six antimicrobials. The remaining four isolates were obtained from four different pigs reared in the same pen in "Farm d." All isolates were classified as ST398 and a novel *spa* type, t16450 (08-16-02-111-02-25-34-24-25). All four ST398 isolates were resistant to six or more antimicrobials.

Table. Isolation of MRSA from pigs

Farm code	Date of sampling	Prevalence of MRSA	No. of isolates	characteristics of MRSA isolates (ST/*spa* type/*mec* type/SCC*mec* type/antimicrobial resistance profile)
First investigatoin				
a	20 Nov. 2012	1/10	1	ST5/t002/A/atypical/ABPC, CLDM, CP, EM, MPIPC, TC
d	15 Nov. 2012	4/10	2	ST398/t16450/A/atypical/ABPC, CLDM, CP, EM, MPIPC, TC, GM
			2	ST398/t16450/A/atypical/ABPC, CLDM, CP, EM, MPIPC, TC
Second investigation				
a	28 Jan. 2014	4/20	2	ST5/t002/B/IVb/ABPC, CLDM, CP, EM, MPIPC, TC
			2	ST5/t002/B/IVb/ABPC, CLDM, EM, MPIPC, TC
b	17 Dec. 2013	12/20	1	ST10/t002/B/IVa/ABPC, CLDM, CP, EM, MPIPC, TC
			11	ST10/t002/B/IVa/ABPC, CP, MPIPC, TC
c	4 Feb. 2014	8/20	8	ST97/t1236 /C/V/ABPC, CLDM, CP, EM, MPIPC, TC
d	9 Jan. 2014	18/20	18	ST398/t16450/A/atypical/ABPC, CLDM, CP, EM, MPIPC, TC
e	9 Jan. 2014	2/20	2	ST398/t16450/A/atypical/ABPC, CLDM, CP, EM, MPIPC, TC
f	9 Jan. 2014	9/20	6	ST398/t16450/A/atypical/ABPC, CLDM, CP, EM, MPIPC, TC
			3	ST398/t3934/A/atypical/ABPC, CLDM, CP, EM, MPIPC, TC
g	9 Jan. 2014	11/20	3	ST398/t16450/A/atypical/ABPC, CLDM, CP, CPFX, EM, MPIPC, TC
			8	ST398/t3934/A/atypical/ABPC, CLDM, CP, CPFX, EM, MPIPC, TC
h	12 Mar. 2014	14/20	4	ST398/t034/C/V/ABPC, CLDM, CP, EM, MPIPC, TC
			3	ST398/t034/C/V/ABPC, CLDM, CP, EM, MPIPC
			3	ST398/t034/C/V/ABPC, CLDM, CP, MPIPC, TC
			4	ST398/t034/C/V/ABPC, CLDM, CP, CPFX, EM, MPIPC, TC

Abbreviation; ST: sequence type, ABPC: ampicillin, CLDM, clindamycin, CP: chloramphenicol, CPFX: ciprofloxacin, EM: erythromycin, MPIPC: oxacillin, TC: tetracycline, GM: gentamicin.

In the second investigation, veterinarians visited 24 pig farms (21 farrow-to-finish and 3 finishing farms) in the Kanto region between November 2013 and March 2014. Of the 24 pig farms, 21 had also participated in the first investigation. Nasal swabs were collected from 20 pigs (6–28 weeks of age) from at least two age groups at each farm, with each age group coming from one pen. The pigs tested in both investigations were determined to be healthy based on visual inspections by veterinarians.

MRSA was isolated from 78 pigs on eight farms, all of which had been surveyed in the initial investigation. Of these eight farms, two (farms a and d) were positive for MRSA in the first investigation. MRSA isolates belonging to ST5, ST10, and ST97 were isolated from three farms (a, b, and c). ST5, ST10, and ST97 isolates were classified as *spa* types t002, t002, and t1236, respectively. MRSA belonging to ST398 were isolated from five farms (d, e, f, g, and h) located within a 2 km radius of each other. From a total of 54 MRSA ST398 isolates, 29, 11, and 14 isolates were classified as *spa* types t16450, t3934, and t034, respectively. ST398/t16450, ST398/t034, and ST398/t3934 were isolated from four (d, e, f, and g), two (f and g) and one (h) farms, respectively. All 78 MRSA isolates were negative for *pvl*. SCC*mec* types of ST5/t002, ST10/t002, ST97/t1236, and ST398/t034 were IVb, IVa, V, and V, respectively. SCC*mec* types of ST398/t16450 and ST398/t3934 were classified as atypical, as no amplicons resulted from PCR for *ccr* typing.

Studies on the presence of MRSA in domestic Japanese pigs were conducted at abattoirs in 2009[3] and 2013[23] showed the presence of MRSA ST5, ST97 and ST221, but not MRSA ST398 or ST10. To the best of our knowledge, the isolation of MRSA ST398 from four pigs on a pig farm in the Kanto region in November 2012, is the first isolation of MRSA ST398 in pigs in Japan. Fourteen months later, in January 2014, MRSA ST398 was isolated from pigs on five farms, including the MRSA-positive farm from the first investigation. The number of sampled pigs at each farm in the second survey was twice that of the first. Although the probability of MRSA detection may have increased due to the larger sample size, these findings indicate that MRSA ST398 may have become established in Japan. Three ST398

lineages, t034, t3934 and t16450, were found in the present study. ST398/t034 is one of the major lineages of LA-MRSA in pigs[1, 8, 16,22] and most of which have SCC*mec* type V and are negative for *pvl*[16, 22]. ST398/t3934 is one of the minor lineages in pigs[7]. ST398/t16450 was first isolated in the world. The isolation of MRSA ST10 in pigs has never been reported in the world. High prevalence (60%, 12/20) in pigs in Farm b suggests that ST10 is also adapted to pigs as well as ST5, ST97 and ST398 lineages.

Koyama et al.[14] described the isolation of *pvl*-positive MRSA ST398 from a Chinese woman receiving steroid therapy for systemic lupus erythematosus in a Japanese hospital in 2015, representing the first documented case of MRSA ST398 in a human in Japan, while until 4 days prior to admission to the hospital, the subject had been outside of Japan for approximately 2 months. The patient had had no contact with animals or persons working or living with animals, and the MRSA ST398 isolate obtained was genetically close to a community-associated MRSA lineage detected in China. Thus, the subject was unlikely to have been infected with this isolate from animals in Japan. Nakaminami et al.[21] recently reported a case of intractable arthritis of the shoulder joint caused by *pvl*-positive MRSA ST1232 (a single-locus variant of ST398 belonging to clonal complex 398) in a patient in 2018. The transmission route was unclear because the patient reported no overseas travel or animal contact.

Furuno et al.[10] recently reported that at least 12 of 125 pigs imported from Europe and North America tested positive for MRSA ST398 during the quarantine period. These pigs infected with MRSA ST398 must have been released to domestic pig farms because the import of infected pigs is not prohibited, suggesting that the MRSA ST398 lineages isolated in this study may have been introduced into Japan by imported pigs. In this study, MRSA ST398 was not isolated from any regions other than Kanto. However, 6 years have passed since the first isolation of MRSA ST398. Because repeated importation of pigs infected with MRSA increases the possibility of MRSA spread throughout Japan, it is necessary to monitor the prevalence of MRSA ST398 in pigs throughout Japan.

Acknowledgements

This work was supported by the Ministry of Agriculture, Forestry and Fisheries of Japan. The authors wish to thank the pig farms and veterinarians for providing samples for this study.

Conflict of interest

None to declare.

References

1) Alt K, Fetsch A, Schroeter A, Guerra B, Hammerl JA, Hertwig S, Senkov N, Geinets A, Mueller-Graf C, Braeunig J, Kaesbohrer A, Appel B, Hensel A, Tenhagen BA. Factores associated with the occurrence of MRSA CC398 in herds of fattening pigs in Germany. BMC Vet Res 7, 69, 2011.
2) Armand-Lefevre L, Ruimy R, Andremont A. Clonal comparison of *Staphylococcus aureus* isolates from healthy pig farmers, human controls, and pigs. Emerg Infect Dis 11, 711-714, 2005.
3) Baba K, Ishihara K, Ozawa M, Tamura Y, Asai T. Isolation of methicillin-resistant *Staphylococcus aureus* (MRSA) from swine in Japan. Int J Antimicrob Agents 36, 352- 354, 2010.
4) Clinical and Laboratory Standards Institute. Performance standards for antimicrobial disk and dilution susceptibility tests for bacteria isolated from animals; approved standard. 4rd ed, CLSI document Vet08-4, Wayne, PA: CLSI, 2018.

5) Clinical and Laboratory Standards Institute. Performance standards for antimicrobial susceptibility testing; 28th informational supplement. CLSI document M100-S28, Wayne, PA: CLSI. 2018.
6) Cuny C, Wieler LH, Witte W. Livestock-associated MRSA: the impact on humans. Antibiotics 4, 521-543, 2015.
7) Dierikx CM, Hengeveld PD, Veldman KT, de Hann A, van der Voorde S, Dop PY, Bosch T, van Duijkeren E. Ten years later: still a high prevalence of MRSA in slaughter pigs despite a significant reduction in antimicrobial usage in pigs the Netherlands. J Antimicrob Chemother 71, 2414-2418, 2016.
8) Emborg HD, Porrero MC, Sanders P, Schuepbach G, Teale C, Tenhagen BA, Wagenaar J. Analysis of the baseline survey on the prevalence of methicillin-resistant *Staphylococcus aureus* (MRSA) in holdings with breeding pigs, in the EU, 2008 - Part A: MRSA prevalence estimates. EFSA Journal 7, 1376, 2009.
9) Enright MC, Day NP, Davies CE, Peacock SJ, Spratt BG. Multilocus sequence typing for characterization of methicillin-resistant and methicillin-susceptible clones of *Staphylococcus aureus*. J Clin Microbiol 38, 1008-1015, 2000.
10) Furuno M, Uchiyama M, Nakahara Y, Uenoyama K, Fukuhara H, Morino S, Kijima M. A Japanese trial to monitor methicillin-resistant *Staphylococcus aureus* (MRSA) in imported swine during the quarantine period. J Glob Antimicrob Resist 14, 182-184, 2018.
11) Harmsen D, Claus H, Witte W, Rothgänger J, Claus H, Turnwald D, Vogel U. Typing of methicillin-resistant *Staphylococcus aureus* in a university hospital setting by using novel software for *spa* repeat determination and database management. J Clin Microbiol 41, 5442-5428, 2003.
12) Köck R, Schaumburg F, Mellmann A, Köksal M, Jurke A, Becker K, Friedrich AW. Livestock-associated methicillin-resistant *Staphylococcus aureus* (MRSA) as causes of human infection and colonization in Germany. PLoS One 8, e55040, 2013.
13) Kondo Y, Ito T, Ma XX, Watanabe S, Kreiswirth BN, Etienne J, HiramatsuK. Combination of multiplex PCRs for staphylococcal cassette chromosome *mec* type assignment: rapid identification system for *mec, ccr,* and major differences in junkyard regions. Antimicrob Agents Chemother 51, 264-274, 2007.
14) Koyama H, Sanui M, Saga T, Harada S, Ishii Y, Tateda K, Lefor AK. A fatal infection caused by sequence type 398 methicillin-resistant *Staphylococcus aureus* carrying the Panton-Valentine leukocidin gene: A case report in Japan. J Infect Chemother 21, 541 - 543, 2015.
15) Lewis HC, Mølbak K, Reese C, Aarestrup FM, Selchau M, Sørum M, Skov RL. Pigs as Source of Methicillin-resistant *Staphylococcus aureus* CC398 infections in humans, Denmark. Emerg Infect Dis 14, 1383-1389, 2008.
16) Lim SK, Nam HM, Jang GC, Lee HS, Jung SC, Kwak HS. The first detection of methicillin-resistant *Staphylococcus aureus* ST398 in pigs in Korea. Vet Microbiol 155, 88-92, 2012.
17) Lina G, Piemont Y, Godail-Gamot F, Bes M, Peter M, Gauduchon V, Vandenesch F, Etienne J. Involvement of Panton-Valentine leukocidin-producing *Staphylococcus aureus* in primary skin infections and pneumonia. Clin Infect Dis 29, 1128-1132, 1999.
18) Lozano C, Rezusta A, Gómez P, Gómez-Sanz E, Báez N, Martin-Saco G, Zarazaga Myrion, Torres C. High prevalence of *spa* types associated with the clonal lineage CC398 among tetracycline-resistant methicillin-resistant *Staphylococcus aureus* strains in a Spanish hospital. J Antimicrob Chemother 67, 330-334, 2012.
19) Ministry of Agriculture, Forestry and Fisheries in Japan. The 89th statistical yearbook of Ministry of Agriculture, Forestry

and Fisheries in Japan, 2015.
20) Molla B, Byrne M, Ableyl M, Mathews J, Jackson CR, Fedorka-Cray P, Sreevatsan S, Wang P, Gebreyes WA. Epidemiology and genotypic characteristics of Methicillin-resistant *Staphylococcus aureus* strains of porcine origin. J Clin Microbiol 50, 3687-3693,2012.
21) Nakaminami H, Hirai Y, Nishimura H, Takadama S, Noguchi N. Arthritis caused by MRSA CC398 in patient without animal contact. Japan. Emerg Infect Dis 26, 795-797, 2020.
22) Normanno G, Dambrosio A, Lorusso V, Samoilis G, Taranto PD, Parisi A. Methicillin-resistant *Staphylococcus aureus* (MRSA) in slaughtered pigs and abattoir workers in Italy. Food Microbiol 51, 51-56, 2015.
23) Sato T, Usui M, MotoyaT, Sugiyama T, Tamura Y. Characterisation of methicillin-resistant *Staphylococcus aureus* ST97 and ST5 isolated from pigs in Japan. J Glob Antimicrob Resist 3, 283-528, 2015.
24) The European Communities. Commission Decision of 20 December 2007 concerning a financial contribution from the Community towards a survey on the prevalence of *Salmonella* spp. and Methicillin-resistant *Staphylococcus aureus* in herds of breeding pigs to be carried out in the Member States (2008/55/EC), 2008.
25) van Rijen MM, Van Keulea PH, Kluytmans JA. Increase in a Dutch hospital of methicillin-resistant *Staphylococcus aureus* related to animal farming. Clin Infect Dis 46, 261-263, 2008.
26) Voss A, Loeffen F, Bakker J, Klaassen C, Wulf M. Methicillin-resistant *Staphylococcus aureus* in pig farming. Emerg Infect Dis 11, 1965-1966, 2005.

Japanese Journal of Veterinary Research 68(3): 203-208, 2020

JJVR

SHORT COMMUNICATION Experimental Research

Clinical evaluation of pentosan polysulfate as a chondroprotective substance in native Mongolian horses

Mijiddorj Tsogbadrakh[1)], Takafumi Sunaga[1, *)], Eugene Bwalya[1)], Suranji Wijekoon[1)], Ekkapol Akaraphutiporn[1)], Yanlin Wang[1)], Carol Mwale[1)], Adiya Naranbaatar[2)], Sangho Kim[1)], Kenji Hosoya[1)], Damdinsuren Alimaa[2)] and Masahiro Okumura[1)]

[1)]Laboratory of Veterinary Surgery, Department of Veterinary Clinical Sciences, Faculty of Veterinary Medicine, Kita18, Nishi9, Kita-ku, Sapporo, Hokkaido 060-00818, Japan

[2)]Department of Veterinary Surgery and Theriogenology, School of Veterinary Medicine, Mongolian University of Life Science, Zaisan, Khan-uul District, Ulaanbaatar 17024, Mongolia

Received for publication, May 11, 2020; accepted, June 22, 2020

Abstract

Pentosan polysulfate (PPS) is widely used as therapeutic intervention for joint diseases in humans and animals, while objective confirmation has not been established yet. The purpose of this study was to provide the objective measure of the efficacy of PPS. Twenty-five healthy Mongolian horses were randomly assigned in three groups. Three different doses of PPS, 0/1.2/3.0 mg/kg, were injected intramuscularly one a week for consecutive 4 weeks. On 14 and 28 days after the initial administration, relative ratios of serum COMP/CPII were 97.9/87.6/61.8 and 94.2/104.3/88.1 in 0/1.2/3.0 mg/kg PPS, respectively. The results revealed that balance of cartilage metabolism could be significantly brought to an anabolism dominant state by PPS injections in dose dependent manor in field fed horses in Mongolia.

Key Words: pentosan polysulfate, chondroprotection, horse

Pentosan polysulfate (PPS) is a semi-synthetic polysulfated xylan derived from beechwood[8)]. PPS is weak heparinoid indicating slight anticoagulant activities[9)] and anti-inflammatory properties, which are widely used for symptomatic managements for selective diseases, including interstitial cystitis[16)], osteoarthritis[1)] and mucopolysaccharidosis[6)] in human beings and veterinary patients. The pathobiology pathways, to which PPS could interfere as therapeutic interventions in osteoarthritis, were speculated to include induction and maintenance of synovitis, microcirculation in subchondral bones and surrounding structures resulting to bone sclerosis, and degradation of articular cartilage[5)]. Despite popularities of use of PPS for equine patients have been increased[18)], clinical factual observations are surely very limited to prove the evidence for PPS to restrain any of the above-mentioned pathways. The objective of the present study was to provide reliable clinical confirmation that PPS could control those pathways, particularly degradative activity of articular cartilage metabolism in horses with ordinally field-feeding.

* Corresponding author: Takafumi Sunaga
Address: Kita18, Nishi9, Kita-ku, Sapporo, Hokkaido 060-0818, Japan
Fax number: 011-706-5228 (Japan) Email: sunaga@vetmed.hokudai.ac.jp
doi: 10.14943/jjvr.68.3.203

Table 1. Blood biochemistry examination on ALT, LDH, BUN and Cr

	days after injection	PPS 3.0 mg/kg bw	PPS 1.2 mg/kg bw	PPS 0 mg/kg bw
ALT(U/l)	0	16.6±6.5	18.4±14.9	11.8±2.8
	14	9.8±2.2	10.3±2.5	8.2±2.2
	28	10.6±2.2	9.2±6.1	7.2±1.2
LDH(U/l)	0	481±105	634±165	465±119
	14	620±112	452±157	363±173
	28	535±73	542±144	351±103
BUN(mg/dl)	0	19.1±2.6	20.9±4.6	19.0±5.2
	14	20.9±3.3	19.8±4.8	17.1±4.1
	28	19.2±1.8	17.3±4.3	11.3±3.4
Cr(mg/dl)	0	0.52±0.24	0.65±0.10	0.54±0.12
	14	0.88±0.08	0.84±0.15	0.60±0.13
	28	0.84±0.05	0.93±0.16	0.59±0.14

Blood specimens were collected every 2 weeks, and serum biochemistry profiles, including total alanine aminotransferase (ALT), lactate dehydrogenase (LDH), blood urea nitrogen (BUN) and creatinine (Cr), were measured (Fuji DryChem NX500, Fujifilm, Tokyo, Japan) after sera being separated and prepared. Parameters of serum biochemistry examined were all in the normal reference ranges. Values were described as mean±standard deviation.

In the present study, a total of 25 native Mongolian horses (average body weight±standard error: 242±9 kg; 14 males and 11 females), which were two years of age and all after breaking, were randomly selected at a feeder in one plain in Khentii province, Mongolia, in September, 2017. All the horses had free access to grass and water daily in the same pasture condition. Before being assigned to this study, horses were examined to prove its general physical condition, serum biochemistry profiles including hepatic and renal functional measures and orthopedic fitness being normal and healthy. Four doses of PPS (OJI-200EI, Oji Holdings Co., Tokyo, Japan) at 3.0 mg/kg or 1.2 mg/kg were injected intramuscularly one a week in 20 horses, as of PPS dosage, injected each group of horses was consisted with 10 horses. In the rest five horses, phosphate-buffered saline solutions were injected in the same course of PPS administrations in other 20 horses. Horses were randomly assigned in each treatment group and entire procedures of the administration of PPS in an open label fashion. Use of PPS to these horses assigned in this study was on the basis of the owners' preference of its clinical use for prevention of osteoarthritis and maintained skeletal health[18]. Evaluation of horses in general physical and orthopedic conditions was done every week when PPS was injected. Blood specimens were collected every 2 weeks, and serum biochemistry profiles, including total alanine aminotransferase (ALT), lactate dehydrogenase (LDH), blood urea nitrogen (BUN) and creatinine (Cr), were measured (Fuji DryChem NX500, Fujifilm, Tokyo, Japan) after sera being separated and prepared. Serum cartilage metabolic markers, including cartilage oligomeric matrix protein (COMP; My BioSource., San Diego, CA, U.S.A.) and procollagen II C-propeptide (CPII; IBEX Pharmaceuticals Inc., Montreal, QC, Canada), were quantified by respective commercially available enzyme immune assay kits in accordance to manufacturer's instructions. All procedures were done by registered veterinary professionals in Mongolia under the approval of School of Veterinary Medicine, Mongolian University of Life Science as ethical standards for animals. Analysis of variance (ANOVA) was used to compare relative ratio of COMP/CPII among different PPS dose groups of horses on 14 or 28

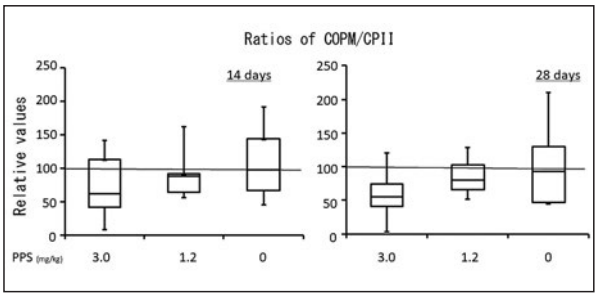

Fig. 1. The ratio of COMP/CPII at 14 and 28 days after the initial injection of PPS.

The ratios of COMP/CPII in horses with 3.0 mg/kg PPS showed some tendency to be lower than those with 0 mg/kg PPS on both 14 and 28 days after the initial injection (P =0.2517; P =0.1762, respectively).

Relative values of each cartilage metabolic marker represented %values in comparison with ones at the initial administration. Analysis of variance (ANOVA) was used to compare ratios of relative values of COMP/CPII among different dose groups of PPS on 14 or 28 days after the initial injections. Significant difference was defined as $P < 0.05$.

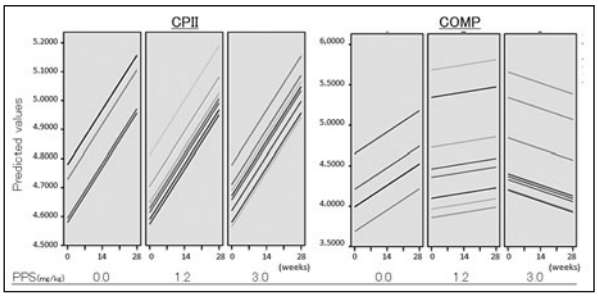

Fig. 2. Analysis of effects of sequential administration of PPS on cartilage metabolism by using the linear mixed effects models.

On the analysis, PPS was positively correlated to values of CPII, an anabolic marker of cartilage metabolism (Left). PPS dose and sequential injections showed negative correlation to vales of COMP with certain significance (Right) (P =0.027).

Each bar represents respective horse on the basis of concentration markers.

Significance of PPS administration on values of the markers in the course was evaluated by the linear mixed effects models fit by REML.

Significant difference was defined as $P < 0.05$.

days after the initial administration. Significance of PPS administration on values of the markers in the course was on the basis of dose-dependent manner, which was evaluated by the linear mixed effects models fit by residual maximum likelihood estimation. P value estimating statistical significance was set less than 0.05.

All horses showed no unbeneficial presentations in relation to series of PPS administration during the observation period. No symptomatic pathologies in joints, its adjacent structures and injection sites in the neck were found, and parameters of serum biochemistry examined were all in the normal reference ranges (Table 1). After 14 and 28 days from the initial administration, the relative ratios of serum relative values of two markers, COMP to CPII, representing balance of articular cartilage metabolism were 97.9/87.6/61.8 and 94.2/104.3/88.1 in three different dosages of PPS including 0, 1.2 and 3.0 mg/kg, respectively (Fig. 1). The ratios in 3.0 mg/kg PPS showed some tendency to be lower than those of 0 mg/ml PPS in both 14 and 28 days after the initial injection (P=0.2517; P=0.1762, respectively) (Fig. 1). The reduction of the ratio of COMP/CPII in different doses of PPS was simulated on the linear mixed effect models (Fig. 2). On the analysis, sequential injections of PPS showed the tendency to be positively correlated to values of CPII, an anabolic marker of cartilage metabolism (P=0.167). PPS dose and sequential injections showed negative correlation to vales of COMP with statistical significance (P=0.027).

This investigation suggested a clinical evidence to prove one of pathobiology pathways, degradative activities of cartilage, where PPS would effectively suppress in the course of joint diseases[5]. In previous studies, PPS is suggested to have suppressive effects on some of classic mitogen activated protein kinase pathways in cultured chondrocytes[1,15], to regulate phenotype of chondrocytes in appropriate condition[4], to down-regulate induction osteoclastic differentiation of hematopoietic stem cells simulating inflamed synovitis[2,17] and to show suppressive inflammatory changes of synovium in rodent models *in vivo*[19]. In horses, while much attention, especially for owners and trainers of racing horses, is being paid to PPS as both

preventive and therapeutic use to joint fitness, some studies suggest some positive opinions but none of them reached to provide clinical evidence using objective measures[3,7]. This would suggest that values of cartilage metabolic markers from large animals would have much variation, which could compromise to comprehend the obtained data properly. Statistical analysis using means or medians were not suitable to absorb the physiological variation of results.

The results on the balance of anabolic (CPII) and catabolic (COMP) markers suggested tendency, which PPS would bring it to more less catabolic in comparison with negative control (Fig. 1). The results analyzed by using the linear mixed effects models fit by REML revealed that degradation marker changes were significant to correlate with doses and sequential uses of PPS, proving that PPS would reduce degradative activities of cartilage in the course of joint diseases (Fig. 2). Domestic Mongolian horses are being fed by nomads in a traditional fashion customized for the specific climate and environment in Mongolian steppe, resulted in excess athletic and regular migration activities in summer and less movement and very limited nutritional intake in winter. On its life style, native horses are forced to have much physical stress on the skeletal system through active movement on the rough surface of the ground in warm season[11,13]. This would surely increase degradative activity of cartilage on joint surfaces causing future osteoarthritis, which would be one of the most prevalent diseases in athletic horses[12]. In human trial to use PPS for mild knee osteoarthritis, significant reduction of C2C, one of degradation markers of cartilage, was observed, which promised suppressive effects for PPS on degradation of cartilage[10]. Our observation of two cartilage metabolic markers would be the first evidence of anti-degradative effects of PPS in horses at a clinical setting.

No adverse effects were seen in serum biochemistry profiles and orthopedic examinations. Basically, this semi-synthetic substance is believed to be very safe and orally used for the only medical treatment for human interstitial cystitis for lifelong use to relief pain under the approval and registration by United States Food and drug Administration[19]. However, recently some ophthalmologists reported the augmentation that long time use of oral PPS for 15 years or more might cause vision threating pathologies in human beings aged more than 60 years old[14]. While short time use of PPS would not be expected to lead any serious adverse events, more knowledge and experience related to long time use of PPS in horses are necessary to establish its safety.

In conclusion, through our results from the analysis of cartilage metabolic markers related to PPS injections, reliable clinical confirmation that this substance could reduce degradative activity of articular cartilage metabolism in native Mongolian horses with ordinally field-feeding.

Acknowledgements

The authors sincerely pay appreciation to OJI Holdings corporation and colleagues to provide injectable PPS and tireless technical supports to complete measure biomarkers.

References

1) Bwalya EC, Kim S, Fang J, Wijekoon HMS, Hosoya K, Okumura M. Pentosan polysulfate inhibits IL-1β-induced iNOS, c-Jun and HIF-1α upregulation in canine articular chondrocytes. PLoS ONE 12, e0177144, 2017.
2) Bwalya EC, Kim S, Fang J, Wijekoon HMS, Hosoya K, Okumura M. Effects of pentosan polysulfate and polysulfated glycosaminoglycan on chondrogenesis of canine bone marrow-derived mesenchymal stem cells in alginate and micromass culture. J Vet Med Sci 79, 1182-1190, 2017.

3) Cruz AM, Hurtig MB. Multiple pathways to osteoarthritis and articular fractures: is subchondral bone the culprit? Vet Clin North Am Equine Pract 24, 101–116, 2008.
4) Francis DJ, Hutadilok N, Kongtawelert P, Ghosh P. Pentosan polysulphate and glycosaminoglycan polysulphate stimulate the synthesis of hyaluronan in vivo. Rheumatol Int 13, 61–64, 1993.
5) Ghosh P. The pathobiology of osteoarthritis and the rationale for the use of pentosan polysulfate for its treatment. Semin Arthritis Rheum 28, 211-267, 1999.
6) Hennermann JB, Gökce S, Solyom A, Mengel E, Schuchman EH, Simonaro CM. Treatment with pentosan polysulphate in patients with MPS I: results from an open label, randomized, monocentric phase II study. J Inherit Metab Dis 39, 831-837, 2016.
7) Jambaldorj S. Horse treasure book (Морин эрдэнэ судар), 1st ed. Central library of Mongolian, Ulaanbaatar, Mongolia. pp. 11-14, 1996. (in Mogolian)
8) Koenig TJ, Dart AJ, McIlwraith CW, Horadagoda N, Bell RJ, Perkins N, Dart C, Krockenberger M, Jeffcott LB, Little CB. Treatment of experimentally induced osteoarthritis in horses using an intravenous combination of sodium pentosan polysulfate, N-acetyl glucosamine, and sodium hyaluronan. Vet Surg 43, 612-22, 2014.
9) Kramer CM, Tsang AS, Koenig T, Jeffcott LB, Dartb CM, and Dartc AJ. Survey of the therapeutic approach and efficacy of pentosan polysulfate for the prevention and treatment of equine osteoarthritis in veterinary practice in Australia. Australian Vet J 92, 482-487, 2014.
10) Kumagai K, Shirabe S, Miyata N, Murata M, Yamauchi A, Kataoka Y, Niwa M. Sodium pentosan polysulfate resulted in cartilage improvement in knee osteoarthritis--an open clinical trial. BMC Clin Pharmacol 28, 7, 2010.
11) Losonczy H, Nagy I, Menyhei G. Management of chronic venous insufficiency with the combination of coumarin (Syncoumar) and oral pentosan polysulfate (PPS, SP 54) (preliminary report)]. Orv Hetil 134, 291–295, 1993.
12) McIlwraith CW, Frisbie DD, Kawcak CE. Evaluation of intramuscularly administered sodium pentosan polysulfate for treatment of experimentally induced osteoarthritis in horses. Am J Vet Res 73, 628–633, 2012.
13) Orgil D, Lo Y. Racehorse lameness and treatment (Хурдан морь доголох эмгэг ба эмчилгээ), 1st ed. Mongolian University of Life Science, Ulaanbaatar, Mongolia. pp. 16–21, 2019. (in Mongolian)
14) Pearce WA, Chen R, Jain N. Pigmentary maculopathy associated with chronic exposure to pentosan polysulfate sodium. Ophthalmology 125, 1793-1802, 2018.
15) Sunaga T, Oh N, Hosoya K, Takagi S, Okumura M. Inhibitory effects of pentosan polysulfate sodium on MAP-kinase pathway and NF-κB nuclear translocation in canine chondrocytes in vitro. J Vet Med Sci 74, 707–711, 2012.
16) van Ophoven A, Vonde K, Koch W, Auerbach G, Maag KP. Efficacy of pentosan polysulfate for the treatment of interstitial cystitis/bladder pain syndrome: results of a systematic review of randomized controlled trials. Curr Med Res Opin 35, 1495-1503, 2019.
17) Wijekoon S, Bwalya EC, Fang J, Kim S, Hosoya K, Okumura M. Chronological differential effects of pro-inflammatory cytokines on RANKL-induced osteoclast differentiation of canine bone marrow-derived Macrophages. J Vet Med Sci 79, 2030-2035, 2017.
18) Wijekoon HMS, Bwalya EC, Fang J, Kim S, Hosoya K, Okumura M. Inhibitory effects of sodium pentosan polysulfate on formation and function of osteoclasts derived from canine bone marrow. BMC Vet Res 14, 152, 2018.

19) Wijekoon HMS, Kim S, Bwalya EC, Fang J, Aoshima K, Hosoya K, Okumura M. Anti-arthritic effect of pentosan polysulfate in rats with collagen-induced arthritis. Res Vet Sci 122, 179-185, 2019.

JJVR

The Japanese Journal of Veterinary Research